國立臺灣大學工學院環境工程學研究所

碩士論文

Graduate Institute of Environmental Engineering
College of Engineering
National Taiwan University

Master Thesis

球狀活性碳對揮發性有機物的吸附與微波再生

Adsorption of Volatile Organic Compounds and Microwave Regeneration on Beaded Activated Carbon

蕭世盈
Shih-Ying Hsiao

指導教授：席行正 博士
Advisor: Hsing-Cheng Hsi, Ph.D.

中華民國 109 年 7 月

July 2020

doi:10.6342/NTU202003443

國立臺灣大學碩士學位論文
口試委員會審定書

球狀活性碳對揮發性有機物的吸附與微波再生

Adsorption of Volatile Organic Compounds and Microwave Regeneration on Beaded Activated Carbon

本論文係蕭世盈君(學號 R07541119)在國立臺灣大學環境工程學研究所完成之碩士學位論文，於民國 109 年 7 月 22 日承下列考試委員審查通過及口試及格，特此證明

論文審查委員：

席行正	席行正博士 國立台灣大學環境工程學系教授
林進榮	林進榮博士 國立宜蘭大學環境工程學系教授
余炳盛	余炳盛博士 國立台北科技大學材料及資源工程系副教授
江右君	江右君博士 元智大學機械工程學系副教授

指導教授：席行正

所　　長：闕蓓德

doi:10.6342/NTU202003443

誌謝

時光飛逝，兩年的研究所生活轉眼就要結束了，在台大環工所的這兩年，承蒙許多人的幫助才得以順利完成這個碩士學位。非常感謝席老師這兩年的耐心指導，在實驗上給我方向，不厭其煩的校閱這本論文，並且總是溫和地給予我許多鼓勵。感謝口試委員，林進榮、余炳盛、江右君老師，在口試時給予我許多建議，使此論文能更完整。

謝謝實驗室的學長姐們，在甫入實驗室時就讓我感受到這個研究團隊的熱情活力，也要謝謝學長姐們在實驗上的傳承及生活上的關心。謝謝張慶源老師家的劉柏良學長，出借 TGA 並且協助我使用。更要謝謝政諺學長在實驗各方面的幫助與指導，在學長搬入實驗室後，無論大小問題都能夠從您那得到解答。

謝謝實驗室的夥伴們奕丞、逸萱、書聞、安均、夢圓、廷鈞在學業上互相討論，也互相關心。可惜的是因為疫情緣故，在最後一個學期裡夢圓沒辦法在台灣與我們一同參與畢業典禮。謝謝學弟妹們在實驗及學業上的協助，感謝皓鋕幫忙我產出耗時的 BET 數據，更重要的是要感謝 Adrienne 在我論文的英文用字及文法修改上的鼎力相助，使得我這份論文得以順利完成。

謝謝從中興一起上來台大打拼的同學，雅魚、亭妤、易達、威宇，還有好朋友宗翰，雖然都分處在不同科系及不同實驗室，偶爾見上一面，吃個飯互相鼓勵都讓我的台北生活更加溫暖。謝謝在這段碩班生活給我鼓勵，以及偶爾來台北陪我吃飯的所有朋友同學們，是你們豐富了我的台北生活。

最後要感謝我的父母，讓我在求學的路程上沒有後顧之憂，總是對於我的決定給予全力支持與鼓勵，是我身後最大的支柱。

doi:10.6342/NTU202003443

中文摘要

揮發性有機物(VOC)是重要的空氣汙染物，對環境生態以及人體健康具有短期和長期影響，因此在空氣汙染防制中，如何限制和控制 VOC 的排放是極為重要的課題。活性碳吸附法一直以來被認為是一種有效的 VOC 處理方式，除了可以去除低濃度 VOC 外，也有回收具價值之有機蒸氣的潛力。而球狀活性碳通常具有高機械強度、高比表面積及高度流動性的特性，因此特別適合被應用在流體化床技術中。

本研究使用以酚醛樹酯球為原料，製備出具有高比表面積(大於 2000 m^2 g^{-1})、高微孔體積(大於 0.9 cm^3 g^{-1})且有高度圓球率之球狀活性碳，並將其應用在處理甲苯(TOL)及丁酮(MEK)吸附去除上；並搭配微波加熱再生技術，在惰性氣體環境中加熱使吸附物脫附，達到活性碳再利用的目標。並比較與商用球狀活性碳在吸附及脫附性能的異同。

吸附試驗之實驗結果以 Langmuir、Freundlich 及 Dubinin-Radushkevich(D-R)等溫吸附曲線模式進行擬合均顯示出高擬合度。而以 Clausius-Clapeyron 方程式以及由 D-R 模式所得的參數計算等容吸附熱，表明吸附劑與吸附物的交互作用以物理吸附為主。

而吸附 TOL 及 MEK 至飽和之球狀活性碳以微波加熱方式進行再生，結果表現出自製球狀活性碳(SBAC)能在較小微波功率及較短輻照時間下獲得相對商用球狀活性碳(KBAC)高的再生效率。而在循環吸附試驗方面，經過 8 個循環後，吸附 TOL 的 SBAC 吸附容量有顯著的減少，而在吸附 MEK 方面則些微的提升了吸附效能。然而此現象並沒有顯現在 KBAC 上，經過多個循環後仍維持恆定吸附容量的特性，顯示其在應用上的高可行性。

關鍵字：揮發性有機物、甲苯、丁酮、球狀活性碳、微波再生

doi:10.6342/NTU202003443

Abstract

Volatile organic compounds (VOCs) are a great threat to the environment and human health. Thus, it is very important to abate the emission of VOCs. Activated carbon has been one of the most prevalently used adsorbents for VOC emission control, and in a beaded shape, the activated carbon has potential to be applied in fluidized bed adsorption.

In this study, self-prepared activated carbon beads (SBAC) were synthesized using commercial phenol-formaldehyde resin sphere precursors, which have a very high specific surface area (>2000 m^2 g^{-1}) and micropore volume (>0.9 cm^3 g^{-1}). These experiments used methyl ethyl ketone (MEK) and toluene (TOL) as adsorbates in fixed-bed adsorption tests, and regenerated them via microwave heating with inert gas purging. All adsorption and desorption experiments were also performed using commercial BAC (KBAC) for comparison.

The Langmuir, Freundlich, and Dubinin-Radushkevich (D-R) isotherm models were used to fit the experimental adsorption data. All three models showed good fitting suitabilities. The isosteric heat of adsorption was calculated using the Clausius-Clapeyron (C-C) equation and the parameters obtained from D-R isotherm indicates that the interactions between adsorbate and adsorbent are due to physisorption.

Moreover, microwave heating was applied to the regeneration of saturated adsorbents, in order to analyze the effect of irradiation power and time on the desorption behavior of adsorbate. It was shown that compared to KBAC, SBAC reached relatively higher regeneration efficiencies at lower microwave powers and shorter irradiation times. After eight cycles of regeneration, the adsorption capacity for SBAC was significantly lost when loaded with TOL, whereas in SBAC loaded with MEK it was even greater than the

doi:10.6342/NTU202003443

virgin sample. However, KBAC was able to sustain the adsorption capacities after eight cycles of microwave regeneration, proving its hardiness. In conclusion, this study demonstrates the excellent adsorption performance of SBAC and the possibility for microwave regeneration of BACs.

Keywords: volatile organic compounds, toluene, methyl ethyl ketone, beaded activated carbon, microwave regeneration

doi:10.6342/NTU202003443

Content

誌謝..... III

中文摘要..... IV

Abstract..... V

Content..... VII

List of Figures..... X

List of Tables XIV

Chapter 1 Introduction..... 1

1.1 Background 1

1.2 Objectives..... 2

Chapter 2 Literature Review 4

2.1 Volatile Organic Compounds (VOCs) 4

2.1.1 Definition of VOCs 4

2.1.2 Source of VOCs 4

2.1.3 Effects on Environment and Health 5

2.1.4 VOCs Abatement Methods 8

2.2 Activated Carbon 10

2.2.1 Type of Activated Carbon 10

2.2.2 Preparation of BAC..... 12

2.3 Adsorption/Desorption Systems..... 14

2.3.1 Adsorption Mechanism 14

2.3.2 Adsorbent 17

2.3.3 Adsorption Isotherms 18

2.3.4 Adsorption Heat 25

2.3.5 Adsorbent Regeneration..... 27

doi:10.6342/NTU202003443

2.3.6 Microwave Swing Adsorption (MSA) 29
2.3.7 Heel Formation 34
Chapter 3 Materials and Methods 36
3.1 Research Framework 36
3.2 Materials 38
3.2.1 Preparation of Adsorbent 38
3.2.2 Adsorbate 39
3.3 Material Characterization 40
3.3.1 Surface Area, Pore Volume, and Pore Size Distribution (PSD) 40
3.3.2 Elemental Analysis (EA) 41
3.3.3 Electron Microscopy 41
3.3.4 Thermogravimetric Analysis (TGA) 42
3.4 Adsorption Test 42
3.4.1 VOC Generating System 43
3.4.2 Adsorption Bed Operation 44
3.4.3 THC Detection System 45
3.5 Adsorption Capacity 46
3.6 Microwave Regeneration 47
3.7 Adsorption/Desorption Kinetic Analysis 50
3.8 Cyclic Adsorption Test 52
Chapter 4 Results and Discussion 53
4.1 Physical and Chemical Properties of BAC 53
4.1.1 Elemental Analysis 53
4.1.2 Pore Structures 54
4.1.3 Morphology of BAC 57
4.2 Adsorption Test 61

doi:10.6342/NTU202003443

4.2.1 Adsorption Isotherm Experiments 61
4.2.2 Isosteric Heat of Adsorption 73
4.2.3 Adsorption Kinetics 75
4.3 Thermogravimetric Analysis 78
4.4 Microwave Regeneration 82
4.4.1 Desorption Kinetics 84
4.4.2 Desorption Efficiency 88
4.5 Cyclic Test 93
Chapter 5 Conclusions and Suggestions 98
5.1 Conclusions 98
5.1.1 Adsorption Equilibrium and Kinetics 98
5.1.2 Microwave Regeneration 99
5.1.3 Cyclic Adsorption/Desorption Test 100
5.2 Suggestions 101
Appendix A: Thermodynamic Calculation 102
A.1. Determination of Affinity Coefficient (β) 102
A.2. Determination of Heat of Vaporization (ΔH_{vap}) and Coefficient Expansion (α) 103
References 104

doi:10.6342/NTU202003443

List of Figures

Figure 2-1 Ranges of suitability for VOC control technologies (Cooper & Alley, 2010) 9

Figure 2-2 Schematic model of activated carbon (Henning & Schäfer, 1993) 10

Figure 2-3 Different types of activated carbon: (a) powder (Carbon Activated Corp.), (b) granule (Carbon Activated Corp.), (c) monolith (Applied Catalysis Corp.), (d) fiber cloth (Kureha Corp.), and (e) bead (Kureha Corp.) 12

Figure 2-4 Adsorption terms (Wypych, 2019) 15

Figure 2-5 The IUPAC Classification of physisorption isotherm shapes. 20

Figure 2-6 Illustration of equipotential surfaces 23

Figure 2-7 Dual-bed or three-bed operation of TSA process: (a) adsorption; (b) regeneration; (c) cooling 28

Figure 2-8 Microwaves and (a) conductors, (b) dielectric loss materials, and (c) insulators (Palma et al., 2020) 30

Figure 2-9 Difference in heating between microwave and conductive heat (Palma et al., 2020) 33

Figure 3-1 Flowchart of this study 37

Figure 3-2 The fluidized bed reactor system 38

Figure 3-3 (a) PF resin spheres, (b) SBAC, and (c) KBAC in this study 39

Figure 3-4 Process flowchart of the adsorption testing system 43

Figure 3-5 Calibration curve of microwave muffle furnace 49

Figure 3-6 The scheme diagram of the microwave regeneration system 49

Figure 3-7 (a) the quartz reactor and (b) the quartz boat 50

Figure 4-1 Standard N_2 adsorption-desorption isotherm of SBAC and KBAC 54

Figure 4-2 Mesoporous and macroporous pore size distribution (PSD) of SBAC and KBAC 55

Figure 4-3 Microporous pore size distribution (PSD) of SBAC and KBAC 55

Figure 4-4 SEM images of KBAC 57

Figure 4-5 SEM images of SBAC 58

Figure 4-6 TEM images of SBAC 58

Figure 4-7 SEM images of TOL-KBAC-800W8min 59

doi:10.6342/NTU202003443

Figure 4-8 SEM images of MEK-KBAC-800W8min 60
Figure 4-9 SEM images of MEK-SBAC-800W8min 60
Figure 4-10 SEM images of TOL-SBAC-800W8min 61
Figure 4-11 Experimental and Langmuir modeled adsorption isotherms for MEK and SBAC by (a) integration method and (b) gravimetric method 64
Figure 4-12 Experimental and Langmuir modeled adsorption isotherms for MEK and KBAC by (a) integration method and (b) gravimetric method 64
Figure 4-13 Experimental and Langmuir modeled adsorption isotherms for TOL and SBAC by (a) integration method and (b) gravimetric method 64
Figure 4-14 Experimental and Langmuir modeled adsorption isotherms for TOL and KBAC by (a) integration method and (b) gravimetric method 65
Figure 4-15 Experimental and Freundlich modeled adsorption isotherms for MEK and SBAC by (a) integration method and (b) gravimetric method 67
Figure 4-16 Experimental and Freundlich modeled adsorption isotherms for MEK and KBAC by (a) integration method and (b) gravimetric method 67
Figure 4-17 Experimental and Freundlich modeled adsorption isotherms for TOL and SBAC by (a) integration method and (b) gravimetric method 67
Figure 4-18 Experimental and Freundlich modeled adsorption isotherms for TOL and KBAC by (a) integration method and (b) gravimetric method 68
Figure 4-19 Experimental and D-R modeled adsorption isotherms for MEK and SBAC by (a) integration method and (b) gravimetric method 72
Figure 4-20 Experimental and D-R modeled adsorption isotherms for MEK and KBAC by (a) integration method and (b) gravimetric method 72
Figure 4-21 Experimental and D-R modeled adsorption isotherms for TOL and SBAC by (a) integration method and (b) gravimetric method 72
Figure 4-22 Experimental and D-R modeled adsorption isotherms for TOL and KBAC by (a) integration method and (b) gravimetric method 73
Figure 4-23 Isosteric heat of (a) MEK and (b) TOL adsorption on SBAC; (c) MEK and (d) TOL

doi:10.6342/NTU202003443

adsorption on KBAC 75
Figure 4-24 TG thermal curves of virgin BACs at heating rates of 10 °C/min 78
Figure 4-25 TG thermal curves of (a) MEK-SBAC and (b) MEK-KBAC at heating rates of 5, 10, and 20 °C/min 79
Figure 4-26 TG thermal curves of (a) TOL-SBAC and (b) TOL-KBAC at heating rates of 5, 10, and 20 °C/min 79
Figure 4-27 DTG of MEK-SBAC at various heating rates. (a) DTG peaks; (b) linear form providing the heat of desorption. 81
Figure 4-28 DTG of MEK-KBAC at various heating rates. (a) DTG peaks; (b) linear form providing the heat of desorption. 81
Figure 4-29 DTG of TOL-SBAC at various heating rates. (a) DTG peaks; (b) linear form providing the heat of desorption. 82
Figure 4-30 DTG of TOL-KBAC at various heating rates. (a) DTG peaks; (b) linear form providing the heat of desorption 82
Figure 4-31 Temperature profile of virgin (a) KBAC and (b) SBAC under 12 min of microwave irradiation (5 min for SBAC under 1000 W irradiation) 83
Figure 4-32 THC desorption curves of (a) MEK-SBAC and (b) MEK-KBAC at different microwave power outputs for 12 min of irradiation time 84
Figure 4-33 THC desorption curves of (a) TOL-SBAC and (b) TOL-KBAC at different microwave power outputs for 12 min of irradiation time 84
Figure 4-34 Desorption efficiency for MEK-SBAC evaluated by (a) change of sample weight and (b) desorption curve detected by FID 88
Figure 4-35 Desorption efficiency for MEK-KBAC evaluated by (a) gravimetric measurements and (b) desorption curve detected by FID 88
Figure 4-36 Desorption efficiency for TOL-SBAC evaluated by (a) change of sample weight and (b) desorption curve detected by FID 89
Figure 4-37 Desorption efficiency for TOL-KBAC evaluated by (a) change of sample weight and (b) desorption curve detected by FID 89

doi:10.6342/NTU202003443

Figure 4-38 NO, SO_2, CO, and CO_2 emission curves of (a) MEK-SBAC, (b) MEK-KBAC, (c) TOL-SBAC, (d) TOL-KBAC at 800 W microwave heating for 8 min 92

Figure 4-39 Variation in adsorption capacity of MEK-KBAC over the 8-cycle MSA test..... 94

Figure 4-40 Variation in adsorption capacity of TOL-KBAC over the 8-cycle MSA test 94

Figure 4-41 Variation in adsorption capacity of MEK-SBAC over the 8-cycle MSA test 95

Figure 4-42 Variation in adsorption capacity of TOL-SBAC over the 8-cycle MSA test..... 96

doi:10.6342/NTU202003443

List of Tables

Table 2-1 WHO classification system for indoor organic pollutants 4

Table 2-2 Sources and health effects of dominant VOCs (Zhang et al., 2017) 7

Table 2-3 Technological characteristics of VOC removal methods (Zhang et al., 2017) 9

Table 2-4 Physisorption and chemisorption (Ruthven, 2006) 16

Table 2-5 Classification of pores 17

Table 2-6 Researches of microwave regeneration of activated carbons with VOCs 33

Table 3-1 Properties of MEK and TOL 40

Table 3-2 Saturation vapor pressure data for MEK and TOL 45

Table 4-1 Elemental analysis of the BAC samples 53

Table 4-2 The physical properties of samples 56

Table 4-3 The physical properties of samples after 8-cycle and 800W-8min microwave regenerations 56

Table 4-4 Langmuir parameters for different adsorbate-adsorbent systems at different temperatures 63

Table 4-5 Freundlich parameters for different adsorbate-adsorbent systems at different temperatures 66

Table 4-6 D-R parameters for different adsorbate-adsorbent systems at different temperature 71

Table 4-7 Kinetic parameters of adsorption and correlation coefficient R^2 obtained from PFO and IPD kinetic models 77

Table 4-8 Peak desorption temperatures at different heating rates and activation energies for desorption 81

Table 4-9 Kinetic parameters of desorption and correlation coefficient R^2 obtained from PFO and IPD kinetic models 87

Table A-1 Parameters used in calculating and the affinity coefficient (β) 102

Table A-2 Parameters used in calculating and thermal expansion coefficient (α) 103

Table A-3 Wagner equation constants used in calculating the heat of vaporization 103

doi:10.6342/NTU202003443

Chapter 1 Introduction

1.1 Background

In urban environments, anthropogenic activities have emitted numerous air pollutants, and volatile organic compounds (VOCs) are one of the major air pollutants. Some organic vapors are dangerous to human health and natural ecosystems, and may be accompanied by severe odor problems. The possible impact of VOCs on health is far-reaching, and may cause eye and respiratory irritation, as well as allergic reactions. Moreover, some VOCs, such as some carbonyls and aromatic compounds, are mutagenic and carcinogenic, posing a serious threat to our health. Also, VOCs are essential precursors for the formation of photochemical smog, and some VOCs, such as chlorofluorocarbons (CFC) and hydrochlorofluorocarbons (HCFC), are recognized to contribute to the global greenhouse effect.

Among the stationary sources, the primary sources of VOCs are the chemical, electronics manufacturing, and petrochemical industries. In Taiwan, the major VOC emission source is the polyurethane (PU) industry, which produced about 5000 tons/year of VOCs. Methyl ethyl ketone (MEK) and toluene (TOL) are the major emission of VOCs from solvents (Chang & Lin, 2006; Shen et al., 1999).

In general, many VOC abatement techniques have been developed and applied, including destructive methods (such as thermal/catalytic oxidation and biofiltration) and recovery methods (such as absorption, adsorption, condensation, and membrane separation). Among them, adsorption is considered a very economical method, due to its simplicity and high removal efficiency, in addition to its recoverability for valuable

doi:10.6342/NTU202003443

organic vapors.

Activated carbon (AC) is a very common adsorbent for the removal of hazardous pollutants. Recently, many novel forms of carbon materials have been developed and applied. Beaded activated carbon (BAC) is a novel morphology of this carbonaceous material. Owing to its high mechanical strength, high specific surface area, and high fluidity, it is suitable for many industrial applications.

Microwave heating technology has been widely used since the 1960s. This heating technology can directly heat materials. Thus, it has been used in the regeneration of adsorbents in recent years. Contrary to the conventional conduction heating regeneration methods, microwave heating has a higher heating rate, yet lower energy consumption, and thereby improves the efficiency. Therefore, microwave heating can potentially replace traditional conductive heating.

1.2 Objectives

This study concentrates on BAC adsorption performances of toluene (TOL) and methyl ethyl ketone (MEK), as well as the microwave regeneration of saturated BAC. The BAC prepared from the phenol-formaldehyde resin sphere was compared with commercial BAC.

The specific objectives of this study were as follows:

1. Establish equilibria and kinetic mechanisms of the TOL and MEK adsorption process on BAC, as both mechanisms are recognized as useful tools to understand the interactions between adsorbate and adsorbent surfaces.

doi:10.6342/NTU202003443

2. Explore the effect of microwave power output and irradiation time on the regeneration of spent BACs.
3. Identify and report the effect of regeneration heating on heel buildup during adsorption/regeneration cycling of a VOC, and subsequently proving the feasibility of this technology.

doi:10.6342/NTU202003443

Chapter 2 Literature Review

2.1 Volatile Organic Compounds (VOCs)

2.1.1 Definition of VOCs

The U.S. EPA defines VOCs as "any compound of carbon, excluding carbon monoxide, carbon dioxide, carbonic acid, metallic carbides or carbonates, and ammonium carbonate, which participates in atmospheric photochemical reactions." (Spengler et al., 2001). Organic compounds can be classified into various sub-groups according to their boiling points (World Health Organization, 1989). Although a large number of substances are considered VOCs, the most abundant in the environment are benzene and some of its organic derivatives like toluene, ethylbenzene and xylene, which are collectively named BTEX (Montero-Montoya et al., 2018).

Table 2-1 WHO classification system for indoor organic pollutants

Group	Boiling Point (^{o}C)
VVOC – very volatile organic compounds	< 0 to 50-100
VOC – volatile organic compounds	50-100 to 240-260
SVOC – semi volatile organic compounds	240-260 to 380-400
POM – organic compounds associated with particulate matter	>380

2.1.2 Source of VOCs

Globally, natural VOCs are abundant, and isoprene and monoterpenes are the most prominent compounds, followed by alcohols and carbonyls (Kesselmeier & Staudt, 1999).

doi:10.6342/NTU202003443

Although VOCs emitted into the atmosphere from biogenic sources are the primary sources overall, anthropogenic VOCs often dominate in urban areas (Atkinson & Arey, 2003).

Since the industrial revolution, many activities have emitted anthropogenic pollutants, including toxic gases and VOCs. The major classes of emitted VOCs are alkanes, alkenes, aromatic hydrocarbons, and oxygenated compounds (Atkinson & Arey, 2003). For stationary emission sources, the primary sources of VOCs are the chemical, electronics manufacturing, and petrochemical industries. Some solvents are used as cleaners, thinners, and plasticizers, etc. Consequently, VOCs can be emitted from the vent gas, water separation techniques, industrial wastewater, batch processes, petroleum refining, natural gas processing, petrochemical processes, and painting processes (Chang & Jeng, 1994; Khan & Kr. Ghoshal, 2000; Mirzaei et al., 2016). Anthropogenic activities have become an inevitable source of VOC emissions, and they account for 25% of VOCs in our global atmosphere (Montero-Montoya et al., 2018). Additionally, vehicular emissions are another source of VOCs, accounting for about one-half to two-thirds of airborne VOCs in an urban area. Among these benzene, toluene, ethylbenzene, and m/p/o-xylene are the main components (Chang et al., 2010; Fujita, 2001).

2.1.3 Effects on Environment and Health

From an environmental perspective, it is necessary to limit and control the emissions of VOCs. These vapors may have both short- and long-term impacts on the natural ecosystem as well as on human health (Collins et al., 2013; Kampa & Castanas, 2008; Mirzaei et al., 2016). Furthermore, the emitted VOCs generate severe odor problems, which frequently lead to disputes between factories and nearby residents (Chang & Chiou,

doi:10.6342/NTU202003443

2006).

VOCs are central to atmospheric chemistry from the urban to the global scale. For example, VOCs are known to be crucial precursors of tropospheric ozone. In the presence of sunlight, VOCs react with nitrogen oxides and other airborne chemicals to undergo photochemical reactions by forming secondary organic compounds, or degrading to free radical species that contribute to the formation of ozone. Those compounds are components of environmentally hazardous photochemical smog (Atkinson, 2000; Seinfeld & Pandis, 2016; Sillman, 1999). A significant fraction of the excess secondary organic aerosol is formed from anthropogenic VOCs' oxidation products, which could be responsible for an additional 3-25 Tg yr^{-1} secondary organic aerosol production globally (Volkamer et al., 2006).

Besides this, some greenhouse gases, such as chlorofluorocarbons (CFCs) and hydrochlorofluorocarbons (HCFCs), are also part of a group of VOCs (Hansen et al., 1989). The infrared bands of these greenhouse gases absorb radiation from the earth's surface and emit it. These bands lead to a reduction in the net infrared radiative flux emitted to space, where the trapping of surface radiation by the infrared bands affects the atmospheric temperature and climate (Ramanathan, 1975).

Several VOCs have been perceived as toxic, carcinogenic, or mutagenic at concentration levels present in the urban environment. The possible health effects of VOCs span quite a broad range. Adverse health effects from exposure to VOCs are caused by a wide range of reactions and interactions occurring in the body, which depend mainly on the chemical structure and reactivity of the substance. These contaminants' short-term effects include sensitivity, irritation and allergic reactions, respiratory effects, and

doi:10.6342/NTU202003443

carcinogenic effects (Rumchev et al., 2007). For example, methyl ethyl ketone (MEK), which resembles acetone in odor and physical properties, is more irritating to the eyes and upper airway than acetone, and has even been known to cause dermatosis (Chang & Chiou, 2006). The long-term health effect of these pollutants may be life-threatening diseases. Some carbonyl and aromatic compounds like HCHO, CH_3CHO, benzene, toluene, and xylene have been correlated with the development of cancer in the human body. It has also been proven that polycyclic aromatic hydrocarbons (PAHs), after metabolic activation in vivo, are capable of inducing mutations in oncogenes and may result in tumor growth after multiple mutations (Baird et al., 2005; Soni et al., 2018).

Table 2-2 Sources and health effects of dominant VOCs (Zhang et al., 2017)

Classification	Representatives	IDLH*	Sources	Health effects
Alcohols	Methanol Ethyl alcohol Isopropyl alcohol	6000 ppm 3300 ppm 2000 ppm	Antiseptics Preservative Cosmetics and personal care products	Throat irritation and shortness of breath Eye irritation Central nervous system depression
Aldehydes	Formaldehyde Acetaldehyde	20 ppm 2000 ppm	Decorative and construction materials Cosmetics and plastic adhesives Fabrics and bio-waste decomposition Biomass burning Degradation of VOCs in multiple steps oxidations	Irritation of the throat, eyes and skin Nasal tumors Predecessor of ozone
Alkenes	Propylene Ethylene	–	Petrochemical syntheses Production of varnishes Synthetic resins, adhesives, printing ink Organic intermediates of pharmaceutical and perfumes	Photochemical ozone creativity potential Potentially carcinogenic and adversely affects the odor and taste of drinking water
Aromatic compounds	Benzene Toluene Ethylbenzene	500 ppm 500 ppm 800 ppm	Petroleum products Incomplete combustion of liquid	Carcinogen Damage the ozone layer

doi:10.6342/NTU202003443

Classification	Representatives	IDLH*	Sources	Health effects
			fuels Adhesives Lacquers	Produce photochemical smog, and pose mutagenic hazards
Halogenated VOCs	Carbon tetrachloride Chlorobenzene 1,1,2-Trichloroethane 1,1,2,2-Tetrachloroethane Trichloroethylene Tetrachloroethylene Dichloromethane	200 ppm 1000 ppm 100 ppm 100 ppm 1000 ppm 150 ppm –	Chemical extractant Paints Adhesives Polymer syntheses Water purification systems	Strong bioaccumulation potential Acute toxicity Destruction of the ozone Cause greenhouse gas effects
Ketones	Acetone Ethyl butyl ketone	2500 ppm 1000 ppm	Varnishes, window cleaners, paint thinners, adhesives	Irritation of eyes, nose, and throat Central nervous system depression Headache and nausea
Polycyclic aromatic hydrocarbons	Phenanthrene Pyrene	–	Release from creosote and incomplete combustion of organic matter, coal, oil, and biofuels	Carcinogen

*IDLH (immediately dangerous to life or health) from the National Institute of Occupational Safety and Health.

2.1.4 VOCs Abatement Methods

Table 2-3 lists several methods used for controlling VOCs. These methods can be broadly divided into recovery methods and destruction methods, based on whether the VOCs can be recovered. The destruction techniques involve incineration, catalytic oxidation, and biological treatment, while the recovery methods include condensation, absorption, and adsorption (Zhang et al., 2017). Different techniques are appropriate for different uses, depending their pollution characteristics (see Figure 2-1).

Adsorption is a very prevalent method for VOC emission control with the potential to recover valuable vapors. Adsorption can be seen as the removal of VOCs from an exhaust stream by adhering these compounds to the surface of a porous solid. High removal efficiencies are attainable with a suited adsorbent and enough contact time between the

doi:10.6342/NTU202003443

sorbent and the exhaust stream (Cooper & Alley, 2010). Generally, the adsorbents have high porosity and large surface areas. There are four kinds of commercial adsorbents commonly used in industrial applications, including activated carbon, zeolites, silica gel, and activated alumina (Yang, 2003). The carbon adsorption systems are flexible and economical to operate and install. Despite some disadvantages such as hygroscopicity and pore-blocking, carbon materials are low-cost, efficient, and stable adsorbents for VOC abatement. (Khan & Kr. Ghoshal, 2000; Zhang et al., 2017)

Details of the theory of activated carbon adsorption are introduced in subsequent sections.

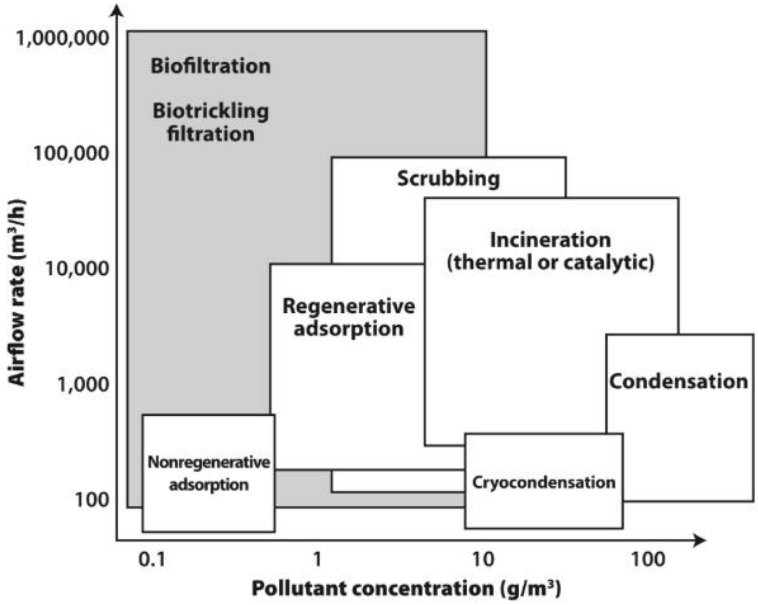

Figure 2-1 Ranges of suitability for VOC control technologies (Cooper & Alley, 2010)

Table 2-3 Technological characteristics of VOC removal methods (Zhang et al., 2017)

Methods	Efficiency	Market sales	Reuse	Waste generation	Energy consumption	VOCs concentration
Incineration	>99% (40 min)	High	No	CO, NOx	Moderate	20%–25%

doi:10.6342/NTU202003443

Methods	Efficiency	Market sales	Reuse	Waste generation	Energy consumption	VOCs concentration
Condensation	Moderate	High	Yes	–	High	>5000 ppm
Biological degradation	100% (~7 months)	Nc[a]	No	Acetaldehyde, Propanal, Acetone	Low	<5000 ppm
Absorption	–	Low	Yes	Spent absorbent	Moderate	–
Adsorption	>90%	High	Yes	Spent adsorbent	Moderate	700–10000 ppm
Plasma catalysis	74%–81%	Nc[a]	No	Formic acid, Carboxylic acids, NOx, O_3	High	–
Photocatalytic oxidation	100% (5 min)	Low-moderate	No	Strong oxidant $OH^{\cdot}$ radicals	Moderate	–
Ozone-catalytic oxidation	100% (2 h)	High	No	Secondary organic aerosols	High	–
Membrane separation	–	Nc[a]	Yes	Clogged membranes	High	<25%

[a] Not widely commercialized.

2.2 Activated Carbon

In a broad definition, activated carbon (AC) can be seen as a wide range of processed amorphous carbon-based materials, and has a highly developed porous structure and an extensive internal surface area (Bansal & Goyal, 2005).

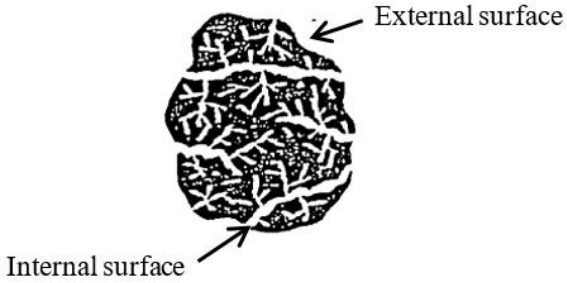

Figure 2-2 Schematic model of activated carbon (Henning & Schäfer, 1993)

2.2.1 Type of Activated Carbon

Activated carbon has been extensively applied in various fields, such as in the removal

doi:10.6342/NTU202003443

of toxic substances from aqueous phase (Perrich, 1981) and gas phase (Mohamad Nor et al., 2013), as well as being catalysts or catalyst supports (Jüntgen, 1986; Pereira et al., 1999). The conventional AC types are powdered activated carbon (PAC) and granular activated carbon (GAC), as shown in Figure 2-3(a) and (b), respectively. However, there are some disadvantages in the application of conventional powdered and granular ACs, such as their high demand, difficult regeneration, and the high pressure drop they cause.

For more industrial applications, some novel morphologies have been developed, such as the monolith, fibrous, and bead forms (Luo et al., 2006). Activated carbon monolith, as (ACM) shown in Figure 2-3(c), has been developed to overcome the existing problems with the direct application of carbon materials. Compared to the conventional AC types, ACM has better mass transfer, reusability, and dispersion of catalysts (Hosseini et al., 2020). Activated carbon fibers (ACF), as shown in Figure 2-3(d), are relatively costly, but the advantages of ACF are that they can be more easily molded to the shape of the adsorption system, and produce lower hydrodynamic resistance to flow (Bansal & Goyal, 2005). Lastly, activated carbon beads (BACs), shown in Figure 2-3(e), have unique characteristics. Due to their high mechanical strength, excellent adsorption performance, good fluidity, and high micropore volume, they have a wide range of uses, including as catalyst supports and adsorbents (Romero-Anaya et al., 2014; Wang et al., 2012; Xu et al., 2007).

doi:10.6342/NTU202003443

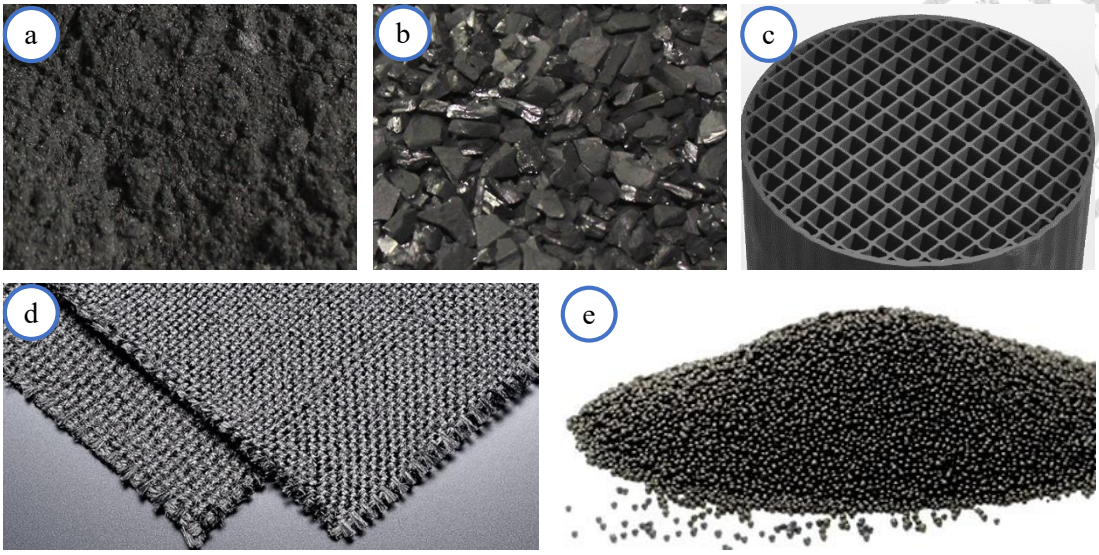

Figure 2-3 Different types of activated carbon: (a) powder (Carbon Activated Corp.), (b) granule (Carbon Activated Corp.), (c) monolith (Applied Catalysis Corp.), (d) fiber cloth (Kureha Corp.), and (e) bead (Kureha Corp.)

2.2.2 Preparation of BAC

The preparation of AC involves two main steps: (1) carbonization and (2) activation. During the carbonization process, raw materials are heated at a moderate temperature (below 800°C) in an inert atmosphere. Most of the non-carbon elements (e.g., oxygen, hydrogen and nitrogen) are released as volatile gaseous species in the pyrolytic decomposition processes. The residual elementary carbon atom groups rearrange into irregular stacks of aromatic sheets. These interstices lead to pores, and the pores are filled or partially blocked by disorganized carbon (Bansal & Goyal, 2005). Afterwards, the activation process can further develop the pore structure of the materials. Although the porosity type of carbon materials is typically determined by the carbonaceous precursor, the activation method used is another parameter that influences the final pore size distribution (Laine & Yunes, 1992).

In chemical activation, the char is impregnated with chemical agents, such as H_3PO_4,

doi:10.6342/NTU202003443

NaOH, and KOH, and subsequently pyrolyzed. The chemical additive is eliminated by heat treatment, and the pore structure is produced during the pyrolysis process (Jagtoyen & Derbyshire, 1998; Lozano-Castelló et al., 2001; Tseng, 2007). On the other hand, in physical activation, the carbonized product is usually implemented in a temperature range between 800 to 900°C in air, carbon dioxide, or steam. During the process, oxidation of some regions within the char are preferential to others, resulting in the selective elimination of carbon atoms and the development of a large internal surface (Bansal & Goyal, 2005).

A variety of materials can be precursors for BAC, including coal, pitch and many other manufactured polymeric materials (e.g. resins). Traditionally, coal-based BAC uses tar or phenolic resin as adheres, and the carbon beads are formed with a disc pelletizer machine. As for pitch-based BACs, the emulsion method is a mainstream technology. In this preparation method, molten pitch particles are spheroidized in a heat-stable liquid medium as it has a lower solubility. This adheres-free method improves sphericity and enhances mechanical intensity (Kodama et al., 1991; Qi et al., 2017).

The precursor of resin-based BAC is a spherical resin, which can be produced by polymerization in heterogeneous systems, such as emulsion, suspension, and other methods. Due to the minimization of interfacial free energy between the particle and the medium, the polymer particles have a spherical shape (Liu et al., 2012; Yuan et al., 1991). Typically, coal and pitch based carbons are manufactured from impure and non-uniform feedstocks, and result in non-uniform porous solids. On the contrary, resin is a more pure and uniform precursor, and the activated carbons made from it have relatively uniform pores distribution (Pelekani & Snoeyink, 2000).

doi:10.6342/NTU202003443

2.3 Adsorption/Desorption Systems

In Taiwan, there are a number of solvents used in many industrial processes. According to the Taiwan Industrial Development Bureau, the PU industry and PVC wallpaper production industry account for roughly 5000 tons and 113,000 tons per year, respectively, of solvent use. Main emission sources of VOCs from factories are the coating, adhering, drying, and surface treating processes. Emitted VOCs include methyl ethyl ketone (MEK), toluene (TOL), dimethylformamide (DMF), and cyclohexanone (ANONE), which can be recovered to reduce production cost and air contamination (Chang & Chiou, 2006). In recent years, numerous adsorption studies of MEK and TOL on activated carbons have been performed (Cha et al., 2004; Cherbański, 2018; Coss & Cha, 2000; Emamipour et al., 2007; Kim & Ahn, 2010; Lee et al., 2008; Romero-Anaya et al., 2010; Shah et al., 2014).

2.3.1 Adsorption Mechanism

Generally, adsorption is the term for the enrichment of molecules, atoms, or ions in the vicinity of the adsorbent (Thommes et al., 2015). The adsorbents' surfaces have active sites that can bind with foreign molecules, and when bound, are referred to as adsorption. Desorption can be described as the reversal of the adsorption process, which is the liberation of the adsorbed molecules (Wypych, 2019). A distinction is made between two types of adsorption mechanisms: physical adsorption (physisorption) and chemical adsorption (chemisorption) depending on the interaction between adsorbate and adsorbent. Physisorption is driven by van der Waals forces between the molecules located on the surface of adsorbents, and are assisted with various electrostatic contributions (e.g.

doi:10.6342/NTU202003443

from polarization, field–dipole and field gradient–quadrupole interactions). During adsorption, there are no violent or disruptive structural changes that occur on the surface of the adsorbent. In contrast, the molecular interaction potentials of chemisorption are more robust and involve a chemical reaction between the surface of the adsorbent and the adsorbate, which leads to high heats of adsorption, often approaching the value of chemical bonds. (Khan & Kr. Ghoshal, 2000; Lowell et al., 2012; Ruthven, 2006). The general characteristics of physisorption and chemisorption are shown in Table 2-4.

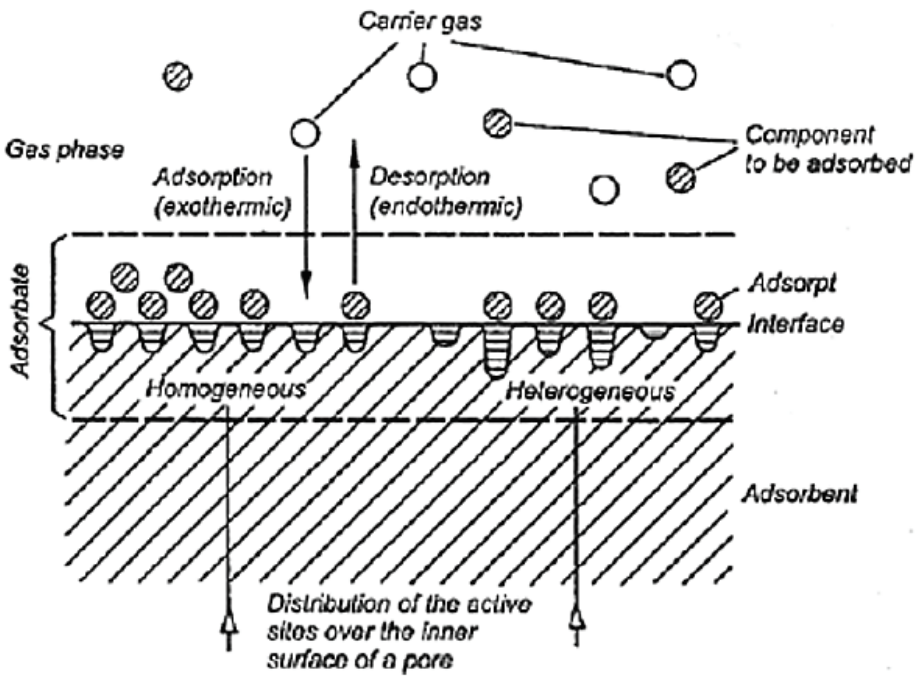

Figure 2-4 Adsorption terms (Wypych, 2019)

doi:10.6342/NTU202003443

Table 2-4 Physisorption and chemisorption (Ruthven, 2006)

Physisorption	Chemisorption
Low heat of adsorption (1.0 to 1.5 times latent heat of evaporation)	High heat of adsorption (> 1.5 times latent heat of evaporation)
Nonspecific	Highly specific
Monolayer or multilayer	Monolayer only
No dissociation of adsorbed species	May involve dissociation
Only significant at relatively low temperature	Possible over a wide range temperatures
Rapid, non-activated, reversible	Activated, may be slow and irreversible
No electron transfer although polarization of sorbate may occur	Electron transfer leading to bond formation between sorbate and surface

In the context of physisorption, the surface area and pore size distribution (PSD) of the adsorbent are factors of primary importance in the adsorption process. Generally, due to the availability of adsorption site, the higher the specific surface area, the higher the adsorption capacity will be. Nevertheless, the surface area within the adsorbent must be accessible (Wypych, 2019). Pore size and PSD are affected by the precursor, degree of activation, and the regeneration frequency. It is convenient to classify pores according to their size, which is determined by the analysis of nitrogen (77 K) adsorption-desorption isotherms. According to the International Union of Pure and Applied Chemistry (IUPAC) classification of pore size, pores are divided into three categories as shown in Table 2-5 (Thommes et al., 2015).

These are distinguished by the type of adsorption controlling force. The overlapping surface forces from opposite walls within the pore play an important role in the micropore range. Surface forces and capillary forces are dominant in mesopores, and for macropores,

doi:10.6342/NTU202003443

pore characteristics contribute very little to the adsorption capacity, but rather, they are essential in for transport properties (Choi et al., 2001).

Table 2-5 Classification of pores

Categories	Width of pores
Micropores	d < 2 nm
Mesopores	2 nm < d < 50 nm
Macropores	d > 50 nm

2.3.2 Adsorbent

Generally, the surfaces of activated carbon are nonpolar, which have a relatively low water affinity and strong affiliation to organic substances with non-polarity or weak polarity, which are often described as hydrophobic. With those carbonaceous adsorbents, physisorption is the dominant adsorption mechanism. The affinity between adsorbent and adsorbate is the primary interaction force controlling adsorption, and is dependent on the size and polarizability of the sorbate molecules, as well as the pore size (Ruthven, 2006).

Activated carbon has attracted considerable attention for its remarkable properties, such as its predominantly hydrophobic surface properties, high thermal stability, low cost, chemical inertness, excellent mechanical stability, and low energy requirement for regeneration (Guo et al., 2009; Wickramaratne & Jaroniec, 2013).

The adsorbent applied in this study is activated carbon with a beaded shape, also termed BAC. Its unique properties, such as high mechanical strength, excellent attrition resistance, high fluidity, and high specific surface area, all contribute to the broad utilization of this carbonaceous material in industries (Romero-Anaya et al., 2014).

doi:10.6342/NTU202003443

In this study, the phenol-formaldehyde (PF) resin beads have been used as a precursor to prepare activated carbon beads. Compared to other feedstock (e.g. coal and pitch), the advantage of using synthetic polymers is owing to their chemical composition, rendering better control of the resulting carbon materials' morphology and pore structure (Sun et al., 2013). The essential advantage of the phenolic resin-based BACs is that the ash content of the synthesized phenolic resin is very low. Thus, the impurities of BACs can be kept to a very low level (Cai et al., 2004). These resin-based BAC adsorbents have ideal spherical shapes, high mechanical strength, and low dusting properties, which are the ideal features for fluidized bed looping applications (Wickramaratne & Jaroniec, 2013).

2.3.3 Adsorption Isotherms

The surface microstructure of activated carbons is generally relative to its adsorption capacity. In the 2015 IUPAC reports, the physisorption isotherms were grouped into eight types, as shown in Figure 2-5, which were identified and shown to be closely related to particular pore structures. The classifications of physisorption isotherms are discussed as follows (Thommes et al., 2015):

(1) Type I isotherms typically depict microporous materials with relatively small external surfaces. A Type I isotherm is concave to the P/P_0 axis, and the amount adsorbed approaches a limiting value. In lieu of of the high adsorbent-adsorptive interactions in narrow micropores, a precipitous uptake at very low P/P_0 occurs. Type I(a) isotherms are found with microporous materials having mainly narrow micropores, and Type I(b) isotherms are given by materials with broader pore size distributions, including wider micropores and narrow mesopores.

doi:10.6342/NTU202003443

(2) Type II isotherms are typically used to describe the physisorption of most gases on nonporous or macroporous sorbents. Its shape is the outcome of unrestricted monolayer-multilayer adsorption, reaching high P/P_0. The inflection point is called point B, which corresponds to the completion of monolayer coverage.

(3) Type III isotherms are convex to the P/P_0 axis without a point B, indicating that there is no identifiable monolayer formation. This isotherm represents a relatively weak gas-solid interaction; therefore, the adsorbed molecules are clustered around the most favorable sites on the surface of a nonporous or macroporous solid.

(4) Type IV isotherms are usually observed in mesoporous adsorbents. The curve takes the same path of the corresponding part of a Type II isotherm by rising steeply, with a prominent intermediate saturation of the adsorption surface at low P/P_0. Then, at higher P/P_0, there is a limiting value as saturation pressure is reached. In the Type IV(a) isotherm, when the pore width exceeds a certain critical width, a hysteresis loop occurs due to the pore condensation. If an adsorbent has mesopores with smaller widths or conical and cylindrical shapes, an utterly reversible Type IV(b) isotherms are observed.

(5) Type V isotherms are usually observed for water adsorption on hydrophobic microporous and mesoporous adsorbents. This results from relatively weak adsorbent–adsorbate interactions. Adsorption is low at low P/P_0, but increases at higher P/P_0 once capillary condensation takes place, and then levels off at high concentrations.

(6) Type VI isotherms are observed in a highly uniform nonporous surface. This is a more complicated case, showing that the adsorption isotherms can have more than one step,

doi:10.6342/NTU202003443

which is representative of layer-by-layer adsorption, and illustrates an adsorption of adsorbate molecules up to the limit of condensation phenomenon (Ng et al., 2017).

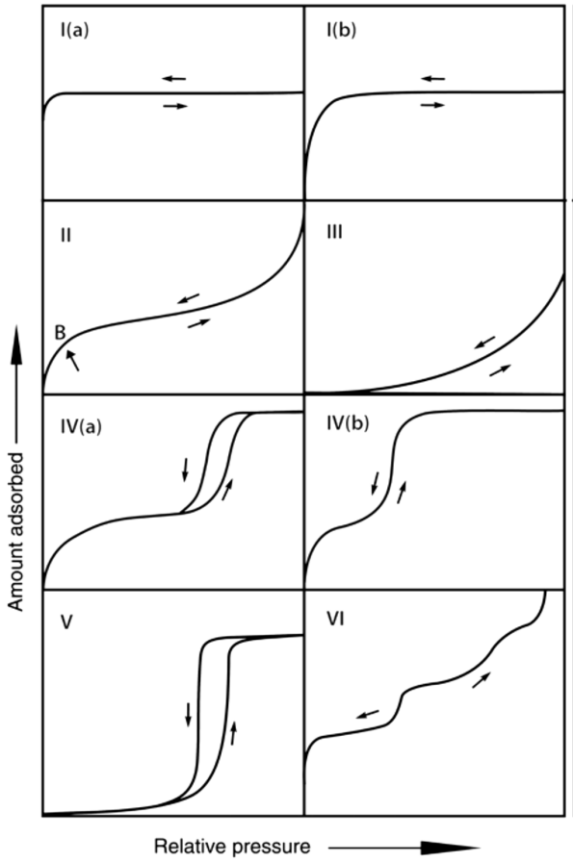

Figure 2-5 The IUPAC Classification of physisorption isotherm shapes.

2.3.3.1 Adsorption isotherm models

Since activated carbon has multiple isotherm properties, the adsorption processes are attributed to various interactions. Adsorption isotherm models are beneficial tools to describe the adsorbate-adsorbent interactions. They provide essential information on the adsorption mechanisms and the surface properties and affinities of the adsorbent (Vargas et al., 2011). More importantly, such isotherm models provide the design data required for developing adsorption systems (Ng et al., 2017). Linear regression analysis has been one of the most applied tools for defining the best fitting adsorption models. There are a

doi:10.6342/NTU202003443

variety of equations for analyzing experimental adsorption equilibrium data (Ayawei et al., 2017; Vargas et al., 2011). The most commonly used models are as follows:

(1) Langmuir isotherm model

The Langmuir isotherm model broadly utilizes gas-solid phase adsorption. The Type I isotherm is characterized by Langmuir-type adsorption (Ng et al., 2017). Langmuir introduced a concept of monomolecular adsorption on energetically homogeneous surfaces. This model assumes uniform energies of adsorption onto the surface and no transmigration of adsorbate on the plane of the surface. (Chiou, 2003; Dąbrowski, 2001) The form of the Langmuir isotherm is as follows (Yang, 2003):

$$q = \frac{q_s K_L P}{1+K_L P} \tag{2-1}$$

where q_s is the maximum capacity of adsorption, q is the amount of adsorbate on the adsorbent at equilibrium, and P is the partial pressure of the adsorbate in the gas-phase. The constant K_L is a Langmuir isotherm constant related to the affinity of the binding sites.

(2) Freundlich isotherm model

The Freundlich isotherm is a classical empirical adsorption model rather than a physical model. This model was formulated to define the surface heterogeneity and the exponential distribution of active sites and their energies. As a result, the Freundlich model is a considerably simple mathematical tool for many applications. It is regarded as an excellent way to present the toluene adsorption on activated carbon (Ayawei et al., 2017; Benkhedda et al., 2000; Chiou, 2003). The Freundlich exponential equation is

doi:10.6342/NTU202003443

expressed as:

$$q = K_F \cdot P^{1/n} \tag{2-2}$$

where K_F and n are empirical constants, which indicate a relative distribution of energy and the heterogeneity of the adsorbent sites, q is the amount of adsorbate in the adsorbent at equilibrium, and P is the partial pressure of the adsorbate in the gas-phase (Ayawei et al., 2017).

(3) Polanyi-theory-based models

In the case of highly energetic heterogeneous adsorption, the adsorption data show a considerable deviation from the Langmuir model or the BET model. It usually happens in high-surface-area, microporous solids, as the force field within a pore space of a microporous material varies by location. The Polanyi adsorption potential theory has been recognized as one of the most influential models for describing gas adsorption on energetically heterogeneous adsorbents. The theory considers that the attractive adsorption potential (ε) between the molecule and the solid surface is highest in the narrowest pore (Chiou, 2003). Polanyi thought that the potential energy (ε) could be expressed by the isothermal compression work of the adsorbed gas as such (Wang et al., 2014):

$$\varepsilon = RT \ln\left(\frac{P_0}{P}\right) \tag{2-3}$$

where R is the gas constant (8.31 $Jmol^{-1} k^{-1}$), T is absolute temperature, P_0 is the saturation pressure corresponding to the adsorption temperature, and P is the adsorption equilibrium pressure.

doi:10.6342/NTU202003443

Connecting the points in adsorption space with the same ε forms a series of equipotential surfaces, as depicted in Figure 2-6 (Chiou, 2003).

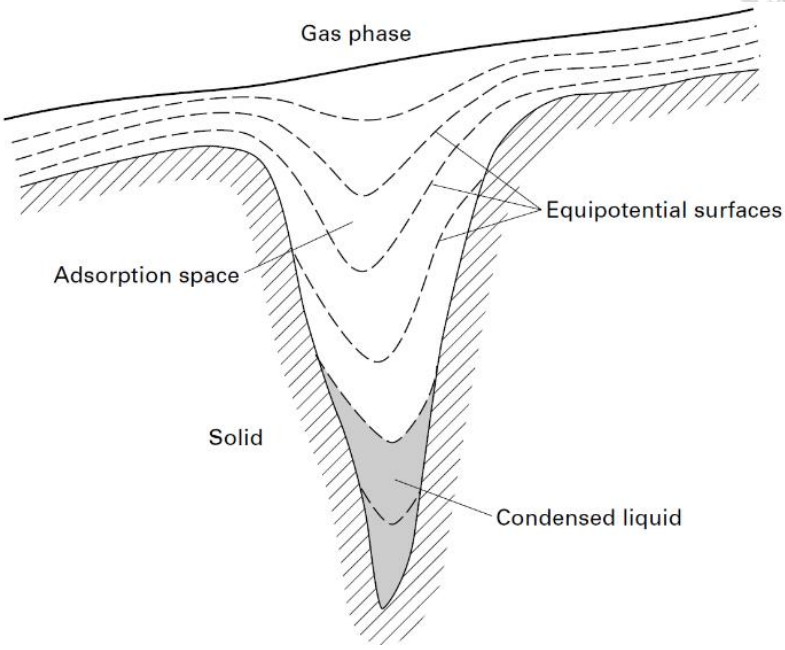

Figure 2-6 Illustration of equipotential surfaces

Dubinin's approach was developed from the Polanyi concept of adsorption potential and from the concept of the volume filling of micropores, rather than a defined model process to describe the physisorption of the adsorbate (Dąbrowski, 2001; Hutson & Yang, 1997). It is regarded as a suitable way to characterize the equilibrium adsorption process between the adsorbate vapor and activated carbon (Wang et al., 2014).

The Dubinin-Radushkevich (D-R) isotherm model is a semi-empirical adsorption expression, which has a significant correlation with temperature; therefore, when adsorption data at different temperatures are plotted as a function of the logarithm of the amount adsorbed versus the square of potential energy, all suitable data can be obtained. The D-R isotherm is derived as:

doi:10.6342/NTU202003443

$$W = W_0 \exp\left\{-\left[A\frac{\varepsilon}{\beta}\right]^2\right\} \tag{2-4}$$

where W is the total volume of the adsorbed space, and W_0 is the limiting volume of the adsorbed space. E is the characteristic energy of the tested adsorbate and E_0 is that for the reference adsorbate. β is an affinity coefficient characterizing the polarizability of the adsorbate, which is equal to the ratio of E and E_0, or $\beta = E/E_0$.

Alternatively, the D-R isotherm can also be shown as:

$$q = q_s \exp[-K_{DR}\varepsilon^2] \tag{2-5}$$

where K_{DR} is the D-R equation constants, q_s is the maximum capacity of adsorption, and q is the amount of adsorbate in the adsorbent at equilibrium. The constant K_{DR} gives the characteristic energy (or free energy) E, which was computed using the relationship (Ayawei et al., 2017):

$$E = \frac{1}{\sqrt{2K_{DR}}} \tag{2-6}$$

The modified D-R equation is vital to the adsorption methods analysis of properties in most industrial adsorbents. These sorbents have complex pore structures, and micropores play an essential role in the structures (Dąbrowski, 2001). The Dubinin−Astakhov (D-A) approach is a revised equation from the D-R equation:

$$W = W_0 \exp\left[-\left(A\frac{\varepsilon}{\beta}\right)^n\right] \tag{2-7}$$

where n is the D-A equation adjustment parameter, generally ranging from 1.5 to 3 in the case of activated carbon (Monneyron et al., 2003).

(4) Brunauer–Emmett–Teller (BET) model

doi:10.6342/NTU202003443

The BET theory is a special type of Langmuir isotherm, in which the assumption is that the Langmuir equation applies to every adsorption layer (Dąbrowski, 2001; Khan et al., 1997). It represents the entire course of the isotherm, including the areas of monomolecular adsorption, polymolecular adsorption, and capillary condensation. This model is the theoretical basis for calculating the surface area of fine powders and porous materials (Chiou, 2003). The BET equation for physical adsorption is given as:

$$q_e = \frac{q_0 CP}{(P_0 - P)\left(1 + (C-1)\frac{P}{P_0}\right)} \tag{2-8}$$

$$C = A \exp\left(\frac{E_1 - E_L}{RT}\right) \tag{2-9}$$

where q_e is the amount adsorbed at a pressure P, q_0 is the amount the gas required to form a monolayer on the surface of the adsorbent, and P_0 is the saturation vapor pressure of the adsorbate at the adsorption temperature. E_1 is the mean enthalpy of adsorption of the first layer and E_L the enthalpy of liquefaction of the adsorbate (Parra et al., 1995).

2.3.4 Adsorption Heat

Adsorption heat is composed of two parts: one part is the condensation heat of the vapor, and the other is called surface energy. The first part can be found in the steam table, whereas the second part is difficult to measure. Fortunately, the adsorption heat can be estimated by the adsorption equation (Wang et al., 2014).

The isosteric heat of adsorption is the differential heat of adsorption, which reflects the interaction between the adsorbate molecules and the active sites on adsorbent surfaces (Bansal & Goyal, 2005). Adsorption is an exothermic process. When the vapor condenses on the surface of the solid adsorbent under constant temperature and pressure, the degree

doi:10.6342/NTU202003443

of freedom decreases. Thus, the degree of disorder decreases, and the entropy (S) decreases. The free enthalpy (H) on the surface of the adsorbent also declines (Wang et al., 2014). Free enthalpy is:

$$\Delta H = \Delta G + T\Delta S \tag{2-10}$$

When it is under constant temperature and pressure conditions, the Equation 2-10 is less than 0 ($\Delta H < 0$). Hence, heat is released in the adsorption process. Conversely, desorption is an endothermic process ($\Delta H > 0$) and requires a large amount of heat when the adsorbed gas is discharged (Menon & Komarneni, 1998). Nevertheless, a large exothermic heat of adsorption can result in a significant temperature increase during the adsorption process, which can be detrimental to the performance of the adsorption unit. For instance, the reduction of dynamic adsorption capacities and induction of the oxidation reaction, may even lead to bed ignition at a rather low temperature (Giraudet et al., 2009). Consequently, in lieu of ensuring the efficiency and safety of the adsorption process in practical application, a high ΔH_s is not always an advantage.

Conventionally, to explain the variation in adsorption heat, the isosteric heats of adsorption can be calculated from isotherms at different temperatures by using the Clausius-Clapeyron (C-C) equation (Ruthven, 2006):

$$\Delta H_s = -RT^2 \left(\frac{\partial \ln P}{\partial T}\right)_q \tag{2-11}$$

Assuming that the heat of adsorption is independent of temperature, integration of Equation 2-11 yields:

doi:10.6342/NTU202003443

$$\ln P = -\frac{\Delta H_s}{RT} + \text{constant} \tag{2-12}$$

where ΔH_s (kJ/mol) is the isosteric heat and P (Pa) is the vapor pressure.

Substituting the Polanyi's potential (Equation 2-3) into Equation 2-11 yields an analytical solution for ΔH_s (Ramirez et al., 2005):

$$\Delta H_s = \Delta H_{vap} + \varepsilon - T\left(\frac{\partial \varepsilon}{\partial T}\right)_q \tag{2-13}$$

where the ΔH_s is the summation of the heat of vaporization (ΔH_{vap}), the adsorption potential (ε), and the change of maximum adsorption capacity with temperature.

The change in maximum adsorption capacity with temperature can be modified and combined with Equation 2-13 to become:

$$\Delta H_s = \Delta H_{vap} + \varepsilon - T\left(\frac{\partial \varepsilon}{\partial T}\right)_\theta - \alpha T\left(\frac{\partial \varepsilon}{\partial \ln q}\right)_T \tag{2-14}$$

Assuming that ε is temperature independent, it can be rewritten as:

$$\varepsilon = E\left(\ln\frac{W_0}{W}\right)^{1/2} \tag{2-15}$$

Yielding a modified Equation 2-14 expressed as:

$$-\Delta H_s = \Delta H_{vap} + E\left(\ln\frac{W_0}{W}\right)^{1/2} + \frac{E\alpha T}{2}\left(\ln\frac{W_0}{W}\right)^{-1/2} \tag{2-16}$$

where E is the characteristic energy and α is the coefficient of thermal expansion of the adsorbate.

2.3.5 Adsorbent Regeneration

Regeneration (or desorption) is implemented by changing the conditions in the adsorber to achieve a lower equilibrium capacity by methods including pressure swing

doi:10.6342/NTU202003443

adsorption (PSA) and temperature swing adsorption (TSA) (Wypych, 2019). Because the PSA process requires constant pressure control which causes enormous energy consumption, the TSA process is currently most prevalent. This is based on the periodic variation in the temperature of an adsorbent bed, where the bed is regenerated by raising the temperature (Di, 2016). A typical TSA system is dual- (adsorption and regeneration) or three-bed (adsorption, regeneration and cooling), as shown in Figure 2-7 (Ko, Moon, & Choi, 2001). In order to optimize the AC bed regeneration process, efficiency and energy requirement are important parameters for the advancement of VOC capture technologies. Moreover, parameters such as the selection of a carbon adsorbent, bed design, and effect of gas inlet conditions have effects on abatement performances (Shah et al., 2014).

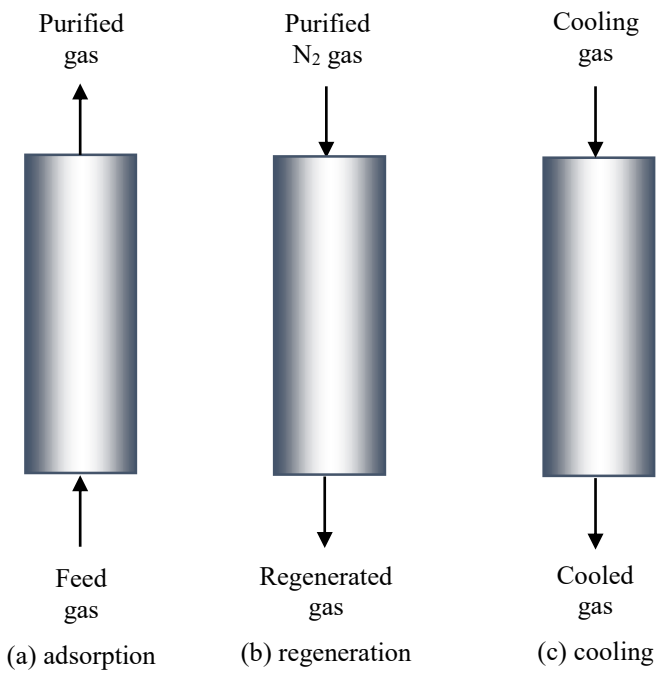

Figure 2-7 Dual-bed or three-bed operation of TSA process: (a) adsorption; (b) regeneration; (c) cooling

doi:10.6342/NTU202003443

The regeneration of ACs has numerous economic advantages and has relative operational ease in adsorption processes. In the past, when AC became saturated, it was simply discarded, generating a secondary source of pollution (Ania et al., 2005). Additionally, the spent carbon adsorbents, which may have been toxic and flammable or explosive, needed to be treated as hazardous waste. Regeneration allows for the stabilization of spent ACs, and the solvents can be recovered for reuse, minimizing the demands of both solvents and virgin adsorbents (Shah et al., 2014).

2.3.6 Microwave Swing Adsorption (MSA)

Microwaves are a form of electromagnetic energy, which incorporates those wavelengths roughly between 1 m to 1 mm or the bands of frequencies from 300 MHz to 300 GHz. The two standard frequencies in commercial applications are 915 and 2450 MHz (Chandra, 2011; Metaxas, 1991). Materials can be classified into three groups according to their interaction with microwaves: absorbers (or dielectric loss materials), insulators, and conductors, as shown in Figure 2-8. Figure 2-8 illustrates several points: (1) electrical conductors, such as aluminum or stainless steel, can reflect microwaves; (2) most carbon-based materials are absorbers of microwaves (depending on their structural composition) and convert microwave energy to heat; (3) insulating materials like quartz are microwave transparent. Microwaves are transmitted through the material with little attenuation. (Binner et al., 2014; Chandrasekaran et al., 2012)

doi:10.6342/NTU202003443

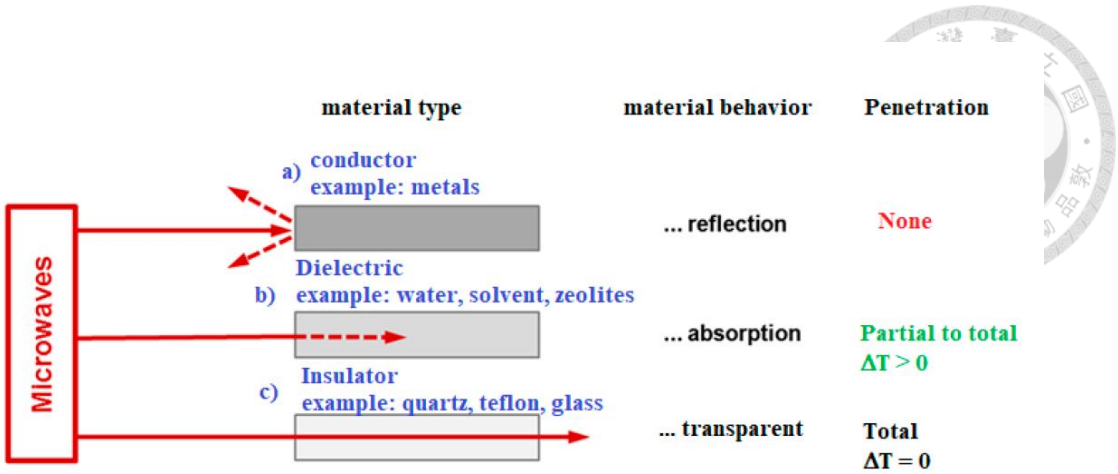

Figure 2-8 Microwaves and (a) conductors, (b) dielectric loss materials, and (c) insulators (Palma et al., 2020)

Microwave heating is caused when applied energy is transformed into heat by mutual interactions between media. The materials or media, which absorb the microwave radiation, are termed as dielectrics. With microwaves, the energy transfer is not primarily by conduction or convection as in conventional heating, but by dielectric loss. The literature reveals that microwave heating occurs by dipolar and interfacial polarization (Menéndez et al., 2010). When microwaves are applied to the dielectric materials with an oscillating electric field, its electric field polarizes the workload's molecules. The dipoles within the material then realign themselves and flip around in the presence of the high-frequency electric field. Due to the high frequency, this realignment occurs at a million times per second, causing an internal friction of molecules, and thereby resulting in volumetric heating of the material (Binner et al., 2014; Chandrasekaran et al., 2012; Metaxas, 1991; Nigar et al., 2016). In the case of dielectric solid materials with charged particles that are free to move in a delimited region of the material, such as π-electrons in carbon materials, a current traveling in phase with the electromagnetic field is induced. As the electrons cannot couple to the changes in the phase of the electric field, energy is

doi:10.6342/NTU202003443

released in the form of heat due to the interfacial polarization (Menéndez et al., 2010).

It has been reported that carbon is a proper receptor of microwaves (Yuen & Hameed, 2009). Charcoal is classified as a hyperactive material with regards to its interaction with microwaves. Depending on the power of the irradiation microwave, very high temperatures (>1000°C) can be achieved within seconds. Therefore, it would be expected that activated carbon would absorb microwave energy and display a high heating rate (Amankwah et al., 2005).

Molecules with symmetric charge distributions are nonpolar, meaning they have a very small dipole moment and loss factor. Hence, they exhibit a limited absorption of microwaves. The aliphatic hydrocarbon structures are inclined to have weak microwave absorbing potential. By contrast, water and a wide range of organic compounds such as MEK are polar because they have charge asymmetry, which can affect a molecule's otherwise non-polar structure and lead to an increased absorbing capability of microwaves (Binner et al., 2014; Hashisho et al., 2005; Metaxas, 1991).

There is a growing body of evidence that microwave technology is a promising available technology for the regeneration of carbon materials (Table 2-6). Microwave swing adsorption (MSA) is a system that uses microwave energy to capture and recover organic vapors from airstreams for reuse (Hashisho et al., 2005). Compared with conventional heating techniques, the additional advantages of microwave heating are rapid heat transfer, volumetric and selective heating, compactness of equipment, speed of switching on and off, and no by-products of combustion (Metaxas, 1991). The benefits of microwave regeneration are the microwave regeneration capability of molecular-level heating, which leads to homogeneous and quick thermal reactions (Ania et al., 2007).

doi:10.6342/NTU202003443

Consequently, the heating mechanism of microwaves is dependent on the dielectric properties of the workload rather than the purge gas flow rate during regeneration (Hashisho et al., 2005). Due to the direct and homogeneous heating from microwaves on adsorbents, Kim and Ahn (2012) reported that microwave heating regeneration showed a higher desorption efficiency than conventional heating regeneration methods.

Generally, the traditional conductive heating regeneration methods (e.g. hot gas or steam purge) have low energy efficiency not only because the adsorbent was heated, but also because of the need to heat the purge gas. In contrast, microwaves can offer target heating of the material, and directly heat the inside of the workload (i.e. adsorbate and/or adsorbent). It allows for a higher energy efficiency and the rapid and precise control of the workload temperature, resulting in energy savings and shortening in processing time. (Hashisho et al., 2005). Heating times using microwave treatment can be decreased to less than 1% of those needed using conventional conductive heating methods with the associated reduction in inert gas consumption (Jafarinejad, 2017; Jones et al., 2002). Hazervazifeh et al. (2017) reported that the microwave technology using in fruits dehydrate could decrease 60% of energy costs compared with conventional heating methods (Hazervazifeh et al., 2017). Though the capital costs of microwave regeneration units were higher than those of conventional heating units, the total operating cost for microwave regeneration is likely to be less. A comparison between a microwave system and a conventional kiln regenerating 120 kg/h activated carbon revealed that operating costs could be reduced by 1/3 using the microwave unit (Bradshaw et al., 1997).

Carbons can not only be recycled and reused several times by microwave regeneration, but this technique sometimes increases its surface area and accordingly increases its

doi:10.6342/NTU202003443

adsorption capacity (Ania et al., 2004). Liu et al. (2004) have shown that after seven cycles of adsorption/microwave regeneration of GAC, the adsorption capacity was higher than the virgin, and attributed to the increase in the surface area and total pore volume during microwave heating.

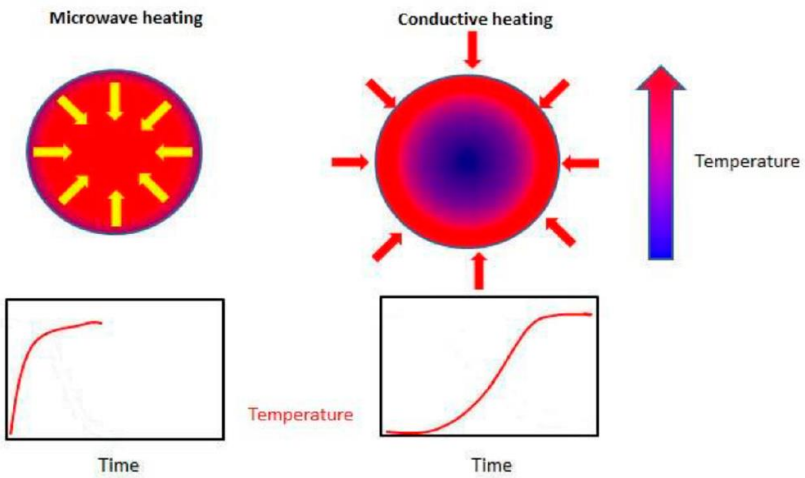

Figure 2-9 Difference in heating between microwave and conductive heat (Palma et al., 2020)

Table 2-6 Researches of microwave regeneration of activated carbons with VOCs

Type of AC	Adsorbate	Reference
PAC	The aqueous solutions of ethanol and acetone	Fang and Lai (1996)
Coal-based GAC	Methyl ethyl ketone, acetone, and tetrachloroethylene vapors	Coss and Cha (2000)
GAC	Methyl ethyl ketone	Cha and Carlisle (2001)
GAC and natural zeolite	Toluene, ethyl acetate and methylene chloride	Cha et al. (2004)
GAC	The aqueous solutions of pentachlorophenol, dichloromethane, sodium hydroxide, hydrochloric acid, methanol and acetonitrile	Liu et al. (2004)
GAC	Phenol	Ania et al. (2004)
ACF	Methyl ethyl ketone, water vapor and tetrachloroethylene	Hashisho et al. (2005)
ACF	Methyl ethyl ketone	Emamipour et al. (2007)
BAC	n-Dodecane	Fayaz et al. (2015)
GAC	Toluene	Cherbański (2018)

doi:10.6342/NTU202003443

2.3.7 Heel Formation

One of the challenges of adsorbent regeneration is the amount of adsorbate left on the BAC following the regeneration cycle, which is commonly known as the build-up of the heel and reduces the lifetime of the adsorbent. The heel formation usually can be described as the combined result of strong physisorption, oligomerization, and chemisorption (Niknaddaf et al., 2016), where some solvents may decompose, react, or polymerize when in contact with activated carbon and steam (Wypych, 2019).

The physisorption mechanism in small micropores is mainly pore filling, due to the overlapping of pore wall potentials that enhance adsorption capacity. Still, an increasing portion of adsorbed species is converted into heel on highly microporous adsorbents. Owing to the lower adsorption energy, the larger pores are usually associated with lower VOC adsorption capacities, which also lead to higher adsorbate elimination during desorption. In other words, there is lower heel formation during regeneration of the adsorbent in larger pores (Pelekani & Snoeyink, 2000). Lashaki et al. (2012) reported that micropore volume reduction for BACs confirmed that heel accumulation took place in the highest energy pores. That is, a more significant portion of adsorbed species was converted into heel on highly microporous adsorbents due to a higher share of high energy adsorption sites in their structure. They also reported that heel formation decreases with increasing regeneration temperature, which is possibly due to the desorption of chemical compounds from narrow micropores.

However, some researchers noted that AC regeneration at high temperatures (> 400°C) and high heating rates can cause permanent pore blockage due to coke formation, along with an increased heel formation (Niknaddaf et al., 2020; 2016). Although the microwave

doi:10.6342/NTU202003443

regeneration technique has superior performance to conventional heating regeneration, some literature reported that due to an enhanced cracking of the adsorbed compounds resulting from direct adsorbate-microwave interaction, a decrease in the efficiency of the regeneration process occurred, and suggested that rapid heating could be associated with reduced adsorbent performance (Niknaddaf et al., 2016). Ania et al. (2005) reported the formation of coke deposits within the pore because of the high-temperature decomposition of adsorbed phenol molecules after microwave regeneration of activated carbons at 850°C. Çalışkan et al. (2012) considered that for a given compound, especially a polar adsorbate which readily adsorbed microwaves, decomposition was accelerated in the presence of microwaves. Therefore, to find a balance between reversibility and capacity, it is of paramount importance to understand these mechanisms for designing and selecting adsorbents for practical applications.

doi:10.6342/NTU202003443

Chapter 3 Materials and Methods

3.1 Research Framework

This research divided into four parts: adsorbent preparation and characterization, the adsorption test, microwave heating regeneration, and cyclic adsorption/regeneration tests.

For the one thing, the BAC we prepared and the commercial BAC for comparisons characterized by their physical and chemical properties. Then, based on the adsorption isotherm models and kinetic models, we studied the VOC adsorption process onto BAC samples. Using the C-C equation and the parameters obtained from the D-R model fitting calculate the isosteric heat of adsorption process. After that, spent BAC was regenerated by microwave heating with N_2 as a purging gas. Lastly, cyclic microwave regeneration tests appraised the long-term applications of the adsorbents. The change of adsorption capacity was estimated by a new adsorption test after each regeneration. Figure 3-1 illustrates the research procedures of this study in detail.

doi:10.6342/NTU202003443

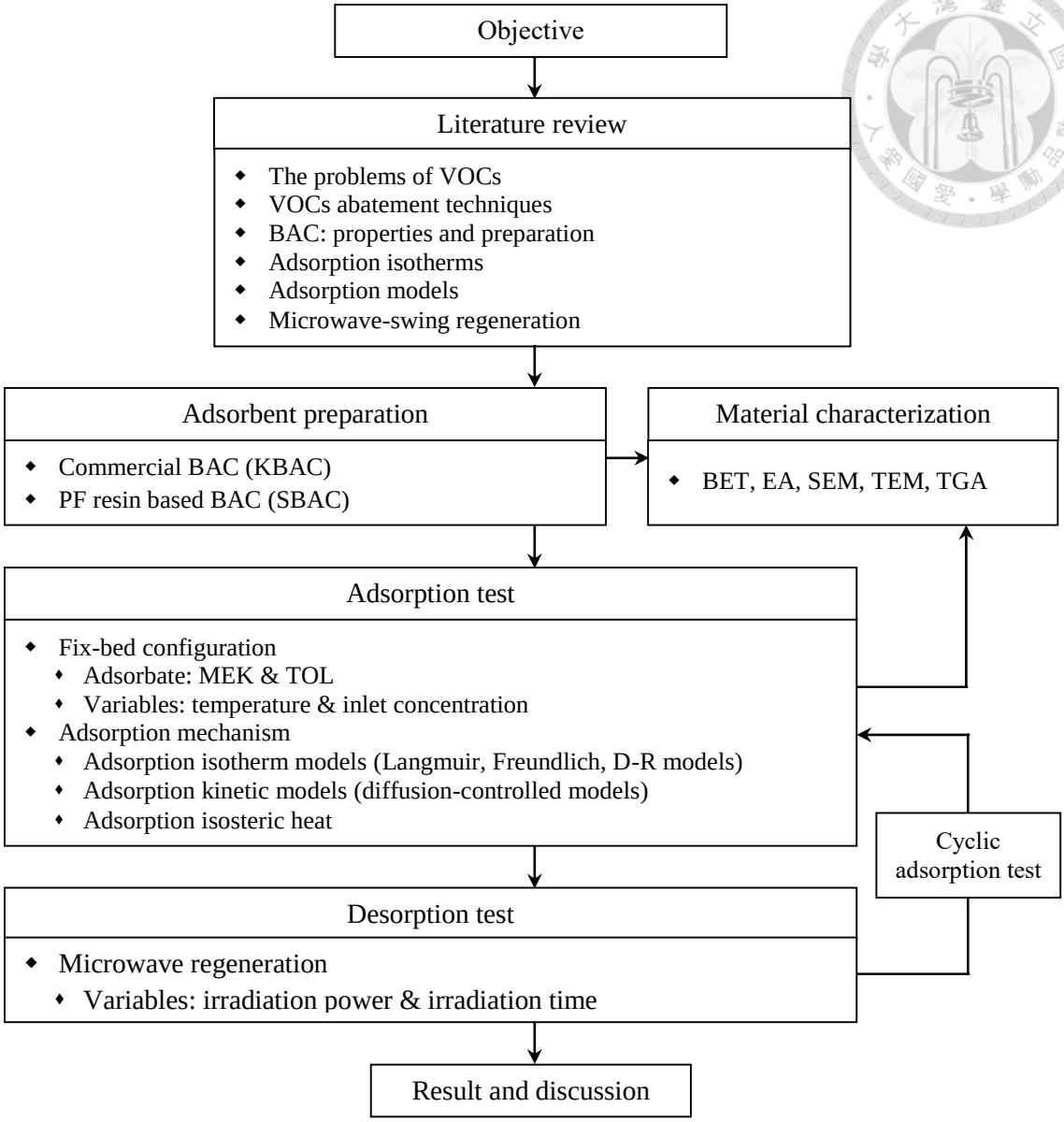

Figure 3-1 Flowchart of this study

doi:10.6342/NTU202003443

3.2 Materials

3.2.1 Preparation of Adsorbent

In this research, the self-prepared adsorbent was BAC prepared from commercial phenol-formaldehyde (PF) resin sphere precursor (Sumitomo Chemical Co., Ltd.). The PF spheres were sieved to select sizes (around 150 μm) and carbonized under 500°C for 1 h and purged with N_2 gas to remove volatile content in the materials and reform the carbon structure. After that, the carbonized sphere underwent physical activation in a fluidized bed reactor. The temperature of the reactor was increased from room temperature to 900°C with high-purity N_2 purging, and then the flow-gas was switched to CO_2 at 900°C for 4 h. During the activation process, the heating rate was set at 10°C min^{-1}, and the flow rate was controlled at 0.1 L min^{-1} by a rotameter. Moreover, the commercial BAC (termed KBAC, where K stands for Kureha CORP.) used for comparison in this study was heated in an oven at 373 K over 24 h to remove adsorbed water vapor. Afterwards, all products were stored in a desiccator until used.

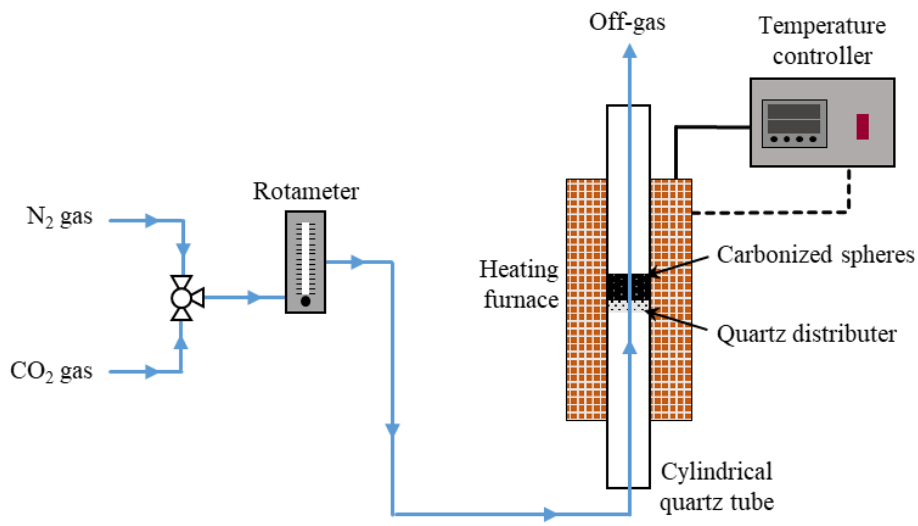

Figure 3-2 The fluidized bed reactor system

doi:10.6342/NTU202003443

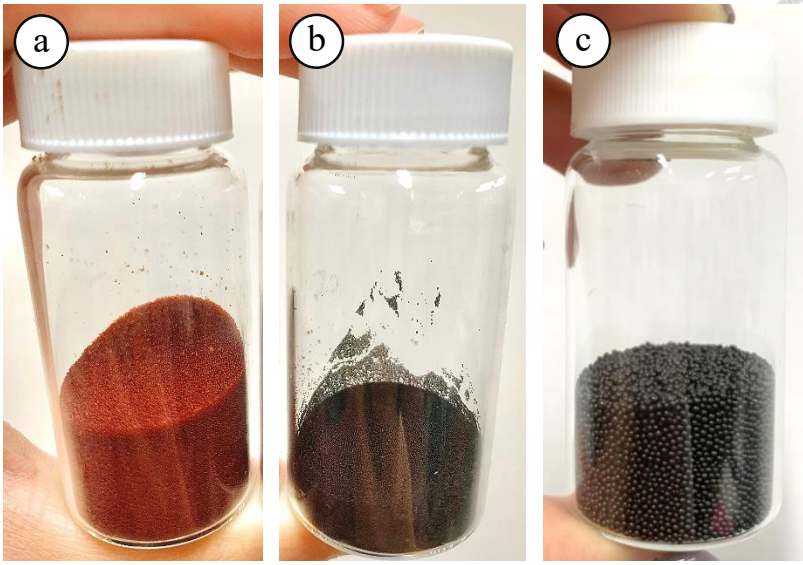

Figure 3-3 (a) PF resin spheres, (b) SBAC, and (c) KBAC in this study

3.2.2 Adsorbate

In Taiwan, according to the Taiwan Emission Data System (TEDS) version 10.0 (2016), the emission of THC was around 627,452 tons in 2016. The industrial plastic products manufacturing, the major VOC emission source in Taiwan, produced about 31500 tons/year, accounting for 5 % of total stationary emissions of VOC. The amount of VOC as a fugitive emission was around 100,027 tons in 2016, and the main source was volatile organic solvents used in the surface coating, which was around 51,000 tons/year (accounting for 8 % of total stationary emissions of VOC). MEK and TOL are the dominant emission of VOCs from the solvents (Chang & Chiou, 2006; Dinh et al., 2016; Zhong et al., 2017). Also, near the petrochemical industrial park, TOL and MEK are also the main species measured in the ambient air (Tsao, 2014).

Since both chemicals were the most abundant solvents commonly used in Taiwan's major industries and have different chemical structures and physical properties. The VOCs studied were MEK (Merck, ≥ 99.0%) and TOL (Honeywell Riedel-de Haën, ≥

doi:10.6342/NTU202003443

99.7%). TOL is aromatic and has a higher boiling point than MEK, while MEK is a ketone with an oxygen group, and has higher polarity compared to TOL. The main properties of MEK and TOL are given in Table 3-1.

Table 3-1 Properties of MEK and TOL

Property	Methyl ethyl ketone (MEK)	Toluene (TOL)
Chemical structure [b]	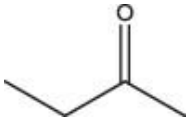	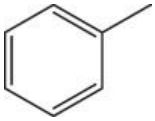
Molecular form	Ketone	Aromatic
Molecular formula	C_4H_8O	C_7H_8
Molar mass (g mol^{-1}) [b]	72.11	92.14
Density at 25 °C (g cm^{-3}) [b]	0.799	0.865
Boiling point at 1 atm (°C) [a]	79.6	110.6
Vapor pressure at 25 °C (kPa) [a]	12.0	3.79
Heat of vaporization at the boiling point (kJ/mol) [a]	31.21	32.80
Kinetic diameter (Å) [b]	5.2	5.8
Dipolar moment (D) [a]	2.78	0.375

[a] (Poling et al., 2001), [b] (Jahandar Lashaki et al., 2012),

3.3 Material Characterization

3.3.1 Surface Area, Pore Volume, and Pore Size Distribution (PSD)

A Micromeritics ASAP 2420 instrument was used to determine the specific surface area (S_{total}), micropore surface area (S_{micro}), total pore volume (V_{total}), micropore volume (V_{micro}), and PSD of the adsorbents. Before starting the analysis, the samples were degassed at 350 °C for more than 15 h to remove impurities and moisture on the surface of samples. Then, the adsorption measurements were carried out by N_2 at 77 K. S_{total} was

doi:10.6342/NTU202003443

calculated using the BET equation. S_{micro} and V_{micro} were obtained from the t-plot analysis by applying the Harkins and Jura thickness curve, $t = [13.99/(0.034 - \log(P/P_0))]^{0.5}$. The range of relative pressures used to determine S_{micro} and V_{micro} based on a statistical thickness t-value of 0.45 - 0.80 nm. V_{total} was determined by the Barrett-Joyner-Halenda (BJH) method and recorded at $P/P_0 = 0.994$. The PSD of the mesopore and macropore range was also evaluated by the BJH method. Nonlocal density functional theory (NLDFT) was used to assess the PSD of the micropore size range.

3.3.2 Elemental Analysis (EA)

The Elementar Vario EL cube instrument was applied to analyze the nitrogen (N), carbon (C), sulfur (S), hydrogen (H), and oxygen (O) content of samples. For the NCSH content determinations, the tested samples were burned in a pure oxygen environment at 1200°C, and all elements were converted into a gas mixture containing nitrogen oxides (NO_x), carbon dioxide (CO_2), sulfur oxide (SO_2), and water vapor (H_2O). NO_x immediately reduced into N_2. Besides N_2, other gases (CO_2, SO_2, and H_2O) were separated by specific absorber columns. The thermal conductivity detector (TCD) at the effluent detected the concentration of each gas to obtain the elemental content ratio of the sample. For the O content determination, the sample was mixed with a high carbon-content compound combusted without oxygen at 1100°C. The oxygen content calculated by the amount of CO_2 and CO produced.

3.3.3 Electron Microscopy

The surface characteristics of the materials were analyzed using scanning electron microscopy (SEM). The Hitachi S-4800 Field-Emission SEM used an accelerating

doi:10.6342/NTU202003443

voltage of 10 kV in this study. It yielded high-resolution images of the samples by scanning the surface with a focused beam of electrons. Hence, it is useful for observing the surface structure of the sample. The materials were also examined by a transmission electron microscope (TEM), which is uses high-energy electron beams to penetrate samples with an ultrathin section. The samples were ground to a fine powder and added into 95% alcohol and shaken for 30 min. The solution was dropped on a copper gridded specimen holder, and left to dry. Afterwards, the image was magnified and focused on a screen.

3.3.4 Thermogravimetric Analysis (TGA)

TGA is an experimental method for assessing a system (element, compound, or mixture) by measuring the weight loss as a function of temperature (Coats & Redfern, 1963). In this study, the pyrolysis tests were performed in a thermogravimetric analyzer (SHIMADZU, model TGA-51). The sample was put into a platinum crucible. The experiments were carried out at atmospheric pressure and purged with 50 ml/min N_2 to desorb the species at a heating rate of 5, 10, and 20°C/min. The weight loss of the sample and the temperature were recorded continuously between the range of 25 to 600°C.

3.4 Adsorption Test

The diagram of the experimental setup of the adsorption testing system is depicted in Figure 3-4. This system comprised of a VOC generating system, a temperature-controlled adsorption bed, and a total hydrocarbon (THC) detecting system.

doi:10.6342/NTU202003443

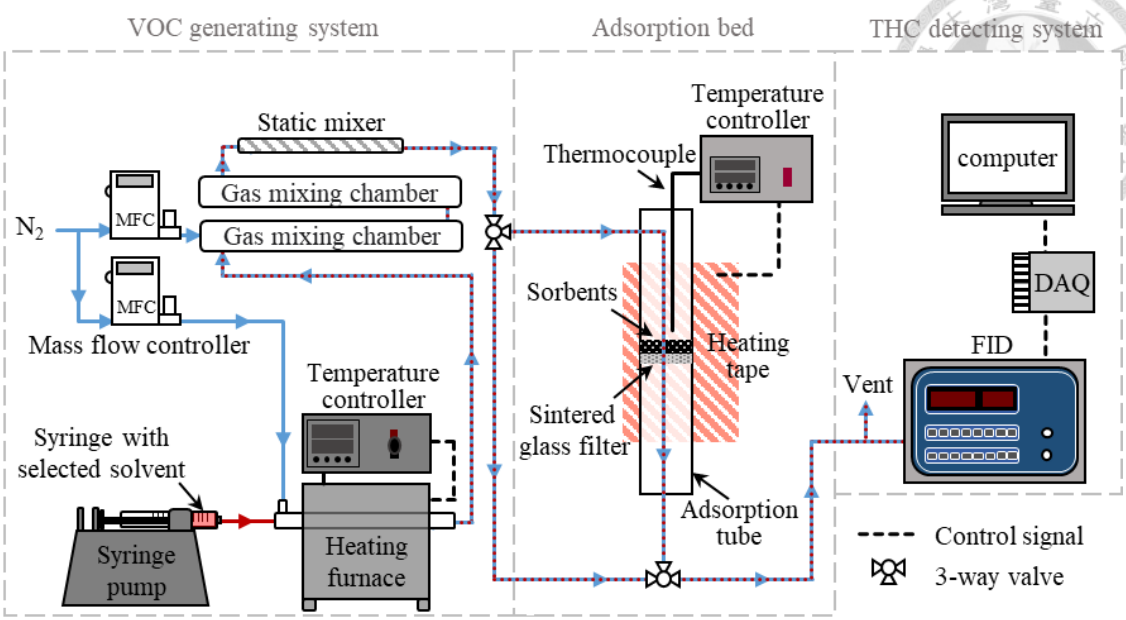

Figure 3-4 Process flowchart of the adsorption testing system

3.4.1 VOC Generating System

In this study, the dynamic gas mixture generation method was chosen for preparing VOC gases, which has the capability of continuously generating a vapor mixture (Nelson, 1992). The mechanically driven injection methods was used to produce a reasonably accurate concentration of vapors, but short-term fluctuations may occur when using pulsed systems (Barratt, 1981).

In this VOC generation system, the selected solvent (TOL or MEK) was supplied at a constant rate with a syringe (Hamilton Company) and a syringe pump (New Era Pump Systems Inc., model NE 1000). The solvent was injected into a small flow of nitrogen and vaporized in a heating furnace (designed by Fortelice International Co., Ltd.). The set temperature of the heating furnace was above the boiling point of the selected solvent to provide adequate heat for immediate vaporization. The solvent injection rate was adjusted according to the desired VOC concentration, and was calculated from the ideal gas law

doi:10.6342/NTU202003443

(Nelson, 1992):

$$C_{ppm_v} = \frac{22.4 \times 10^6 \left(\frac{T}{273}\right)\left(\frac{760}{P}\right) Q_L \rho_L}{Q_G M} \quad (3\text{-}1)$$

Mass flow controllers (Brooks, mode 5850) were used to control the flow rates of the purge gas streams, and the flow rates were calibrated with a gas flowmeter (MesaLabs, model Defender 510). The nitrogen gas stream was directed into the furnace and mixed with the vaporized organic solvent. Furthermore, taking into account that the concentrations of the organic vapor produced may be unstable, two glass bottles in series (nominal volume was 1.4 L) and a static mixer were used to smooth out potential fluctuations. Variations of the concentration were kept within ±5% and checked before each run.

3.4.2 Adsorption Bed Operation

A fixed-bed configuration was used in this study, and a VOC laden air stream was introduced from the top to flow through the adsorption bed. The adsorption tube, made from Pyrex glass, was about 40 cm in length and 1 cm in diameter, and BAC was inserted and supported by a sintered glass filter. The bed was heated by wrapping heating tape (Omega) around the tube. The temperature was measured and controlled by a proportional integral derivative (PID) controller, and a type K thermocouple was inserted from the top and left at the center of the bed. The adsorption of VOCs on the surface of the tube and glass filter was assumed negligible during the test.

Two types of experiments were conducted: (1) adsorption isotherm tests and (2) a dynamic analysis of the fixed bed adsorption. The total gas flow rate was set at 1.6 SLPM to ensure the sufficient uptake of the FID sampling line in both experiments. About 20 to

doi:10.6342/NTU202003443

50 mg of BAC was measured and placed in the adsorption bed. For the adsorption isotherm tests, the concentration of VOCs ranged from 0.0007 to 0.16 P/P_0 and 0.002 to 0.21 P/P_0 for MEK and TOL, respectively. Table 3-2 offers the saturation vapor pressure (P_0) of MEK and TOL at different temperatures (Poling et al., 2001). The operating temperature was set at 30, 40, or 50°C. The saturated adsorption capacity was calculated using the gravimetric and integration method. For the dynamic analysis of the adsorption bed, the operating temperature and the inlet MEK or TOL concentrations were controlled at 40°C and 500 ppm_v. Smooth breakthrough curves were generated, and data were stored for subsequent analysis. The adsorption runs were repeated three times for all experimental concentrations.

Table 3-2 Saturation vapor pressure data for MEK and TOL

Temperature (°C)	Saturated vapor pressure (kpa)	
	MEK	TOL
30	15.10	4.85
40	23.49	7.84
50	35.36	12.22

3.4.3 THC Detection System

The main composition of the THC detecting system was a THC analyzer (Ratfisch Analysensysteme, model RS53-T), which was a flame ionization detector (FID) fueled by a hydrogen cylinder. The outlet VOC concentrations of the adsorption bed were measured continuously by the FID with 1.5 SLPM of the sampling flow rate. For the inlet VOC concentration, five measuring ranges (from 0-10 ppm_v to 0-100,000 ppm_v as methane) were chosen for better accuracy. The two-point calibration was carried out

doi:10.6342/NTU202003443

periodically with pure nitrogen for the zero and methane for the span. The magnitude of the FID measurement signal was approximately proportional to the number of carbon atoms of the sample gas. The actual carbon concentration from the measured FID value was as in the following equation:

$$C_{c,x} = A_c / f_{RC,x} \tag{3-2}$$

where $C_{c,x}$ (mgC m^{-3}) is the actual carbon concentration of gas x, A_c (mgC m^{-3}) is FID reading value, and $f_{RC,x}$ is the carbon related response factor of the gas (0.80 and 0.95 for MEK and TOL, respectively).

The data of outlet VOC concentrations were recorded at 1-second intervals through a data acquisition unit (DAQ), which was consisted of a data logger (National Instruments, model USB 6000) and a LabView software (National Instruments, the program developed by Institute for Information Industry). This equipment transformed an analog output of a voltage signal from the FID into a digital output, so the online measurement can be visualized.

3.5 Adsorption Capacity

Two methods for obtaining adsorption capacities were used. In the gravimetric methods, the adsorption capacity is obtained from the weight change of the adsorbents during the adsorption test. The adsorption capacities were calculated as follows:

$$\text{Adsorption capacity} = \frac{W_{BA} - W_{AA}}{W_{AA}} \tag{3-3}$$

where W_{BA} and W_{AA} is the weight of the adsorbent before and after the adsorption test, respectively.

On the other hand, the adsorption capacities were also calculated from the adsorption

doi:10.6342/NTU202003443

breakthrough curve, determined by integrating the areas above the breakthrough curves. In the integration method, the dynamic breakthrough adsorption capacity of BAC was calculated by the following equation:

$$\text{Adsorption capacity} = \frac{1}{W_{AA}} \sum_{t=0}^{t_{100}} Q_G\,(C_{in} - C_{out})\rho_G \Delta t \tag{3-4}$$

where Q_G is the total gas flow rate, C_{in} and C_{out} are the inlet and outlet concentration during a time step Δt (set at one second in this experiment), ρ_G is the density of the organic vapor, and t_{100} is the time needed to reach 100% breakthrough.

3.6 Microwave Regeneration

Regeneration was attained by microwave heating. Figure 3-6 shows the experimental setup of the microwave regeneration system in this study. Prior to microwave application, all adsorbents were saturated with MEK or TOL under an inlet concentration of 500 ppm_v at 40°C. In the regeneration tests, the spent BAC was heated in a microwave muffle furnace (Milestone, model Pyro 260), which was operated at 2.45 GHz with an adjustable output power. The setting power level ranged from 400 W to 1000 W, and the heating time was between 4 to 12 min in this research. The spent BAC was put into a quartz boat (Figure 3-7(b)), and the boat was put into a 1.5 L quartz reactor (Figure 3-7(a)) inside the microwave furnace. Before each run of the experiment, nitrogen gas purged for more than 5 min to create an oxygen-free atmosphere in the reactor. Then, the heating began. The temperature profile of the adsorbent bed was obtained using a K-type thermocouple with a ceramic sheath, which was inserted into the carbon bed during microwave heating. Nitrogen gas flowed through a rotameter and entered the reactor at the flow rate of 1.5 L min^{-1}, and the desorbed adsorbates were immediately removed from the reactor and

doi:10.6342/NTU202003443

detected for concentration by the FID.

In addition, a portable gas analyzer (HORIBA, model PG-350) was used for measuring NO, SO_2, CO, and CO_2 in the exhaust gas. This analyzer uses two measurement principles, chemiluminescence for NO, and non-dispersive infrared (NDIR) for the measurement CO, CO_2, SO_2. About 20 mg of saturated BACs placed in the microwave furnace. The measurement range is setting at 0 ppm to 200 ppm for SO_2 and CO, 0 ppm to 25 ppm to NO_x, and 0 vol% to 10 vol% for CO_2. The data of outlet gas concentrations were recorded at 1-second intervals.

The desorption efficiency is defined as:

$$\text{Desorption efficiency (\%)} = \frac{W_{BR} - W_{AR}}{W_{BR} \times q_{500ppm}} \times 100\% \qquad (3\text{-}5)$$

where W_{BR} and W_{AR} is the weight of the adsorbent before and after regeneration, respectively, and q_{500ppm} is the adsorption capacity at 40°C and 500 ppm_v.

The adsorption capacities were also calculated from the desorption curve, which were determined by integrating the areas under the curve:

$$\text{Desorption efficiency (\%)} = \frac{1}{W_{BR}} \sum_{t=0}^{t_0} Q\, C \rho_G \Delta t \times 100\% \qquad (3\text{-}6)$$

where Q is the purged gas flow rate, C is the detected concentration, ρ_G is the density of the organic vapor, and t_0 is the time needed for the detected concentration to reach zero.

It should be noted that according to the user manual, the actual applied power was generally not entirely equal to the set power level. Hence, the actual output power of the furnace had to be calibrated. We used one liter of water in a beaker, measured the temperature changes before and after the microwave application, and obtained the actual

doi:10.6342/NTU202003443

applied power in a build-up program of the furnace controller. The calibration curve and correlation between the set power level ($W_{setting}$) and the actual power level (W_{actual}) are shown in Equation 3-7 and Figure 3-6.

$$W_{actual} = 0.8387 \times W_{setting} + 22.4 \quad (3\text{-}7)$$

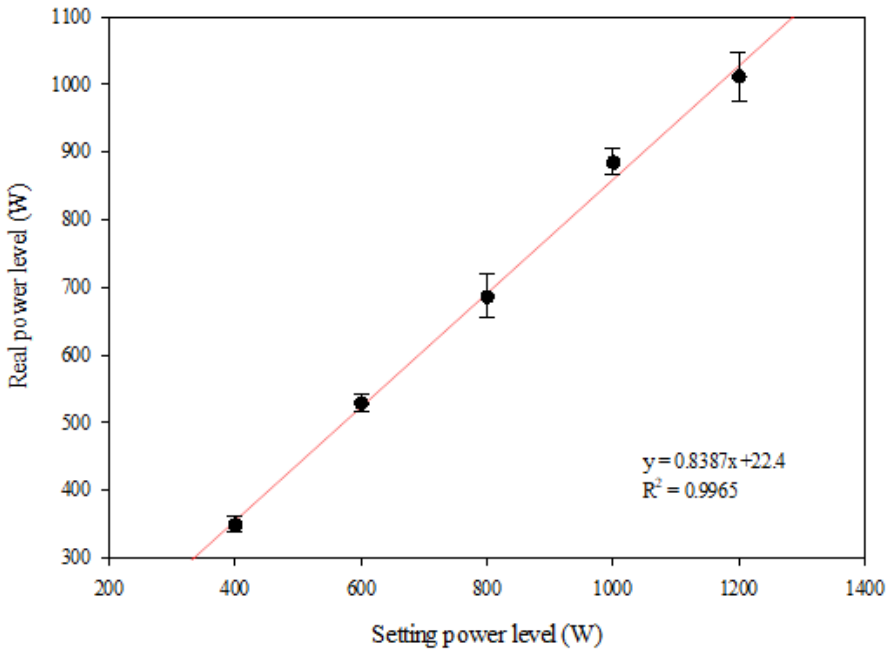

Figure 3-5 Calibration curve of microwave muffle furnace

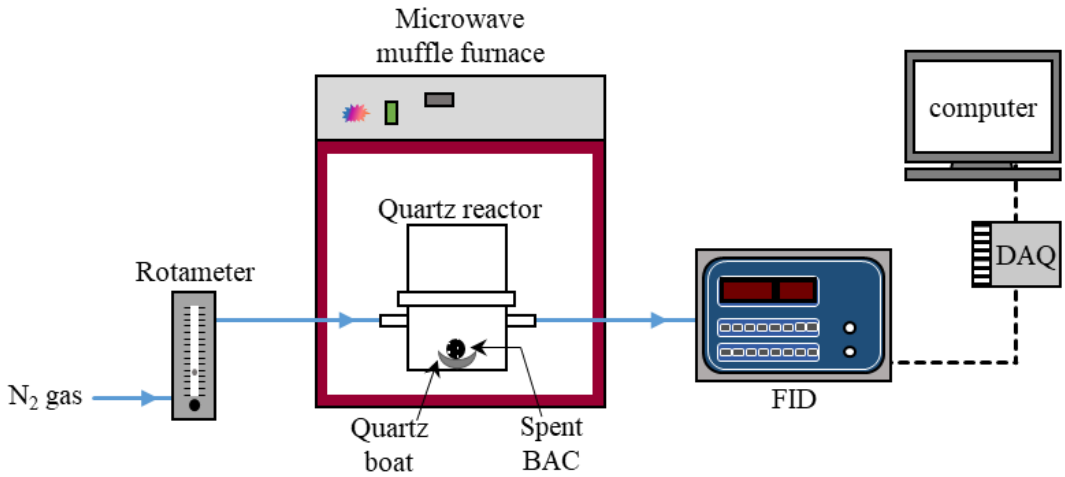

Figure 3-6 The scheme diagram of the microwave regeneration system

doi:10.6342/NTU202003443

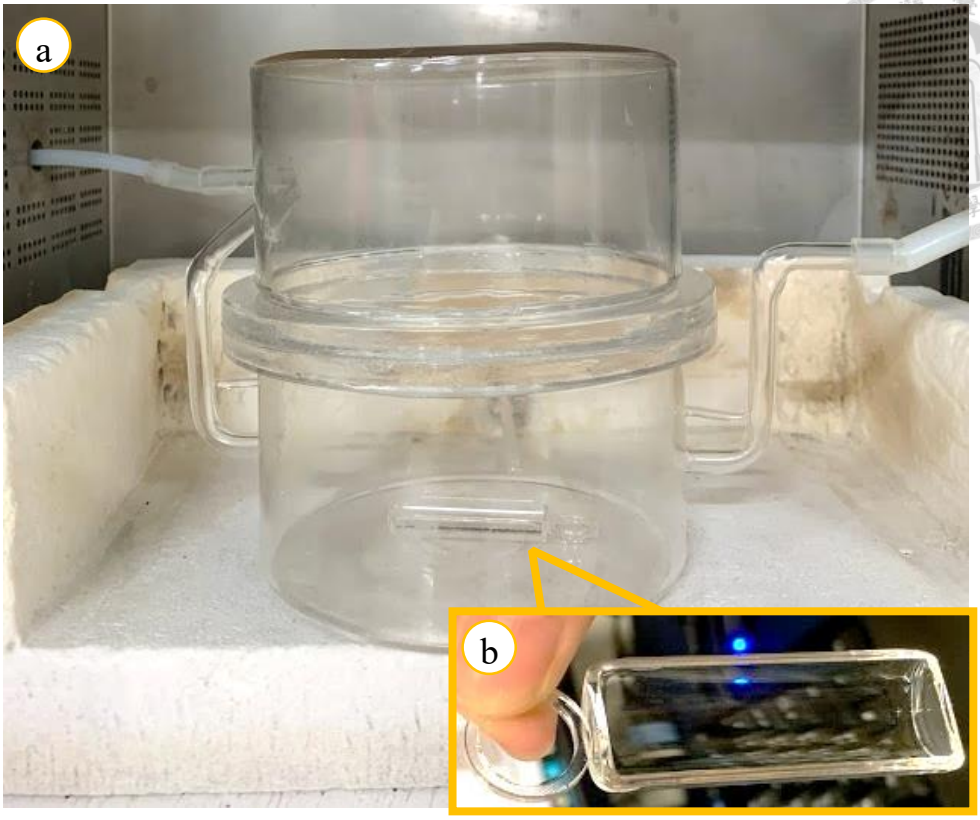

Figure 3-7 (a) the quartz reactor and (b) the quartz boat

3.7 Adsorption/Desorption Kinetic Analysis

It is necessary to understand adsorption equilibrium and kinetics to design an adsorption bed properly. The equilibrium data are easily collected from experiments, while the kinetics data are more difficult to obtain. In this study, we used the diffusion-controlled kinetic models because external diffusion and intraparticle diffusion were considered to be the rate-controlling steps of an adsorption process.

The three consecutive steps of a species physisorbed onto a porous adsorbent are (i) transport of the adsorbate from gas film to the external surface of the solid adsorbent (external diffusion), (ii) transport of the adsorbate within the pores of the adsorbent (intraparticle diffusion), and (iii) adsorption of the adsorbate on the exterior surface of the

doi:10.6342/NTU202003443

adsorbent (surface diffusion). Generally, it is accepted that surface diffusion is very rapid (Singh et al., 2002). The intraparticle diffusion rate is often considered to be the rate-controlling step in an adsorption process (Fournel et al., 2010). In desorption, the process is opposite that of adsorption.

(1) Pseudo-first-order (PFO) model

If external diffusion was the rate-controlling step, the rate of adsorption can be described by PFO model (Zhou et al., 2015):

$$\frac{dq}{dt} = k_1(q_e - q) \tag{3-8}$$

Integral solution of Equation 3-8 is:

$$\ln\left(1 - \frac{q_t}{q_e}\right) = -k_1 t \tag{3-9}$$

where q_e and q_t is the amount of adsorbate uptake to the sorbent at equilibrium and time t, respectively, and k_1 is the PFO adsorption rate constant.

(2) Intraparticle diffusion model (IPD)

If intraparticle diffusion was the rate-controlling step, the IPD model proposed by Weber and Morris is widely used for the analysis of adsorption kinetics (Wu et al., 2009). The IPD model could be described as:

$$q_t = k_p t^{1/2} + I \tag{3-10}$$

where q_t is the amount of adsorption at time t, k_p is the IPD rate constant, and I is the intercept reflecting the extent of the boundary layer thickness.

doi:10.6342/NTU202003443

3.8 Cyclic Adsorption Test

Preliminary tests showed a significant deviation of the adsorption capacities calculated from integration and gravimetric methods. To ensure the accuracy and consistency of the data, in the cyclic test, the adsorption capacity after each cycle was calculated by the gravimetric method.

The regeneration performance was evaluated by regeneration efficiency, which was calculated by Equation 3-11:

$$\text{Regeneration efficiency in cycle } i\,(\%) = \frac{\text{adsorption capacity of regenerated BAC in cycle } i}{\text{adsorption capacity of BAC}} \times 100\% \tag{3-11}$$

where i was the number of the adsorption–regeneration cycles.

doi:10.6342/NTU202003443

Chapter 4 Results and Discussion

In this chapter, code names were used to describe the activated carbon. For instance, MEK-SBAC represents that SBAC (the self-prepared BAC, "S" stands for self-prepared) saturated under 40°C with 500 ppm_v of MEK. TOL-KBAC represents the KBAC (the commercial BAC, "K" stands for Kureha CORP.) saturated under 40°C with 500 ppm_v of TOL. MEK-SBAC-800W4min represents that the MEK-SBAC regenerated at a power level of 800 W, with an irradiation time of 4 min.

4.1 Physical and Chemical Properties of BAC

4.1.1 Elemental Analysis

Table 4-1 shows the concentration of major elements in the BAC samples, including virgin and post-regeneration samples under 800 W for 8 min. In the results of EA, KBAC has a relatively higher proportion of sulfur, but sulfur is not considered as an important factor of VOC adsorption. The percentages of hydrogen and oxygen of both virgin BAC are similar, which may imply that the surface polarities are similar.

Table 4-1 Elemental analysis of the BAC samples

	Elemental analysis (wt%)				
	N	**C**	**S**	**H**	**O**
Virgin samples					
KBAC	0.12±0.17	87.61±0.16	0.77±0.34	2.95±1.57	10.86±0.04
SBAC	1.08±0.31	82.68±14.6	0.09±0.10	2.86±0.87	11.52±8.52
Regenerated samples					
MEK-KBAC-800W8min	0.22±0.01	80.81±0.23	0.13±0.03	4.39±0.11	13.68±0.11
MEK-SBAC-800W8min	1.11±0.08	85.51±0.12	0.37±0.07	4.25±0.13	14.05±3.08
TOL-KBAC-800W8min	0.20±0.02	84.37±0.68	0.13±0.00	4.24±0.30	7.11±0.21
TOL-SBAC-800W8min	0.95±0.04	85.42±2.90	0.00±0.00	2.63±0.48	4.47±0.03

doi:10.6342/NTU202003443

4.1.2 Pore Structures

The N_2 adsorption-desorption isotherms of BAC samples are shown in Figure 4-1. It is worth noting that both KBAC and SBAC presented as Type I isotherm shapes, which is typically indicative of microporous character. The isotherm of SBAC is tended more towards Type I(b), while that of KBAC presented more as Type I(a), revealing that SBAC had wider PSD including wider micropores and narrow mesopores.

The PSDs of BAC samples were examined based on the BJH model (in Figure 4 2), which is suitable for meso and macropore analysis. It can be observed that the width developed pores was mainly below 10 nm. The NLDFT method is applied to examined microporous PSD (in Figure 4-3), which confirms the results obtained from the N_2 adsorption-desorption isotherms, showing the existence of a wider PSD for SBAC, which included wider micropores and narrow mesopores.

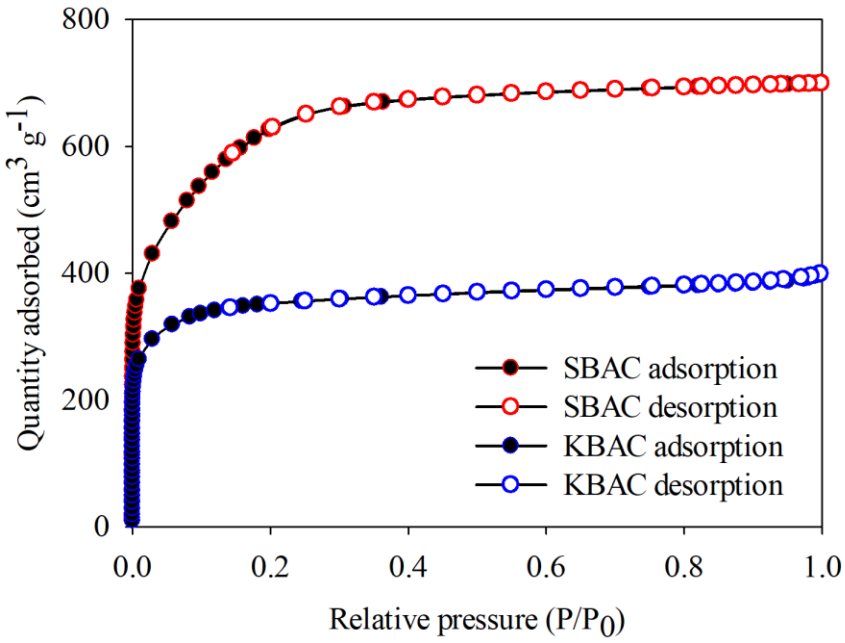

Figure 4-1 Standard N_2 adsorption-desorption isotherm of SBAC and KBAC

doi:10.6342/NTU202003443

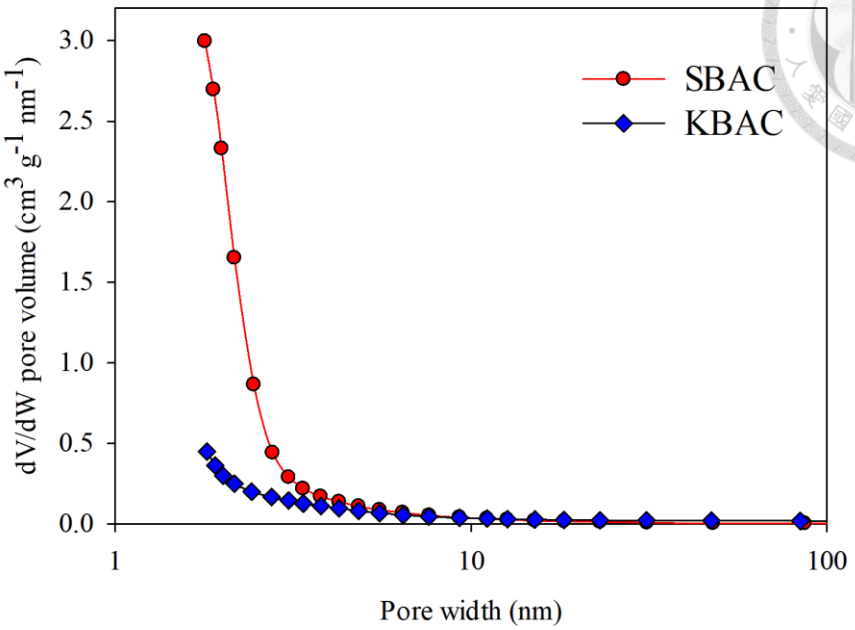

Figure 4-2 Mesoporous and macroporous pore size distribution (PSD) of SBAC and KBAC

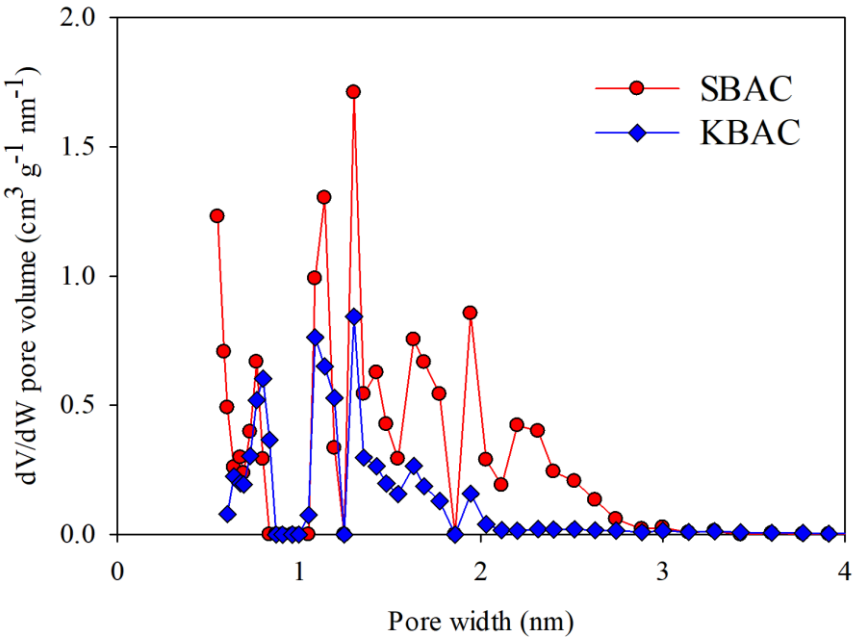

Figure 4-3 Microporous pore size distribution (PSD) of SBAC and KBAC

doi:10.6342/NTU202003443

The physical properties of the BAC samples and 8-cycle regenerated samples are given in Table 4-2 and 4-3, compiling the total BET surface area (S_{total}), micropore surface area (S_{micro}), total micropore volume (V_{total}), micropore volume (V_{micro}), and average pore width (d_{avg}). The porous properties of the commercial KBAC are in accordance with those published previously (Zhu et al., 2004), in which S_{total} was 1300 m^2 g^{-1} and V_{micro} is 0.56 cm^3 g^{-1}. Overall, both BAC samples have excellent development of micropores.

Table 4-2 The physical properties of samples

Sample	SBAC	KBAC
S_{total} (m^2 g^{-1})	2114.29 ± 236.41	1210.41 ± 58.56
S_{micro} (m^2 g^{-1})	2084.97 ± 195.54	1136.03 ± 20.32
S_{micro}/S_{total} (%)	98.61	93.85
V_{total} (cm^3 g^{-1})	1.361 ± 0.66	0.602 ± 0.18
V_{micro} (cm^3 g^{-1})	0.958 ± 0.14	0.534 ± 0.05
V_{micro}/V_{total} (%)	70.39	88.70
d_{avg} (nm)	2.65 ± 0.42	3.66 ± 0.33

Table 4-3 The physical properties of samples after 8-cycle and 800W-8min microwave regenerations

Sample	MEK-KBAC	MEK-SBAC	TOL-KBAC	TOL-SBAC
S_{total} (m^2 g^{-1})	1104.23	1737.98	1115.17	1280.06
S_{micro} (m^2 g^{-1})	1083.89	1708.90	1079.02	1212.13
S_{micro}/S_{total} (%)	98.16	98.33	96.76	94.69
V_{total} (cm^3 g^{-1})	0.535	0.785	0.529	0.598
V_{micro} (cm^3 g^{-1})	0.508	0.771	0.483	0.534
V_{micro}/V_{total} (%)	94.95	98.22	91.30	89.30
d_{avg} (nm)	2.82	2.66	3.11	2.52

doi:10.6342/NTU202003443

4.1.3 Morphology of BAC

Figures 4-4 and 4-5 depict the SEM images of SBAC and KBAC. As we can see from these figures, both samples are spherical with a smooth surface. The size of KBAC is much bigger than that of SBAC, and its surface does not show significant pores. It is noteworthy that the images of SBAC showed a highly developed inner structure, contributing to a higher surface area for SBAC than KBAC. Furthermore, the TEM images of crushed SBAC (see Figure 4-6) revealed a more detailed understanding of its structure, showing that the amount of 3-D pores were randomly combined and constructed amorphous nano-structures.

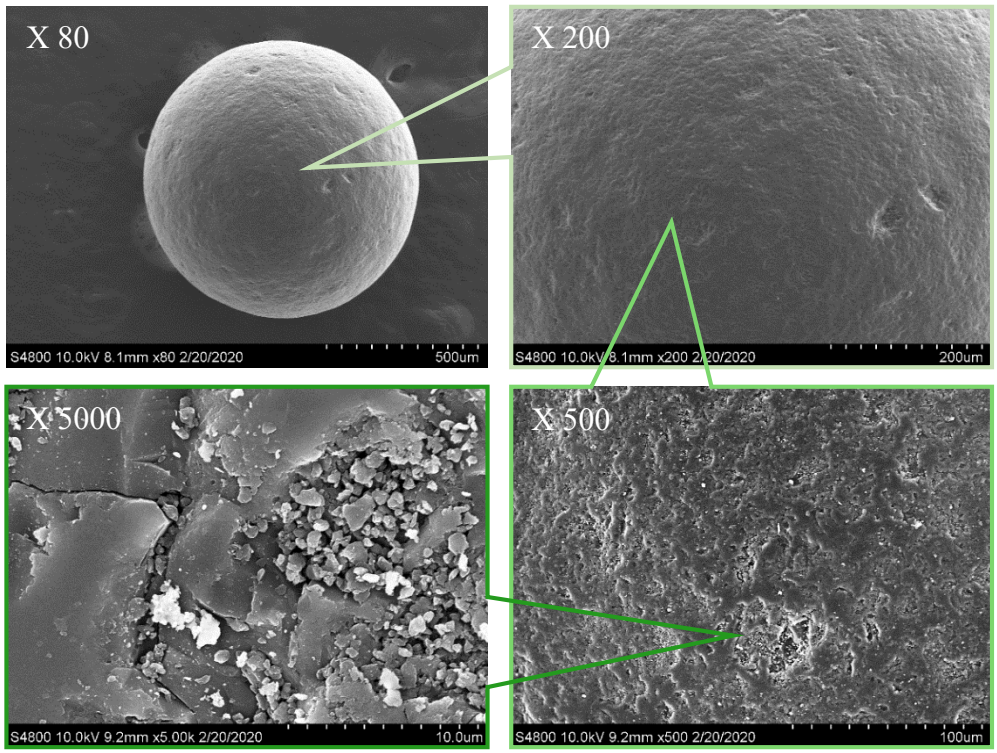

Figure 4-4 SEM images of KBAC

doi:10.6342/NTU202003443

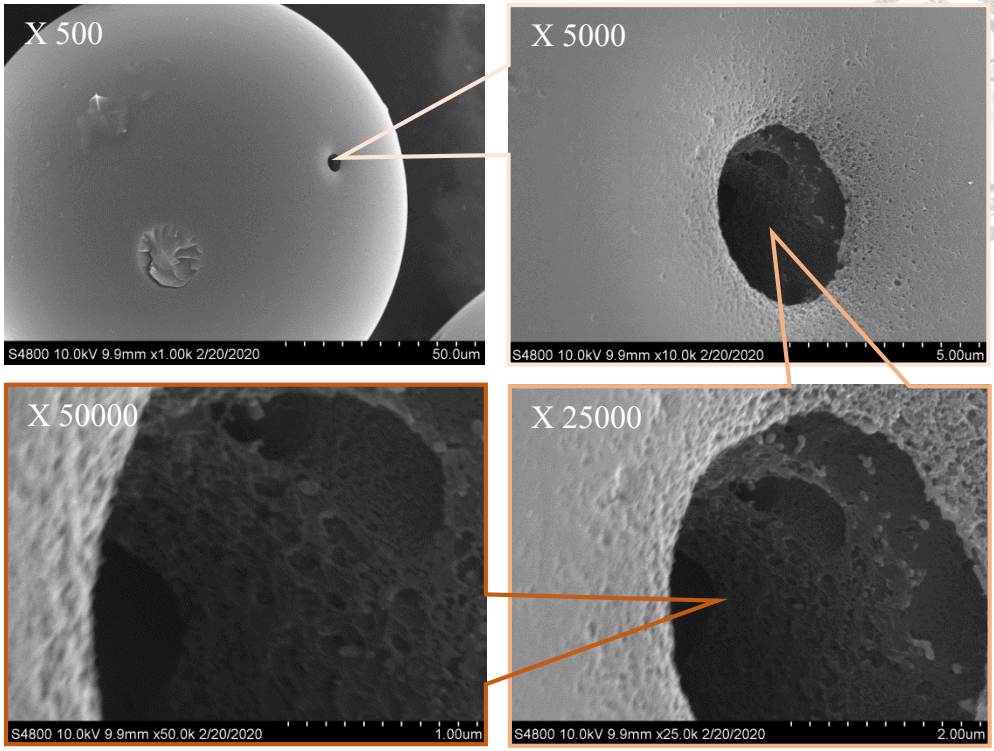

Figure 4-5 SEM images of SBAC

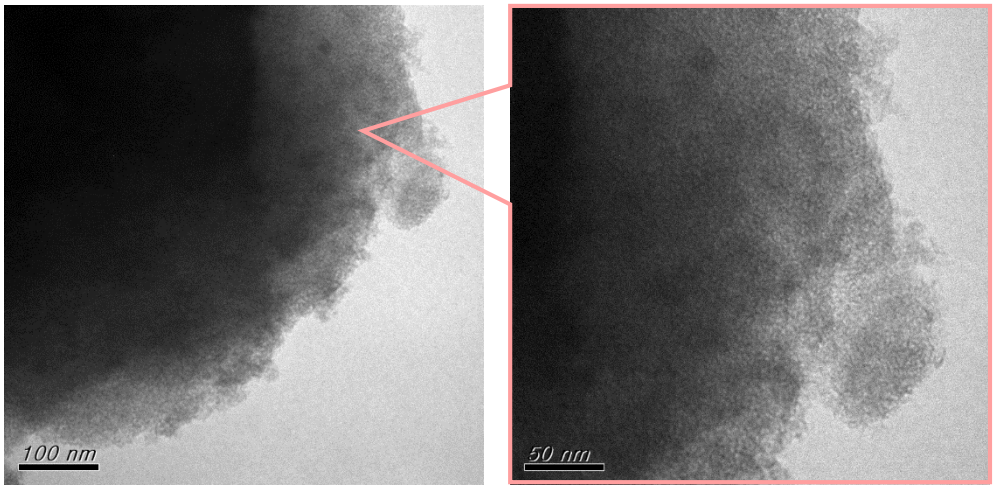

Figure 4-6 TEM images of SBAC

Moreover, the morphologies of BACs were used to evaluate the effects of microwave regeneration. MEK-KBAC, TOL-KBAC, MEK-SBAC, and TOL-SBAC regenerated at 800 W for 8 min were chosen as the SEM samples. As observed in Figures 4-7 and 4-8, there were no significant differences between virgin and post-regeneration KBAC.

doi:10.6342/NTU202003443

However, SEM images of the regenerated MEK-SBAC (Figures 4-9 and 4-10) show changes in pore structure. Due to the polarity of MEK and contact with microwaves, the original structure of the adsorbent changes, as a result of severe heating.

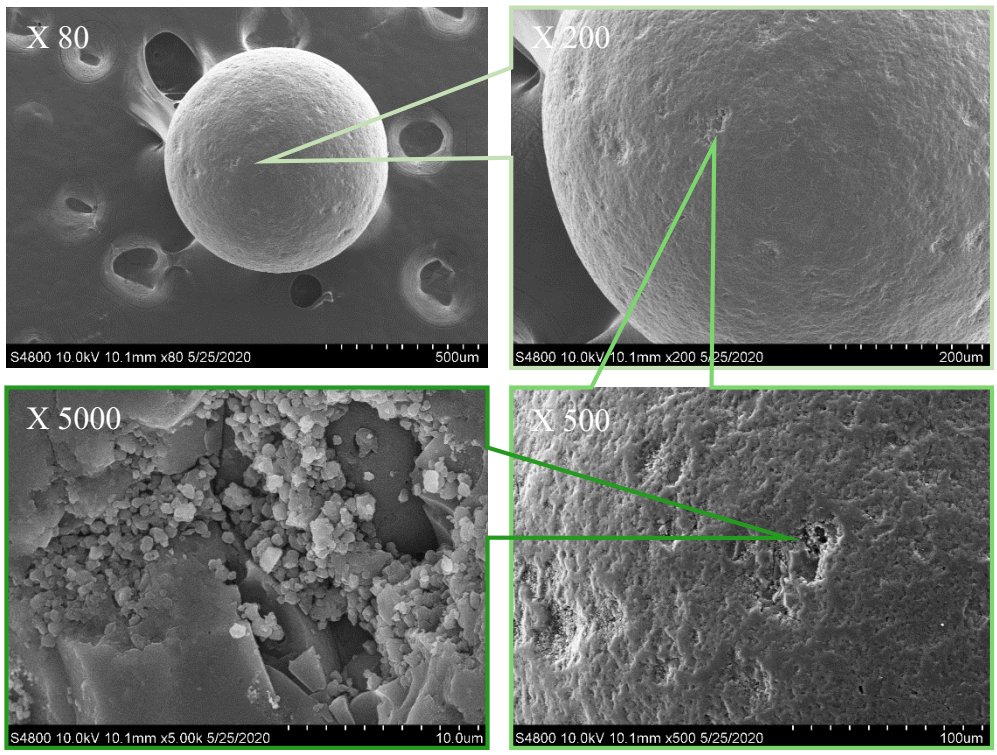

Figure 4-7 SEM images of TOL-KBAC-800W8min

doi:10.6342/NTU202003443

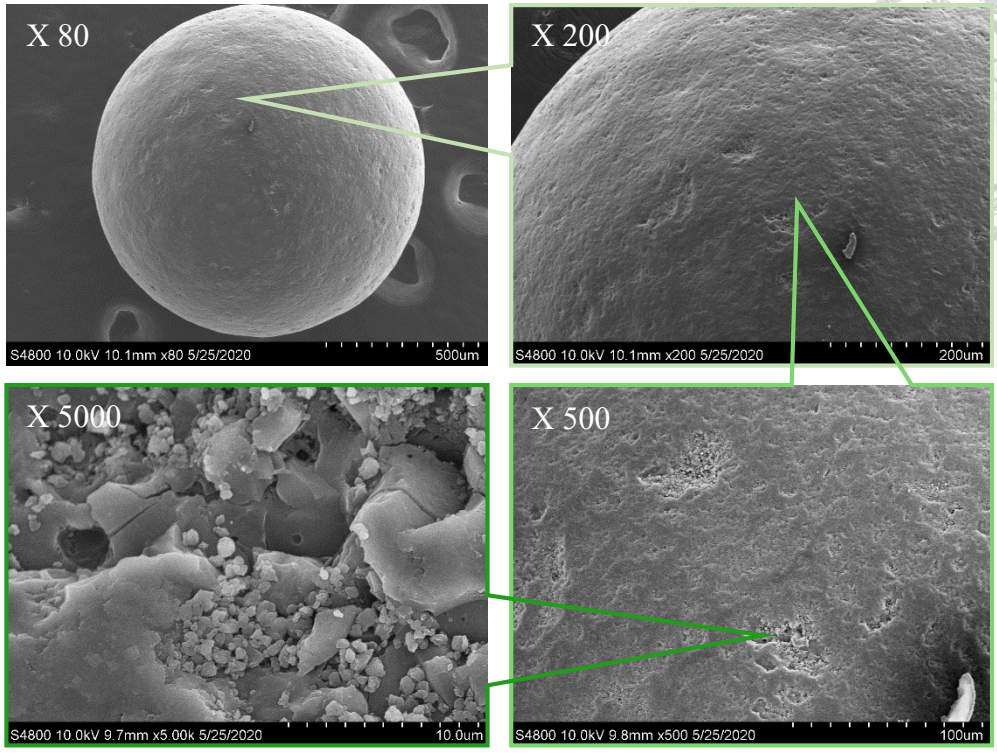

Figure 4-8 SEM images of MEK-KBAC-800W8min

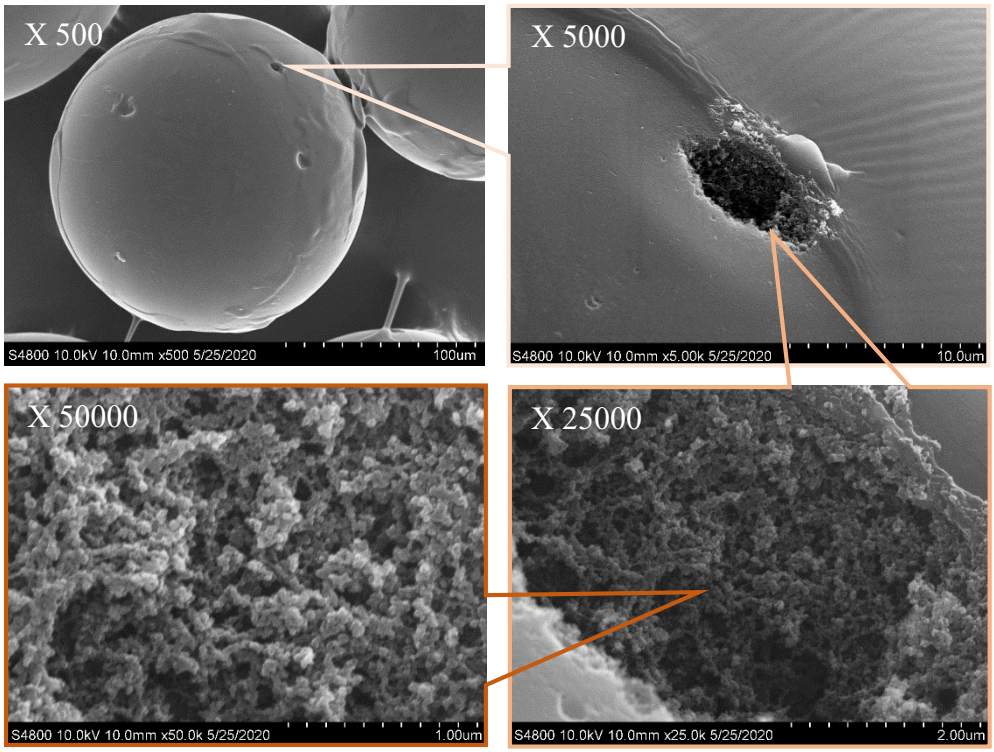

Figure 4-9 SEM images of MEK-SBAC-800W8min

doi:10.6342/NTU202003443

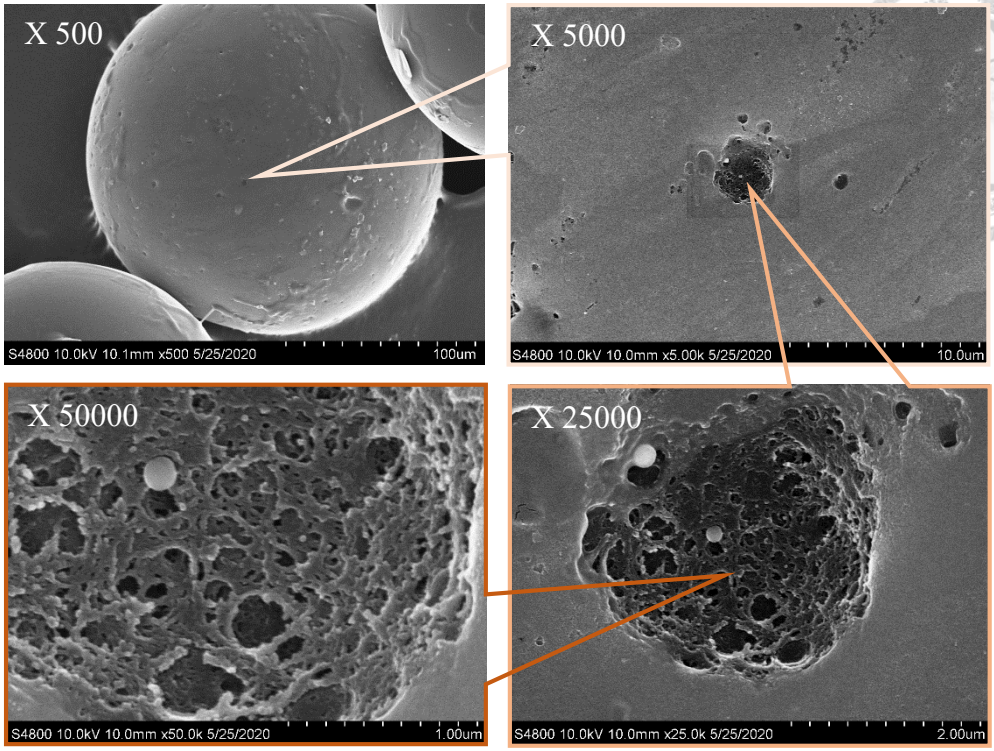

Figure 4-10 SEM images of TOL-SBAC-800W8min

4.2 Adsorption Test

4.2.1 Adsorption Isotherm Experiments

Adsorption isotherm describes the relationship between the adsorbate concentration and adsorption capacity. The data for VOC adsorption was analyzed by three isotherms, namely Langmuir, Freundlich, and Dubinin-Radushkevich (D-R) isotherms. The inlet concentrations of the VOCs were set to range from 100 to 20,000 ppm_v for MEK and 100 to 10,000 ppm_v for TOL, or in other words, from a low to high concentration in the FID detection range. The adsorption capacities were obtained from both integration and gravimetric methods. The parameters of isotherms were determined from fitting the equations using the computer program SigmaPlot version 12.5.

doi:10.6342/NTU202003443

4.2.1.1 Langmuir Isotherm

The Langmuir isotherm is a simple theoretical model for monolayer adsorption and has been widely used to describe the activated carbon adsorption of VOCs. Table 4-4 presents the parameters of the Langmuir isotherm fitting for MEK/TOL adsorption onto SBAC and KBAC. Based on the value of determination coefficient (R^2), the Langmuir isotherm showed a good fit with the experimental data. The plots of the experimental and Langmuir isotherm modeled data are presented in Figures 4-11 to 4-14.

Graphically, the Langmuir isotherm is characterized by a plateau corresponding to a saturated adsorbed amount (q_s). As shown in Figures 4-11 to 4-14 and Table 4-4, the q_s calculated by the integration method seems much higher in comparison to that calculated by the gravimetric method. According to our test data, the adsorption capacities calculated from both methods were similar at a lower concentration range, whereas the capacities showed a significant deviation as the concentration increased. The distinction may be explained by the response time of the THC detector. In the high concentration range (i.e. short breakthrough time), the response time amplified the deviation of the breakthrough curve. As a result, the q_s estimated from the adsorption isotherm calculated by the gravimetric method should be more accurate. According to the result calculated by the gravimetric method, it was observed that adsorption capacities of SBAC are consistently higher than those of KBAC. This can be related to the fact that SBAC has a much higher surface area and larger pore volume (Table 4-2), and therefore has a higher adsorption capacity.

doi:10.6342/NTU202003443

Table 4-4 Langmuir parameters for different adsorbate-adsorbent systems at different temperatures

Langmuir parameter					
Integration method					
Adsorbate	**Adsorbent**	**T (°C)**	**R^2**	**q_s (mg g^{-1})**	**K_L**
MEK	SBAC	30	0.9571	1956.8	40.2
		40	0.9559	1701.5	60.3
		50	0.9904	2382.2	29.9
	KBAC	30	0.9321	547.6	230.6
		40	0.8572	538.9	419.2
		50	0.9730	568.3	238.8
TOL	SBAC	30	0.8669	1686.0	64.6
		40	0.8551	1222.0	168.6
		50	0.9405	1433.7	105.4
	KBAC	30	0.9902	593.1	176.3
		40	0.9838	557.1	218.9
		50	0.9866	555.6	362.9
Gravimetric method					
Adsorbate	**Adsorbent**	**T (°C)**	**R^2**	**q_s (mg g^{-1})**	**K_L**
MEK	SBAC	30	0.9683	962.7	112.5
		40	0.9906	770.2	100.4
		50	0.8936	610.1	211.3
	KBAC	30	0.9924	365.1	368.0
		40	0.9849	358.8	286.0
		50	0.9652	377.4	255.3
TOL	SBAC	30	0.9612	1323.9	71.7
		40	0.9343	997.3	147.5
		50	0.9456	978.2	123.7
	KBAC	30	0.9944	421.8	468.6
		40	0.9995	413.0	491.5
		50	0.9912	400.9	653.6

doi:10.6342/NTU202003443

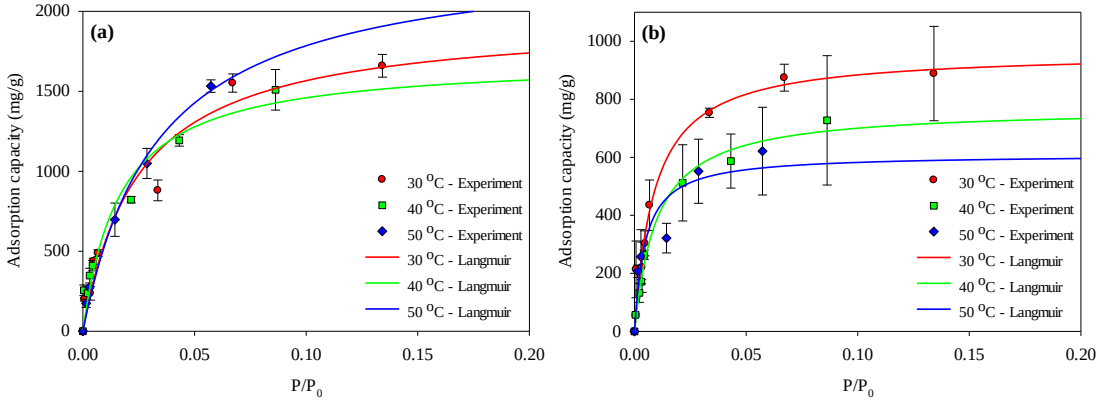

Figure 4-11 Experimental and Langmuir modeled adsorption isotherms for MEK and SBAC by (a) integration method and (b) gravimetric method

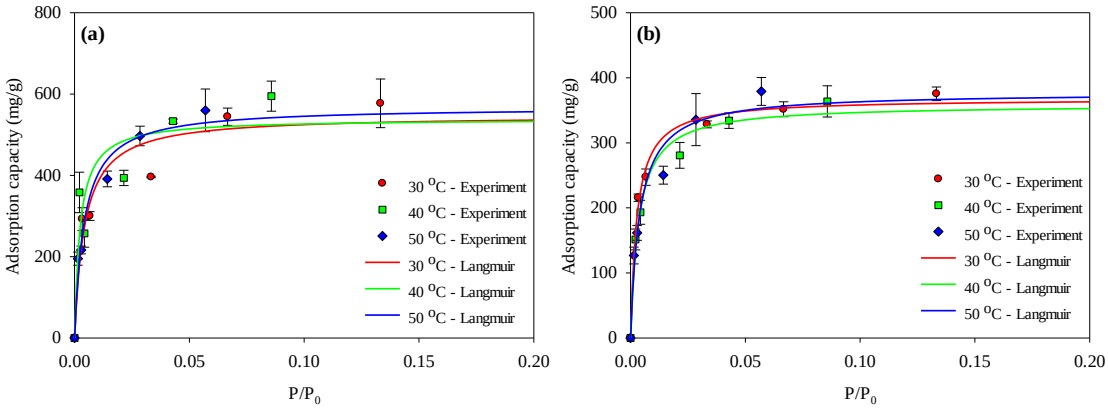

Figure 4-12 Experimental and Langmuir modeled adsorption isotherms for MEK and KBAC by (a) integration method and (b) gravimetric method

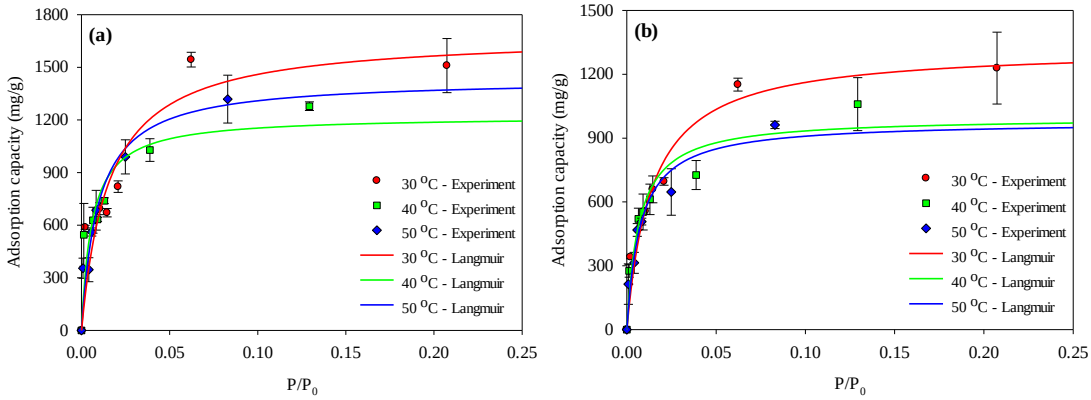

Figure 4-13 Experimental and Langmuir modeled adsorption isotherms for TOL and SBAC by (a) integration method and (b) gravimetric method

doi:10.6342/NTU202003443

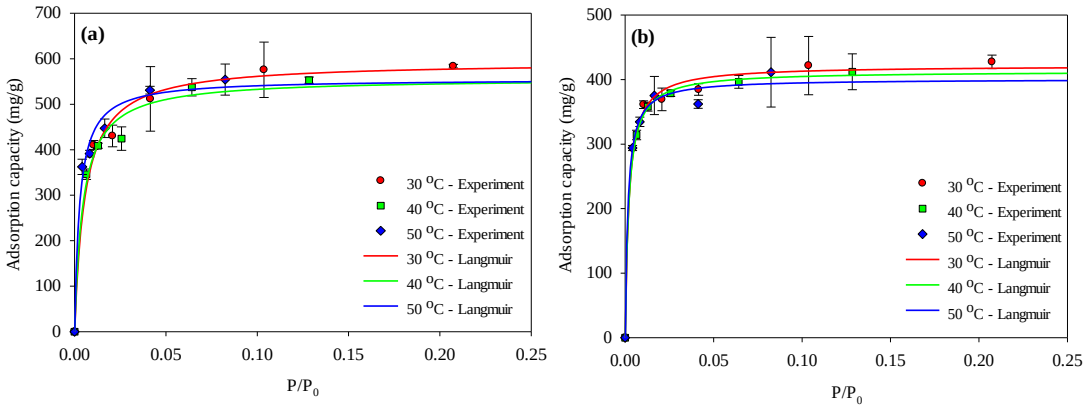

Figure 4-14 Experimental and Langmuir modeled adsorption isotherms for TOL and KBAC by (a) integration method and (b) gravimetric method

4.2.1.2 Freundlich Isotherm

Table 4-5 shows the results from the Freundlich isotherm model fitting for MEK/TOL adsorption onto SBAC and KBAC. Judging by the R^2 values, the Freundlich model also fit the experimental data with a level of conformity. The coefficient K_F is related to the adsorption capacity of the adsorbent, and n is a function of the strength of adsorption or surface heterogeneity. The larger the value of n, the stronger the adsorption affinity, indicating a more heterogeneous adsorption (Do, 1998). As can be seen in Table 4-5, in most cases, K_F increased and n decreased with increasing operating temperature. The value of n was greater than one for all scenarios, revealing the heterogeneity of the carbon surface.

The plots of experimental and Freundlich isotherm modeled data are presented in Figures 4-15 to 4-18. Owing to it lack of a finite limit under high pressure, the Freundlich isotherm cannot be fit for broad concentration ranges. To deepen the understanding of adsorption mechanisms, the D-R isotherm model is presented in the next section.

doi:10.6342/NTU202003443

Table 4-5 Freundlich parameters for different adsorbate-adsorbent systems at different temperatures

Freundlich parameter					
Integration method					
Adsorbate	**Adsorbent**	**T (°C)**	**R^2**	**n**	**K_F**
MEK	SBAC	30	0.9657	2.302	4243.3
		40	0.9896	2.309	4431.1
		50	0.9999	1.746	7927.5
	KBAC	30	0.9822	4.778	890.8
		40	0.9410	4.995	954.2
		50	0.9931	3.352	1360.9
TOL	SBAC	30	0.9486	3.942	2426.1
		40	0.9825	4.496	2013.0
		50	0.9669	3.041	3060.9
	KBAC	30	0.9927	7.886	737.1
		40	0.9925	6.382	783.6
		50	0.9967	6.662	824.7
Gravimetric method					
Adsorbate	**Adsorbent**	**T (°C)**	**R^2**	**n**	**K_F**
MEK	SBAC	30	0.9483	3.336	1793.6
		40	0.9769	2.531	2005.2
		50	0.9637	3.105	1569.8
	KBAC	30	0.9960	6.784	518.7
		40	0.9946	4.407	656.4
		50	0.9947	3.386	905.4
TOL	SBAC	30	0.9555	3.824	1988.3
		40	0.9900	3.902	1777.6
		50	0.9857	3.187	2107.6
	KBAC	30	0.9989	15.97	475.8
		40	0.9960	12.42	494.1
		50	0.9890	10.67	515.3

doi:10.6342/NTU202003443

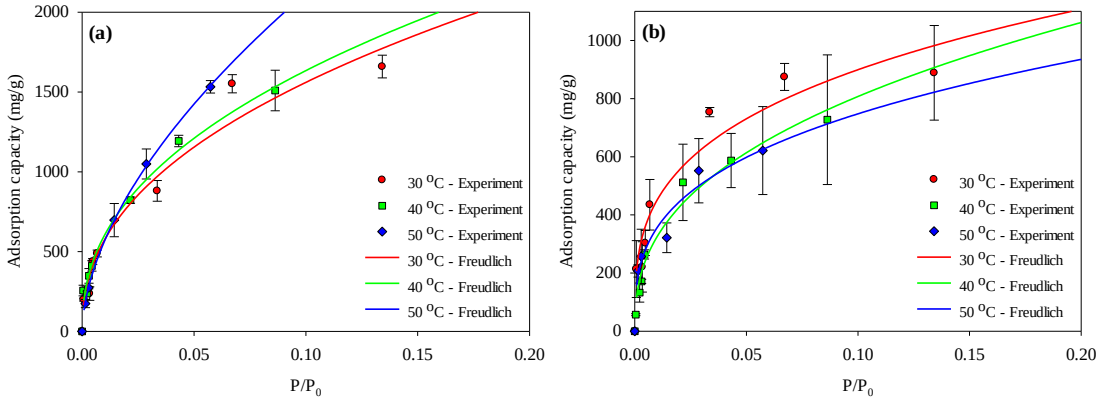

Figure 4-15 Experimental and Freundlich modeled adsorption isotherms for MEK and SBAC by (a) integration method and (b) gravimetric method

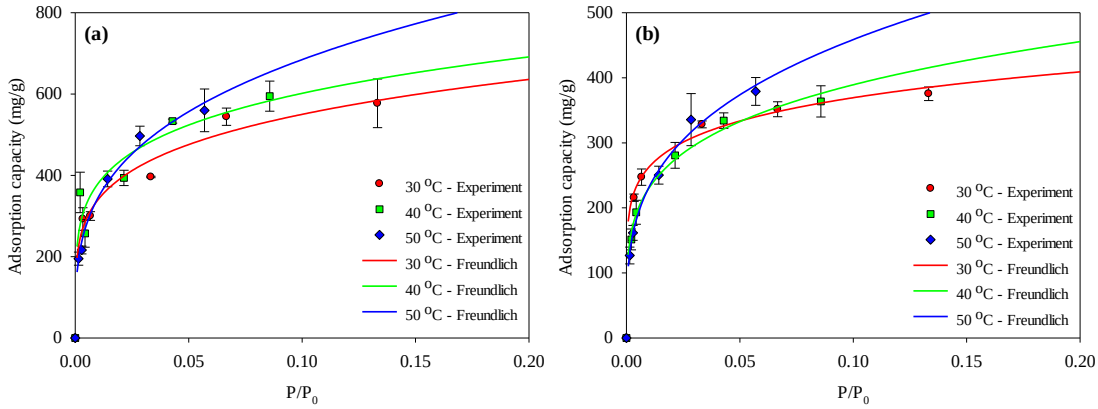

Figure 4-16 Experimental and Freundlich modeled adsorption isotherms for MEK and KBAC by (a) integration method and (b) gravimetric method

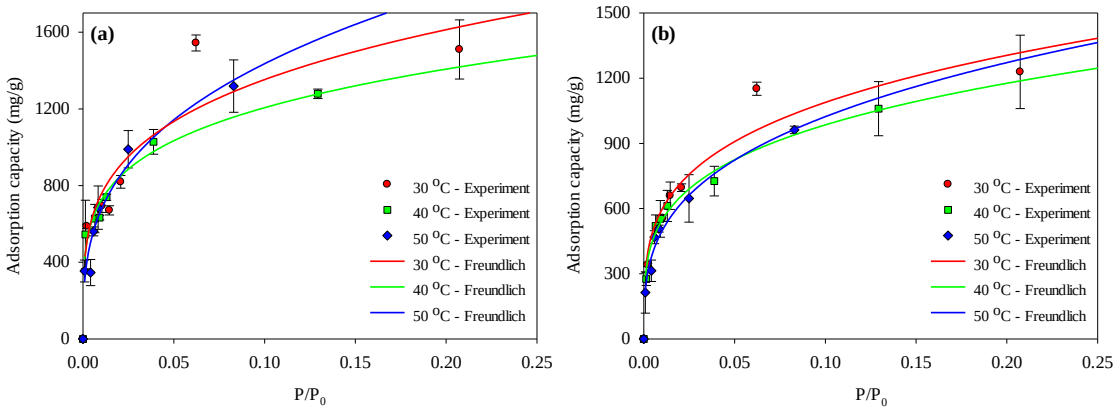

Figure 4-17 Experimental and Freundlich modeled adsorption isotherms for TOL and SBAC by (a) integration method and (b) gravimetric method

doi:10.6342/NTU202003443

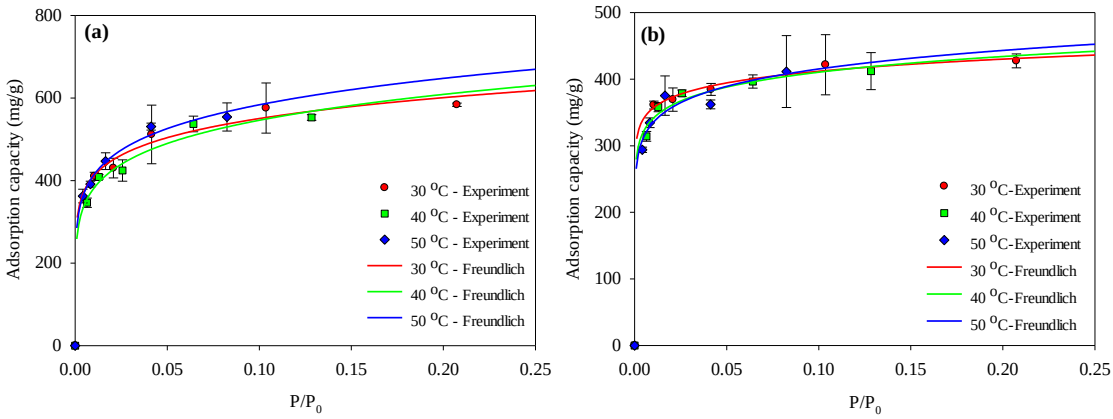

Figure 4-18 Experimental and Freundlich modeled adsorption isotherms for TOL and KBAC by (a) integration method and (b) gravimetric method

4.2.1.3 Dubinin-Radushkevich Isotherm

The D-R model has proven suitable to describe the adsorption isotherms of activated carbon (Ayawei et al., 2017). Since the pore structure analysis revealed that the materials examined in this study have high microporosities, the D-R isotherm model was used in this study. Adsorption isotherms were fit to the D-R equation, with R^2 values mostly above 0.96, to compare adsorbent-adsorbate interactions. The D-R isotherm parameters are summarized in Table 4-6, and the plots of the experimental and D-R isotherm modeled data are presented in Figures 4-19 to 4-22. The affinity coefficient (β) was derived in Appendix A.1.

The characteristic energy, E (or $E_0\beta$), is a parameter concerning pore size, surface chemistry, and adsorbate structure. In brief, the smaller the E is, the easier for adsorbates to adsorb onto the adsorbent (Chiang et al., 2002). It is known that the magnitude of E is useful in the estimation of the type of adsorption mechanism followed. When one mole of the matter is transferred, the value of E in the range below 8 kJ mol^{-1} indicates physical adsorption, whereas a value in the range from 20 to 40 kJ mol^{-1} indicates chemisorption

doi:10.6342/NTU202003443

(Mishra, 2016). In this study, the characteristic energies of adsorption of MEK and TOL onto SBAC were about 8 to 10 kJ mol^{-1}, suggesting that physical adsorption predominates in the adsorption process. Compared with SBAC, the free energy of MEK and TOL adsorbed onto KBAC was higher (10 - 18 kJ mol^{-1}), but still suggests physical adsorption.

Once the characteristic energy is gained from the adsorption isotherm data, the characteristic pore dimensions of a porous carbon can also be estimated. There is an inverse proportionality between E and the slit-pore half-width (x_0) which takes the following form:

$$x_0 = k/E_0 \tag{4-1}$$

For the majority of industrial active carbons whose E is less than 22 kJ mol^{-1}, the corresponding values of k are almost constant, and can be set approximately to 13 kJ nm mol^{-1} (Dubinin & Stoeckli, 1980).

As observed in Table 4-6, the x_0 of SBACs are larger than KBACs. Most results showed an acceptable agreement using MEK or TOL as a probing molecule, while some deviated results could be attributed to data error or narrower pore sizes in adsorbents, which hindered diffusion of larger molecules. It should be noted that the VOCs considered in this study are relatively small, and adsorption capacity trends may differ from those established here for larger adsorbates (e.g. polychlorinated dibenzo-p-dioxins and -furans) (Ghafari & Atkinson, 2018).

W_0 is the limiting pore volume, which is determined by the micropore volume. The calculated W_0 seems inconsistent with that obtained by using N_2 adsorption. The main reason is that the calculated W_0 used MEK or TOL as a probing molecule, and the difference in kinetic diameters of the probing molecules (N_2: 4.02 Å, MEK: 5.25 Å, and

doi:10.6342/NTU202003443

TOL: 5.85 Å) contributed to the different W_0. Generally, the smaller the value of W_0, the less micropore volume it has. As expected, in consistence with the PSD analysis shown previously, SBACs developed higher proportions of small pores compared to KBAC (as seen in Table 4-2).

doi:10.6342/NTU202003443

Table 4-6 D-R parameters for different adsorbate-adsorbent systems at different temperature

D-R parameter							
Integration method							
adsorbate	**adsorbent**	**T (°C)**	**R^2**	**W_0 ($cm^3\ g^{-1}$)**	**E_0 ($kJ\ mol^{-1}$)**	**E ($kJ\ mol^{-1}$)**	**x_0 (nm)**
MEK	SBAC	30	0.9685	2.711	7.44	7.20	1.747
		40	0.9778	2.536	8.17	7.92	1.592
		50	0.9949	3.367	7.30	7.09	1.780
	KBAC	30	0.9709	0.787	11.09	10.74	1.172
		40	0.9200	0.808	12.52	12.14	1.039
		50	0.9954	0.927	10.67	10.36	1.218
TOL	SBAC	30	0.9020	2.014	7.45	8.88	1.745
		40	0.9559	1.590	9.12	10.88	1.425
		50	0.9636	1.962	7.84	9.36	1.658
	KBAC	30	0.9956	0.724	10.19	12.15	1.276
		40	0.9935	0.710	10.21	12.18	1.273
		50	0.9974	0.728	11.45	13.66	1.136
Gravimetric method							
adsorbate	**adsorbent**	**T (°C)**	**R^2**	**W_0 ($cm^3\ g^{-1}$)**	**E_0 ($kJ\ mol^{-1}$)**	**E ($kJ\ mol^{-1}$)**	**x_0 (nm)**
MEK	SBAC	30	0.9690	1.389	9.22	8.92	1.410
		40	0.9932	1.219	8.67	8.41	1.500
		50	0.9477	1.008	10.34	10.04	1.258
	KBAC	30	0.9998	0.510	13.14	12.72	0.989
		40	0.9990	0.540	11.44	11.10	1.136
		50	0.9936	0.618	10.77	10.46	1.207
TOL	SBAC	30	0.9768	1.635	7.83	9.34	1.659
		40	0.9834	1.342	8.41	10.03	1.546
		50	0.9811	1.368	8.13	9.70	1.599
	KBAC	30	0.9982	0.505	14.84	17.68	0.876
		40	0.9982	0.505	14.23	16.98	0.913
		50	0.9905	0.503	14.53	17.34	0.895

doi:10.6342/NTU202003443

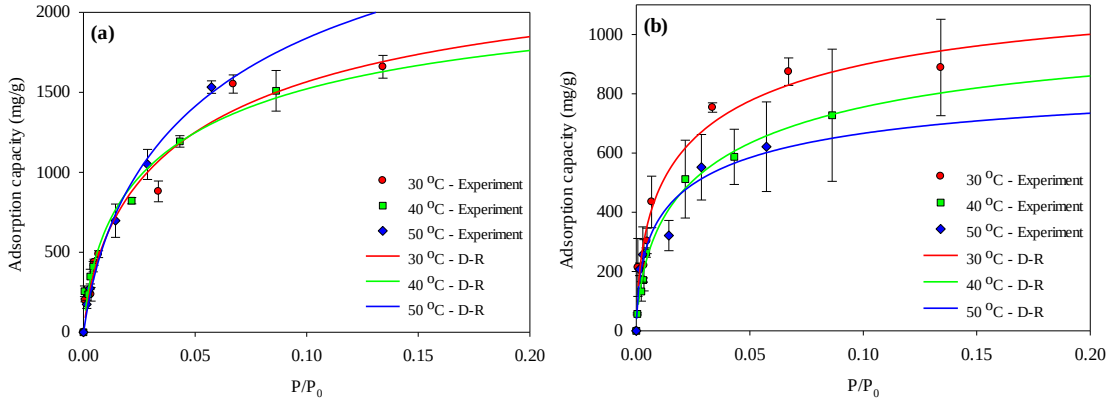

Figure 4-19 Experimental and D-R modeled adsorption isotherms for MEK and SBAC by (a) integration method and (b) gravimetric method

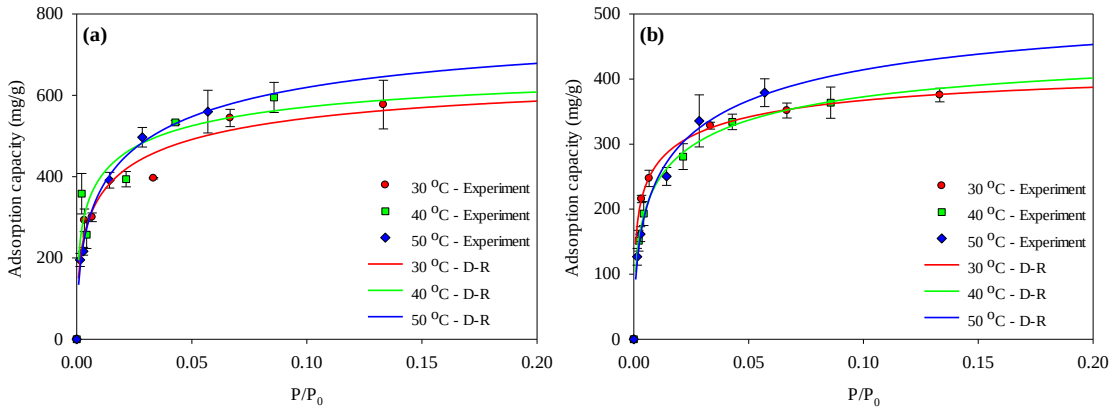

Figure 4-20 Experimental and D-R modeled adsorption isotherms for MEK and KBAC by (a) integration method and (b) gravimetric method

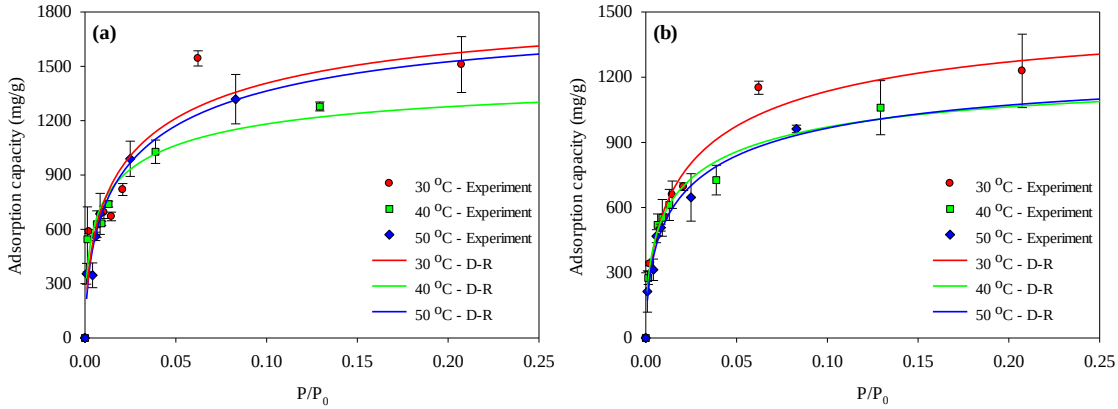

Figure 4-21 Experimental and D-R modeled adsorption isotherms for TOL and SBAC by (a) integration method and (b) gravimetric method

doi:10.6342/NTU202003443

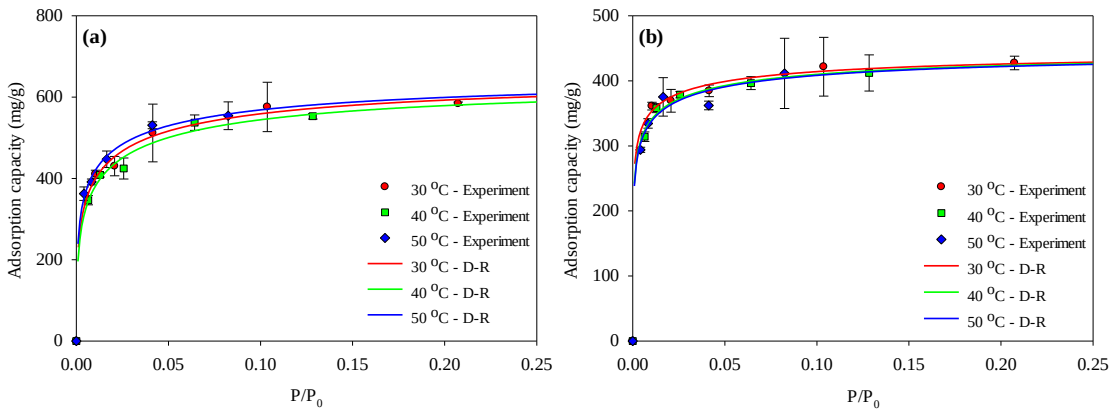

Figure 4-22 Experimental and D-R modeled adsorption isotherms for TOL and KBAC by (a) integration method and (b) gravimetric method

4.2.2 Isosteric Heat of Adsorption

The D-R equation offered an analytically calculable method for the isosteric heat of adsorption (ΔH_s). In our study, ΔH_s was determined via the C-C and D-R equations, where the equation for the ΔH_s is derived in Section 2.3.4 and expressed in Equation 2-16. Details of the thermodynamic parameters (ΔH_{vap} and α) are proposed in Appendix A.2. As mentioned in previous sections, the deviation of adsorption capacities from the different calculation methods was significant. In order to maintain the accuracy and consistency, the data for the D-R isotherms used in calculating ΔH_s are from gravimetric methods. The dependence on adsorbate, temperature, and surface loading in calculating ΔH_s are represented graphically in Figure 4-23.

The isosteric heats may be interpreted as the criterion of the energetic heterogeneity of the adsorbent surface, or it may be represented as an indicator of the interaction strength between the gas molecules and the adsorbent (Cinke et al., 2003; Park et al., 2002). A rule of thumb in adsorption is that for the heat of adsorption of 80 kJ/mole or more, the adsorption process is chemisorption and smaller values are representative of

doi:10.6342/NTU202003443

physisorption (Cinke et al., 2003; Sui et al., 2017; Webb & Orr, 1997). As shown in Figure 4-23, ΔH_s ranges from 35 kJ/mol to 60 kJ/mol, indicating a physical adsorption type.

The data in Figures 4-23(a) and (b) show that ΔH_s of MEK and TOL on the SBAC are nearly constant (≈45.47 and 45.52 kJ mol^{-1}, respectively) and independent of temperature in the range of surface loading. This indicates a relatively energetic homogeneity of the adsorbent surface (Buss, 1995). However, as observed in Figure 4-23(c), ΔH_s of MEK on KBAC at 30ºC is relatively lower. One explanation for this is the surface heterogeneity of adsorbent (Huang, 1972), but this also may be attributed to experimental error in measuring the adsorption isotherm. It should be noted in Figure 4-23(d) that ΔH_s for TOL adsorption on KBAC increased drastically at higher surface loading, which reflected a stronger dependence upon surface loading. Such results are consistent with those of Chen et al. (2020), and can be explained by the following: (1) the surfaces of KBAC are energetically heterogeneous towards adsorption of TOL (Park et al., 2002) , (2) the stronger lateral interactions occur between the adsorbed molecules at higher surface coverage (Chowdhury et al., 2011), or (3) as surface loading increases, a stronger interaction between TOL (weak polarity) and the nonpolar adsorbent resulting in high heats of adsorption.

doi:10.6342/NTU202003443

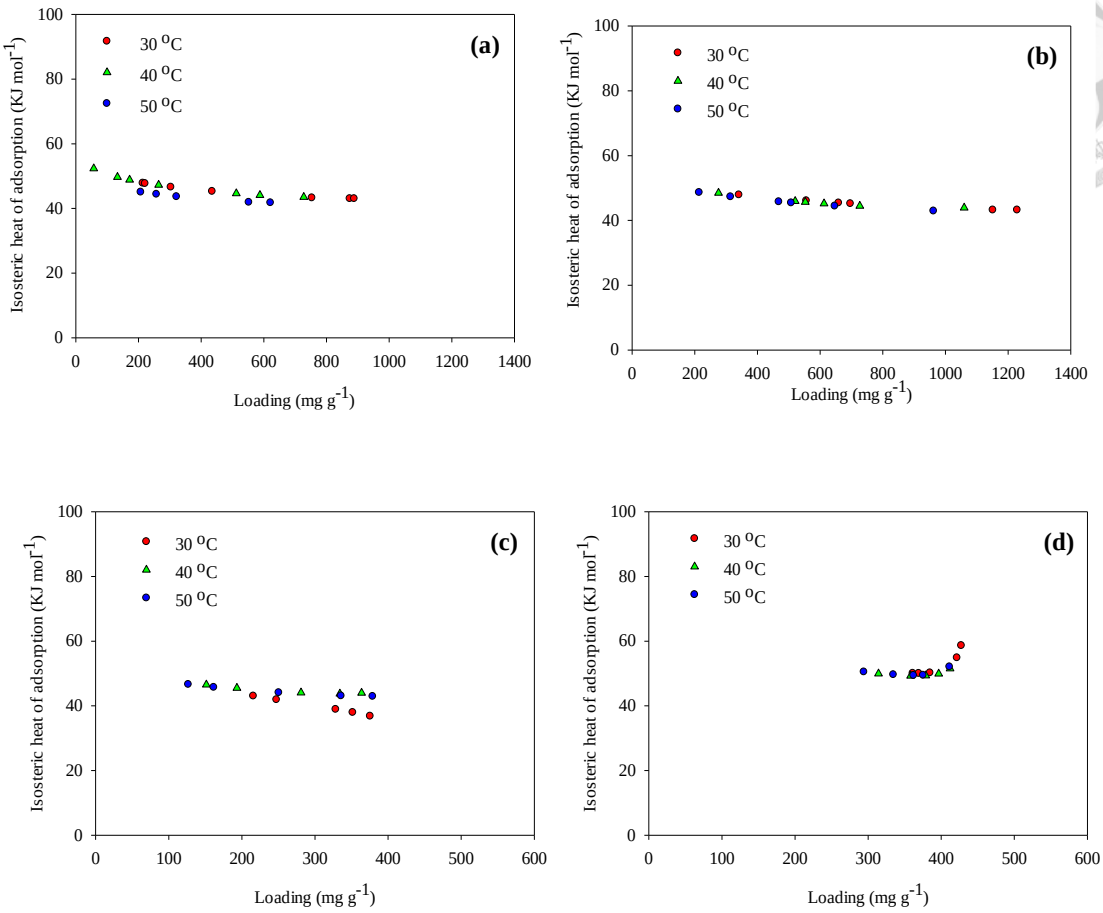

Figure 4-23 Isosteric heat of (a) MEK and (b) TOL adsorption on SBAC; (c) MEK and (d) TOL adsorption on KBAC

4.2.3 Adsorption Kinetics

External diffusion coefficients (k_1) and intraparticle diffusivities (k_p) for adsorption were determined using the PFO (Equation 3-9) and IPD (Equation 3-10) models. The kinetic results were obtained from 500 ppm_v of the inlet adsorbate concentration. The results are given in Table 4-7.

In general, adsorption on an adsorbent is controlled by the intraparticle diffusion step, where the relationship between q_t and $t^{1/2}$ is linear (Zhou et al., 2015). In Table 4-7, the obtained correlation coefficient R^2 for the PFO and IDP kinetic equation was similar,

doi:10.6342/NTU202003443

indicating that MEK and TOL adsorbed onto SBAC and KBAC followed both kinetic models. Consequently, it demonstrated that external and intrapariticle diffusion control are both possible to be the rate-limiting step for adsorption of MEK and TOL on adsorbents.

doi:10.6342/NTU202003443

Table 4-7 Kinetic parameters of adsorption and correlation coefficient R^2 obtained from PFO and IPD kinetic models

Adsorbate	Adsorbent	Temperature	PFO model		IPD model		
		(°C)	k_1 (min^{-1})	R^2	k_p (mg g^{-1} $s^{-1/2}$)	I (mg g^{-1})	R^2
MEK	SBAC	30	0.612 ± 0.054	0.988 – 1.000	17.06 ± 0.90	-32.47 ± 7.40	0.978 – 0.984
		40	0.804 ± 0.083	0.978 – 0.986	17.76 ± 1.14	-38.18 ± 5.61	0.984 – 0.987
		50	0.824 ± 0.094	0.984 – 0.998	13.30 ± 1.52	-21.24 ± 5.97	0.984 – 0.987
	KBAC	30	0.160 ± 0.021	0.982 – 0.997	10.80 ± 0.54	-48.26 ± 7.71	0.985 – 0.991
		40	0.114 ± 0.012	0.996 – 0.998	11.33 ± 0.83	-58.55 ± 6.62	0.980 – 0.991
		50	0.204 ± 0.048	0.988 – 0.998	7.95 ± 0.44	-27.94 ± 8.38	0.985 – 0.989
TOL	SBAC	30	0.268 ± 0.021	0.991 – 0.994	31.45 ± 2.54	-98.98 ± 34.95	0.986 – 0.991
		40	0.244 ± 0.057	0.995 – 0.998	26.83 ± 2.37	-56.75 ± 22.18	0.980 – 0.991
		50	0.352 ± 0.118	0.984 – 0.998	17.16 ± 1.67	-20.81 ± 1.90	0.989 – 0.990
	KBAC	30	0.158 ± 0.015	0.986 – 0.995	14.83 ± 1.09	-69.27 ± 17.93	0.975 – 0.988
		40	0.186 ± 0.026	0.910 – 0.973	11.51 ± 1.40	-72.78 ± 15.09	0.984 – 0.987
		50	0.170 ± 0.015	0.994 – 0.997	14.28 ± 0.20	-67.98 ± 4.12	0.984 – 0.987

doi:10.6342/NTU202003443

4.3 Thermogravimetric Analysis

Thermogravimetric analysis (TGA) has been used to study the thermal regeneration behavior of adsorbents. Virgin BACs (without organics) showed only slight changes in weight during the temperature rise, as shown in Figure 4-24. The weight loss observed around 90°C is attributed to water desorption, which is usually observed in activated carbon previously exposed to ambient air (Popescu et al., 2003).

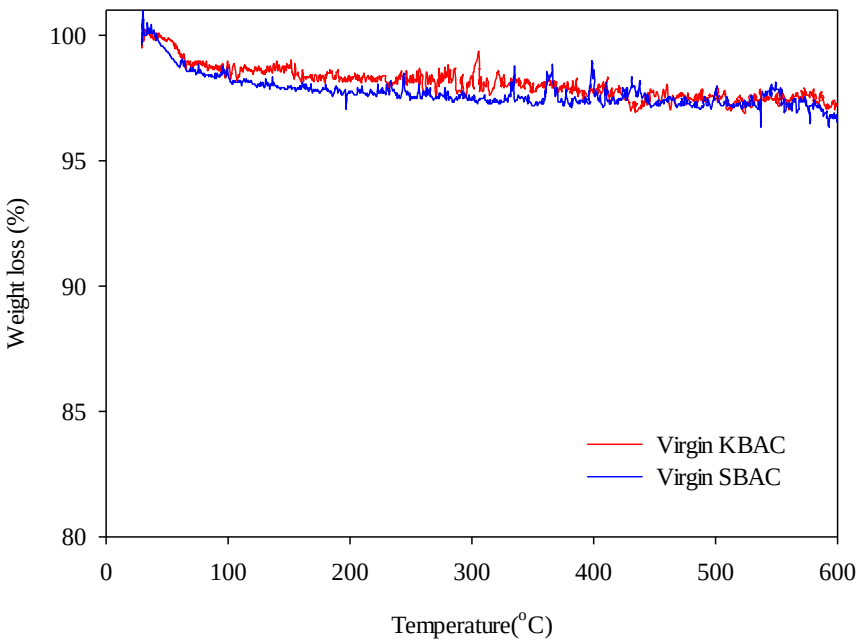

Figure 4-24 TG thermal curves of virgin BACs at heating rates of 10 °C/min

The TGA results of BACs loaded with MEK and TOL at different heating rates are shown in Figures 4-25 and 4-26. The thermal desorption of the adsorbed VOCs and the decomposition of organics on the adsorbent surface were expected to occur during the temperature rise (Suzuki et al., 1978). For all samples, it was observed that the desorption of compounds occurred at temperatures between 100 and 400°C. Hence, the results

doi:10.6342/NTU202003443

showed that these sorbents could be regenerated at temperatures below 400°C.

The TGA results indicate that, under conventional conductive heating, the weight loss percentages of loaded BACs were less significant at rapid heating rates. That may result in more heel formations at rapid heating rates. Niknaddaf et al. (2020) have pointed out that the increase in heel formation is a consequence of the simultaneously rapid heating rates due to higher concentrations of residual VOCs that are exposed to the high temperatures.

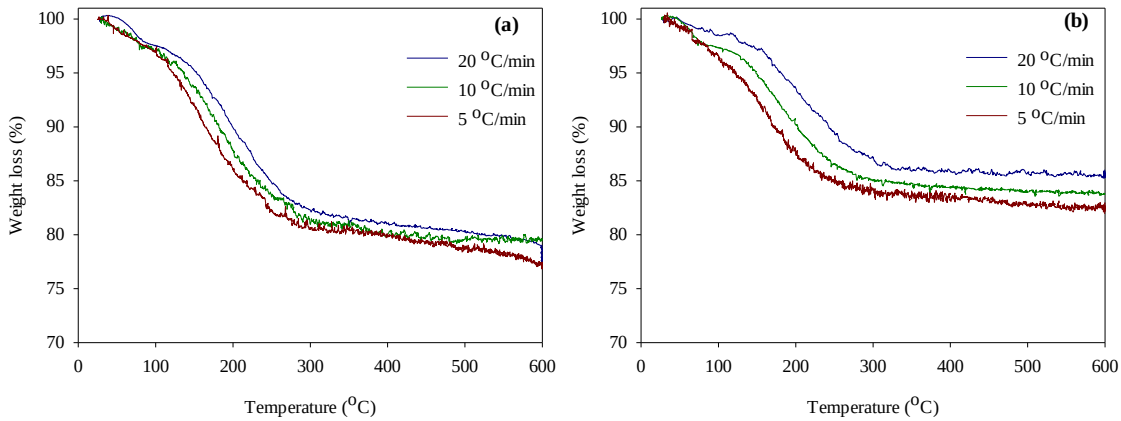

Figure 4-25 TG thermal curves of (a) MEK-SBAC and (b) MEK-KBAC at heating rates of 5, 10, and 20 °C/min

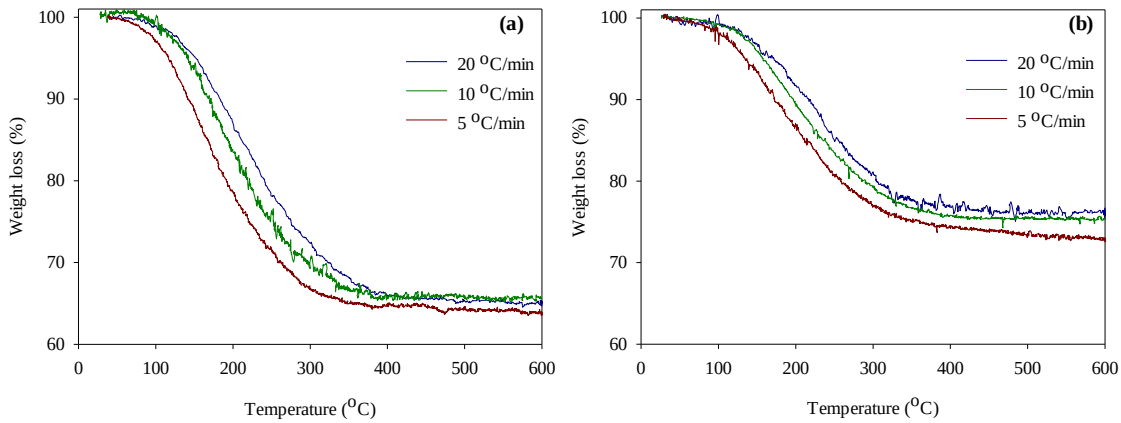

Figure 4-26 TG thermal curves of (a) TOL-SBAC and (b) TOL-KBAC at heating rates of 5, 10, and 20 °C/min

doi:10.6342/NTU202003443

The differential thermal gravimetry (DTG) curve is a plot of the adsorbate's desorption rate as a function of the sample temperature. As a whole, the DTG data were used to evaluate kinetic parameters, such as activation energy of different organic materials. According to the curve, we could easily identify the interactions between the gas and the solid. Since the desorption peak temperature is related to the adsorption strength, a more robust interaction gives rise to a higher peak temperature. A desorbed peak under 100°C is attributed to water desorption (Popescu et al., 2003). Assuming that the desorption followed first-order kinetics and the heating rate is constant (i.e., $T = T_0 + \beta t$), based on the Arrhenius equation, the activation energy for desorption could be calculated from the following equation (Cvetanović & Amenomiya, 1972):

$$\ln\left(\frac{\beta}{RT_M^2}\right) = -\frac{E_d}{RT_M} + C \tag{4-2}$$

where T_M is the peak desorption temperature, β is the heating rate, E_d is the desorption activation energy, R is the gas constant, and C is a constant that depends on the desorption kinetics. Therefore, a plot of $\ln(\beta/RT_M^2)$ versus $1/T_M$ yielded a line with slope: $-E_d/R$.

In general, the desorption energy from a physisorbed state is close to or slightly higher than the heat of vaporization (Popescu et al., 2003). According to the results in Table 4-8, it is seen that E_d is approximately the same or slightly higher than the heat of vaporization for TOL and for MEK (32.8 and 31.21 KJ $mole^{-1}$ at boiling point for TOL and MEK, respectively). This showed that these compounds were physisorbed.

doi:10.6342/NTU202003443

Table 4-8 Peak desorption temperatures at different heating rates and activation energies for desorption

	Peak desorption temperatures (K) at different heating rates			E_d (kJ/mol)	ΔH_{vap} (kJ/mol)[a]
	20 °C/min	10 °C/min	5 °C/min		
MEK-SBAC	488	461	432	36.45	31.21
MEK-KBAC	488	468	441	46.41	
TOL-SBAC	494	459	430	30.40	32.80
TOL-KBAC	520	476	446	27.15	

[a] at boiling point (Poling et al., 2001)

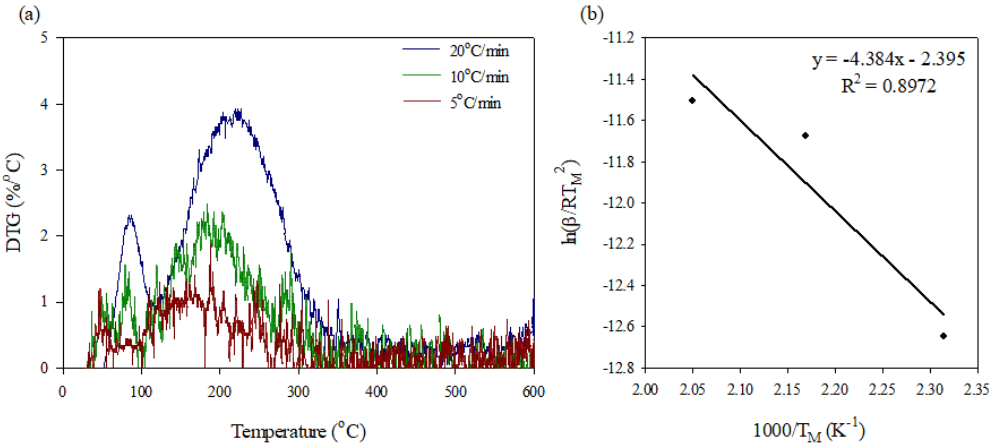

Figure 4-27 DTG of MEK-SBAC at various heating rates. (a) DTG peaks; (b) linear form providing the heat of desorption.

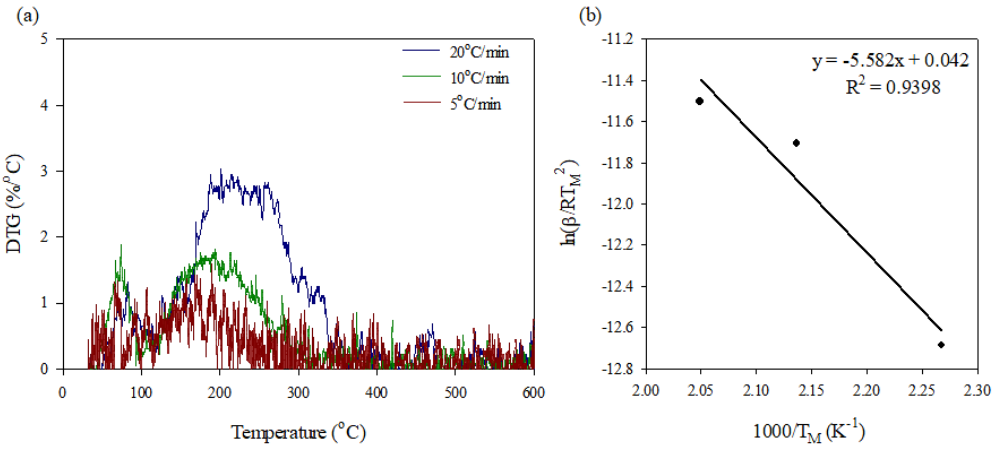

Figure 4-28 DTG of MEK-KBAC at various heating rates. (a) DTG peaks; (b) linear form providing the heat of desorption.

doi:10.6342/NTU202003443

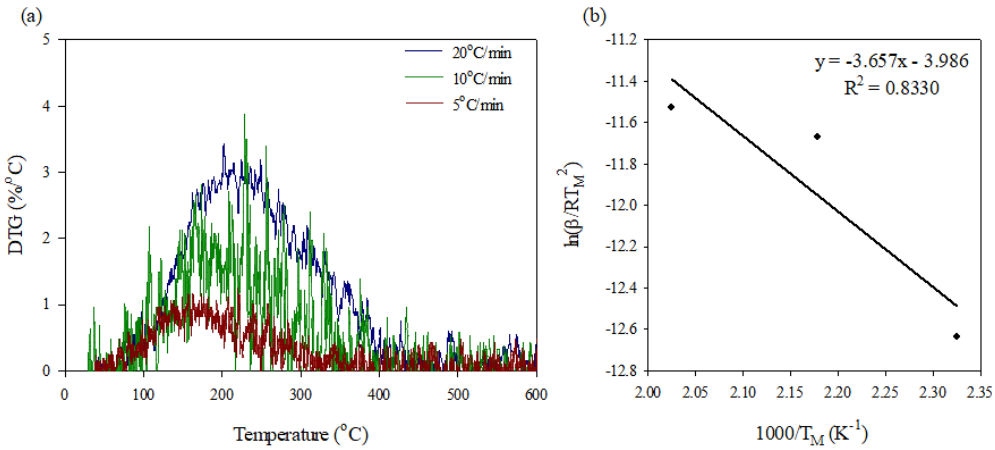

Figure 4-29 DTG of TOL-SBAC at various heating rates. (a) DTG peaks; (b) linear form providing the heat of desorption.

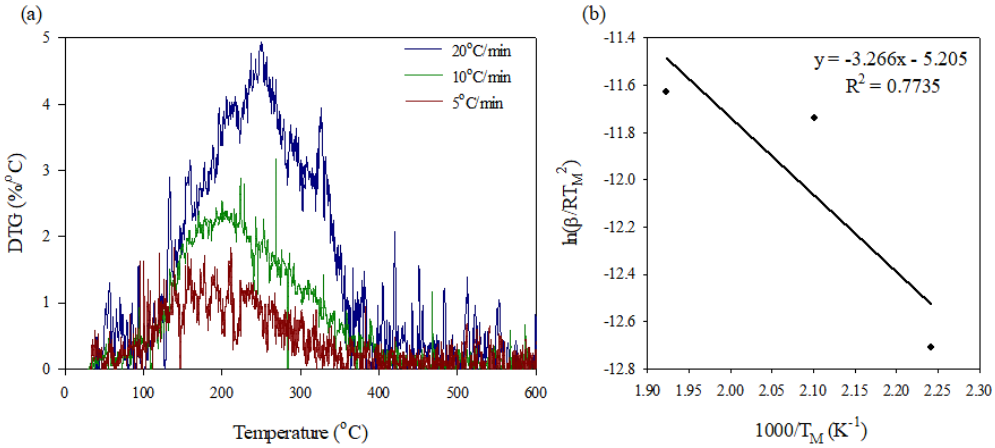

Figure 4-30 DTG of TOL-KBAC at various heating rates. (a) DTG peaks; (b) linear form providing the heat of desorption

4.4 Microwave Regeneration

The saturated BACs (loaded under 40°C and 500 ppm_v of MEK or TOL) were regenerated by microwave irradiation. The desorption tests were evaluated for different durations (2, 4, or 8 min) and different power outputs (400, 600, 800, or 1000 W) of microwave application under a constant flow rate of purging gas (2.0 SLPM). Preliminary tests revealed temperature variations for the virgin BACs (without adsorbate loading) for 12 min at different power outputs, as shown in Figure 4-31. To avoid damaging the

doi:10.6342/NTU202003443

equipment, due to the upper detection temperature limit of the thermocouple, the temperature profile of SBAC under 1000 W was only detected for 5 min.

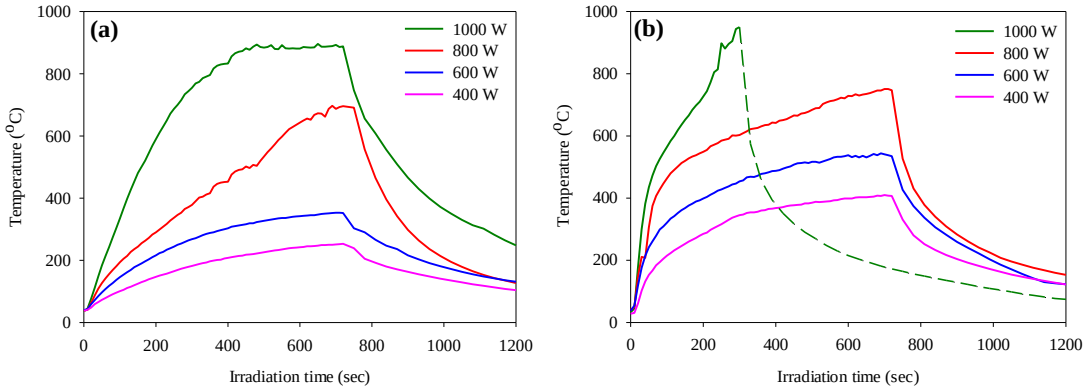

Figure 4-31 Temperature profile of virgin (a) KBAC and (b) SBAC under 12 min of microwave irradiation (5 min for SBAC under 1000 W irradiation)

It was shown that the higher the power output of the microwave, the higher the heating rate. More specifically, this demonstrated the effects of microwave power on the rising temperature of adsorbents. After turning off the microwave, the temperature of the adsorbent quickly decreased to the ambient temperature.

However, some previous studies have reported that the temperature measured by a thermocouple shows significant measurement errors compared to the real reaction temperature of the carbons. Firstly, local high-temperature regions at the contact points of the carbon spheres under microwave irradiation have been observed, whereas the thermocouple can only measure the temperature at a very limited region (Haneishi et al., 2019). Also, the presence of thermocouples in microwave furnaces locally perturbs the microwave field and induces thermal instabilities. That is, the temperature distribution in the BAC bed is non-uniform during desorption processes (Pert et al., 2001). As a result, in order to prevent any temperature interferences from a thermocouple, we removed the

doi:10.6342/NTU202003443

thermocouple during the desorption tests, meaning the temperature profile of virgin BACs is the only reference.

4.4.1 Desorption Kinetics

To study the difference in the desorption performances of TOL and MEK on BACs under different microwave powers, experimental data for the desorption curves of TOL and MEK were obtained for different power outputs, ranging from 400 to 1000 W, respectively. The THC concentration of the outlet nitrogen sweep gas as a function of time during regeneration of the carbon beds at different power outputs are presented in Figures 4-32 and 4-33.

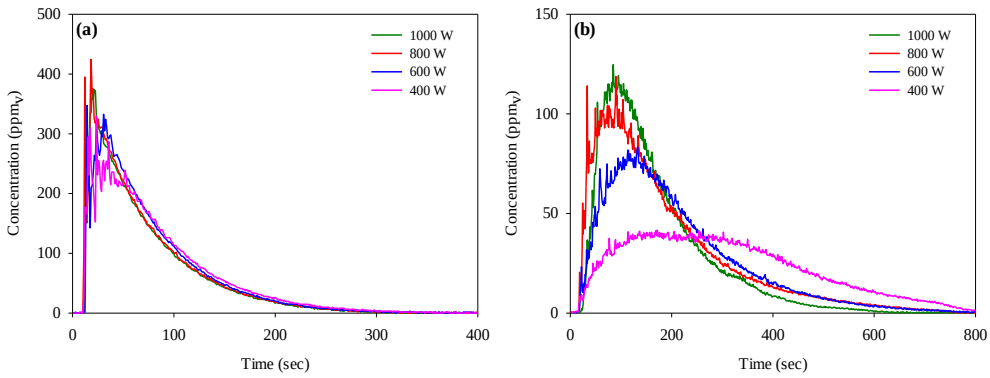

Figure 4-32 THC desorption curves of (a) MEK-SBAC and (b) MEK-KBAC at different microwave power outputs for 12 min of irradiation time

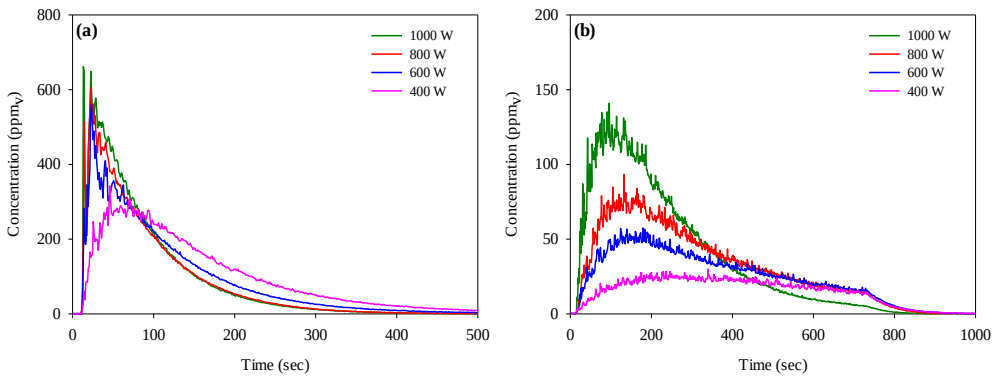

Figure 4-33 THC desorption curves of (a) TOL-SBAC and (b) TOL-KBAC at different

doi:10.6342/NTU202003443

microwave power outputs for 12 min of irradiation time

The results showed that the maximum signal of the VOCs' intensity gradually increased with the increase of microwave power, and this increasing tendency was more significant in KBAC. This could preliminarily confirm that the desorption rate increased when the temperature increased. The desorption rates of SBAC were significantly faster in comparison to those of KBAC. The concentration signal increased sharply as soon as exposure to microwave irradiation. The desorption process of SBAC basically completed within 500 sec. The fast desorption rate and high outlet concentration are crucial factors in optimization the desorption performance.

Moreover, there was sometimes a noticeable, significant peak at the beginning. Foo and Hameed (2012) regenerated activated carbon at 600 W of microwave power, and defined three steps of the heating phenomenon in activated carbon:

(1) At the initial stages of microwave radiation, sudden and intensely bright sparks (known as microplasmas) appeared around the carbon layer. Meanwhile, a large amount of VOCs was released from the carbon samples.

(2) As the microwave radiation continued, the samples were heated rapidly, and the carbon samples facing the microwave source displayed a bright incandescent color.

(3) The carbon samples then turned red and remained incandescent for the entire treatment period, which lead to the desorption of adsorbate from the carbon surface.

In sum, the conspicuous peak at the start is attributed to the presence of microplasmas.

In this section, the diffusion-controlled kinetic models (Equations 3-9 and 3-10) were also used to determine the external diffusion coefficient (k_1) and the intraparticle diffusivities (k_p) for desorption. Results are given in Table 4-9. However, since the

doi:10.6342/NTU202003443

amount of desorbate detected from FID showed deviations between the actual and detected values, the kinetic results from the desorption curve could not represent the real situation. The details of the deviation are explained in the next section.

doi:10.6342/NTU202003443

Table 4-9 Kinetic parameters of desorption and correlation coefficient R^2 obtained from PFO and IPD kinetic models

Adsorbate	Adsorbent	Irradiation power (W)	PFO model		IPD model		
			k_1 (min^{-1})	R^2	k_p ($mg\ g^{-1}\ s^{-1/2}$)	I ($mg\ g^{-1}$)	R^2
MEK	SBAC	400	0.328 ± 0.030	0.889 – 0.921	9.17 ± 0.49	-8.23 ± 4.40	0.889 – 0.912
		600	0.372 ± 0.027	0.900 – 0.934	9.50 ± 0.20	-7.67 ± 5.55	0.886 – 0.916
		800	0.350 ± 0.009	0.895 – 0.926	8.60 ± 1.65	-7.97 ± 6.86	0.881 – 0.912
		1000	0.309 ± 0.030	0.875 – 0.904	8.75 ± 0.64	-3.35 ± 6.15	0.877 – 0.893
	KBAC	400	0.064 ± 0.017	0.953 – 0.975	4.03 ± 0.67	-25.30 ± 6.39	0.973 – 0.985
		600	0.068 ± 0.007	0.842 – 0.987	3.87 ± 0.67	-17.87 ± 8.32	0.949 – 0.988
		800	0.138 ± 0.036	0.902 – 0.973	5.83 ± 0.55	-24.30 ± 21.61	0.901 – 0.955
		1000	0.204 ± 0.021	0.904 – 0.937	7.17 ± 0.12	-23.43 ± 6.95	0.907 – 0.940
TOL	SBAC	400	0.158 ± 0.044	0.868 – 0.951	18.07 ± 1.72	-20.17 ± 49.80	0.896 – 0.944
		600	0.230 ± 0.012	0.887 – 0.926	22.20 ± 0.98	7.23 ± 18.65	0.874 – 0.905
		800	0.212 ± 0.019	0.803 – 0.870	19.90 ± 0.85	54.53 ± 13.78	0.799 – 0.850
		1000	0.232 ± 0.031	0.814 – 0.895	20.43 ± 0.32	33.70 ± 42.86	0.817 – 0.888
	KBAC	400	0.026 ± 0.007	0.949 – 0.972	4.30 ± 1.18	-35.50 ± 7.66	0.958 – 0.976
		600	0.078 ± 0.026	0.981 – 0.985	9.33 ± 1.62	-64.70 ± 8.22	0.975 – 0.987
		800	0.126 ± 0.042	0.963 – 0.990	11.20 ± 0.70	-56.93 ± 20.97	0.928 – 0.982
		1000	0.170 ± 0.009	0.899 – 0.947	11.33 ± 0.64	-10.13 ± 17.22	0.866 – 0.908

doi:10.6342/NTU202003443

4.4.2 Desorption Efficiency

The desorption efficiencies for MEK-SBAC, MEK-KBAC, TOL-SBAC, and TOL-KBAC were evaluated from the change in sample weight Equation 3-5, and the mass balance of the desorption concentration curve detected by FID Equation 3-6. The results are shown in Figures 4-34 to 4-37.

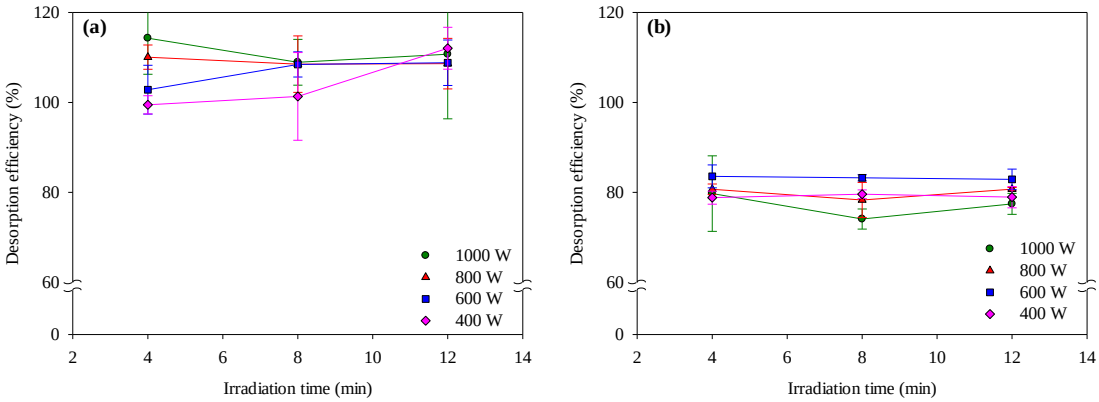

Figure 4-34 Desorption efficiency for MEK-SBAC evaluated by (a) change of sample weight and (b) desorption curve detected by FID

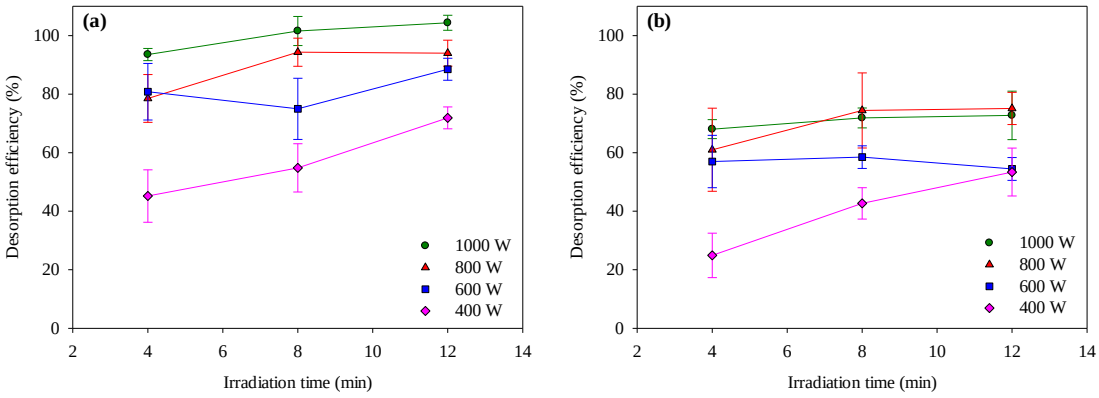

Figure 4-35 Desorption efficiency for MEK-KBAC evaluated by (a) gravimetric measurements and (b) desorption curve detected by FID

doi:10.6342/NTU202003443

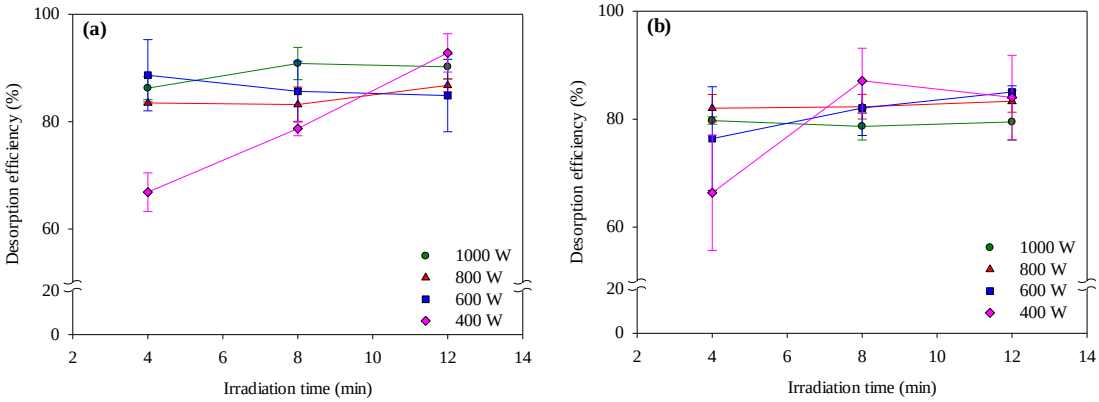

Figure 4-36 Desorption efficiency for TOL-SBAC evaluated by (a) change of sample weight and (b) desorption curve detected by FID

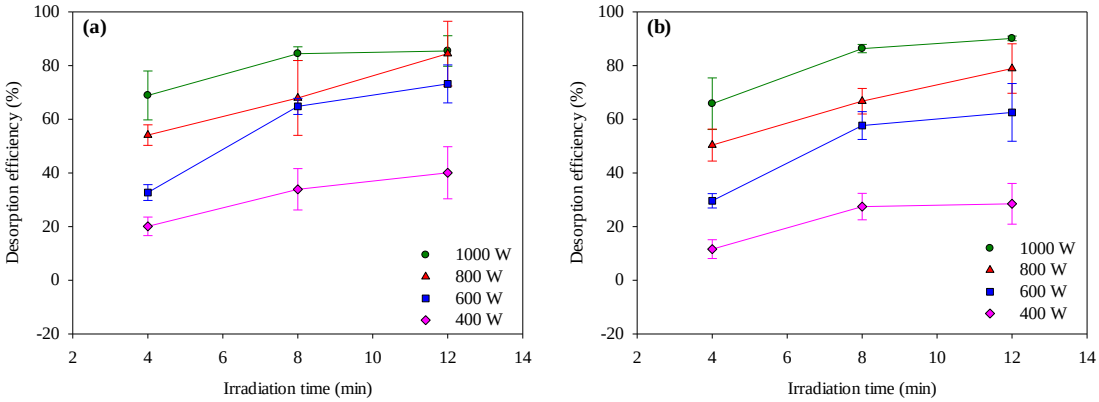

Figure 4-37 Desorption efficiency for TOL-KBAC evaluated by (a) change of sample weight and (b) desorption curve detected by FID

As expected, an increase in irradiation power and time led to an increase in desorption efficiency. The desorption efficiency of MEK and TOL onto SBAC could achieve a higher level with smaller microwave power and shorter irradiation time than KBAC. This may be due to the smaller size of SBAC, which contributed to more “hot-spots” in the carbon bed. In other words, the smaller size of SBAC allowed for better heat retention within the carbon bed. The high-temperature regions accelerated the desorption of VOCs under microwave irradiation. In short, SBAC has better desorption performance and energy

doi:10.6342/NTU202003443

utilization efficiency in the desorption process.

In addition, the amount of MEK desorbed was higher than that of TOL on both SBAC and KBAC. Possible reasons could be the lower boiling point of MEK, or the difference in dielectric permittivity between TOL and MEK. Kim and Ahn (2012) reported that the desorption of VOCs in microwaves becomes more noticeable when the adsorbate is polar. Moreover, the desorption efficiency for MEK-SBAC was beyond 100%. A possible reason for this is that some water and impurities may have existed in the pores or on the surface, and desorbed during the heating processes. A change in the porous structure was also observed from the SEM images. A previous study reported that the dielectric permittivity of adsorbate influenced the heating behaviors in the microwave (Polaert et al., 2010). That is, the polarity of MEK leads to a higher temperature in certain regions of the beaded carbon, which results in the desorption of impurities.

It was worth noting that the difference between the desorption efficiency evaluated by desorption concentration versus that evaluated by weight change. Regarding desorption efficiency evaluated from MEK on BACs, the calculated desorption efficiency from the mass balance of the desorption concentration was significantly lower than that calculated from weight change (-28.01% and -22.37% on the average for MEK-SBAC and MEK-KBAC, respectively).

Originally, we considered that the difference in efficiency obtained from the two methods might be because of the thermal decomposition of MEK. The gas emission curves (including NO, SO_2, CO, and CO_2) of 20 mg samples regenerated under 800 W microwave for 8 min are given in Figure 4-38. For MEK-SBAC, the amount of emitted CO plus CO_2 was approximately 85.52 μg as C (causing about 17.63% of efficiency

doi:10.6342/NTU202003443

difference), and there was no other obvious gas outflow. This phenomenon supports the inference of the thermal decomposition of MEK. Since MEK has a carbonyl group, partial carbons may form inorganic compounds during the heating process. Waring and Spector (1955) reported that MEK was decomposed into several products in an N_2 environment at 550ºC, including 26.6% CO and 1.6% CO_2.

However, the amount of CO and CO_2 released from MEK-KBAC is only about 5.11 μg as C (only cause about 1.15% efficiency difference), but it can be seen that there was a significant SO_2 emission (25.04 μg as S). That is to say, the decomposition of MEK may only account for a small part of the efficiency difference for MEK-KBAC. The removal of impurities such as sulfur under high temperatures might be another reason for the difference of efficiency, which may cause the overestimation of desorption efficiencies obtained from weight change.

On the other hand, for TOL on BACs, the efficiency evaluated by desorption concentration was only slightly lower than that by weight change (-4.31% and -4.48% on average for TOL-SBAC and TOL-KBAC, respectively). A likely explanation for this difference owes to the reaction between TOL and oxygen-containing substances (such as residual water) on the surface of carbon, which released inorganic compounds (i.e. CO or CO_2) that the THC detection system could not detect (Bhandari et al., 2014). This was also reflected in the results of elemental analysis (Table 4-1), in which the percentage of oxygen in the BACs slightly decreased after saturation and regeneration (i.e. the percentage of oxygen of TOL-KBAC-800W8min and TOL-SBAC-800W8min were lower than that of virgin KBAC and SBAC).

According to the gas analysis results, for TOL-SBAC, the amount of CO plus CO_2

doi:10.6342/NTU202003443

obtained from gas analysis results was about 57.02 μg as C (causing about 6.19% of efficiency difference). Nevertheless, for TOL-KBAC, the amount of releasing CO plus CO_2 was only 1.37 μg as C (causing only about 0.22% of difference) and accompanied by 3.08 μg as S of SO_2 release. In brief, the results showed that the efficiency differences of TOL-SBAC were possibly associated with the reaction of TOL on the carbon surface. However, the efficiency difference of TOL-KBAC might be due, in large part, to the release of impurities such as sulfur, accordingly overestimated the efficiency obtained from weight change.

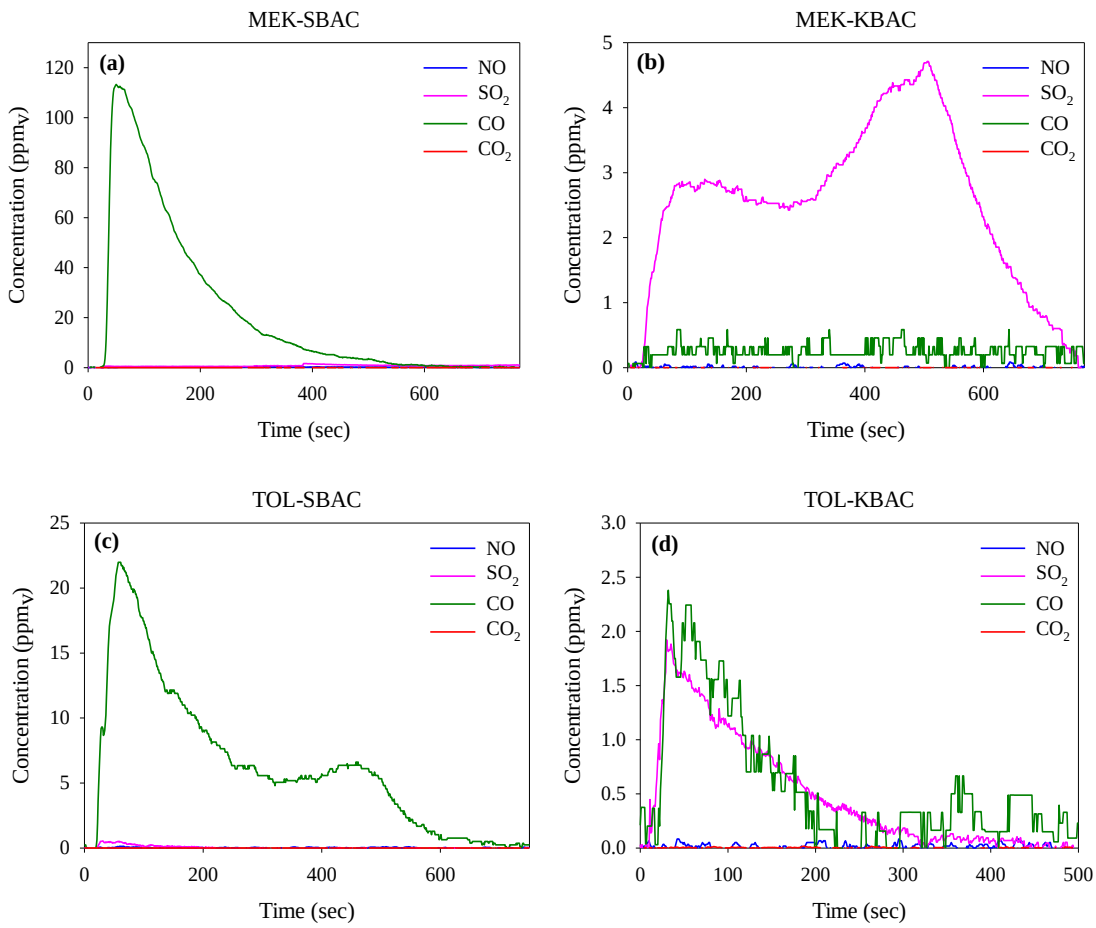

Figure 4-38 NO, SO_2, CO, and CO_2 emission curves of (a) MEK-SBAC, (b) MEK-KBAC, (c) TOL-SBAC, (d) TOL-KBAC at 800 W microwave heating for 8 min

doi:10.6342/NTU202003443

4.5 Cyclic Test

When determining a suitable adsorbent and proper desorption technique, aside from a high desorption efficiency, the cyclic adsorption capability draws attention. The successive cycles may change the porous structure of activated carbon because of the collapse of the porous structure or the formation of coke inside the pores. In this study, BAC samples were subjected to eight adsorption/desorption cycles. The adsorption capacity after each regeneration cycle was evaluated by the gravimetric method.

Figures 4-39 and 4-40 show the effect of different regeneration conditions on MEK-KBAC and TOL-KBAC's capacity loss after eight adsorption/regeneration cycles, and Table 4-3 provides the physical properties of cyclic regenerated samples. While the KBACs showed fluctuating adsorption capacity throughout the cycles, and the adsorption capacity slightly decreased, the results showed that the adsorption capacities of KBAC loaded with MEK and TOL were still in the range of 114.2-151.9 and 237.2-306.4 mg g^{-1} throughout the cycles, respectively. Also, the porous properties maintained after cycles. The slow decline in adsorption capacity also proves a favorable stability.

doi:10.6342/NTU202003443

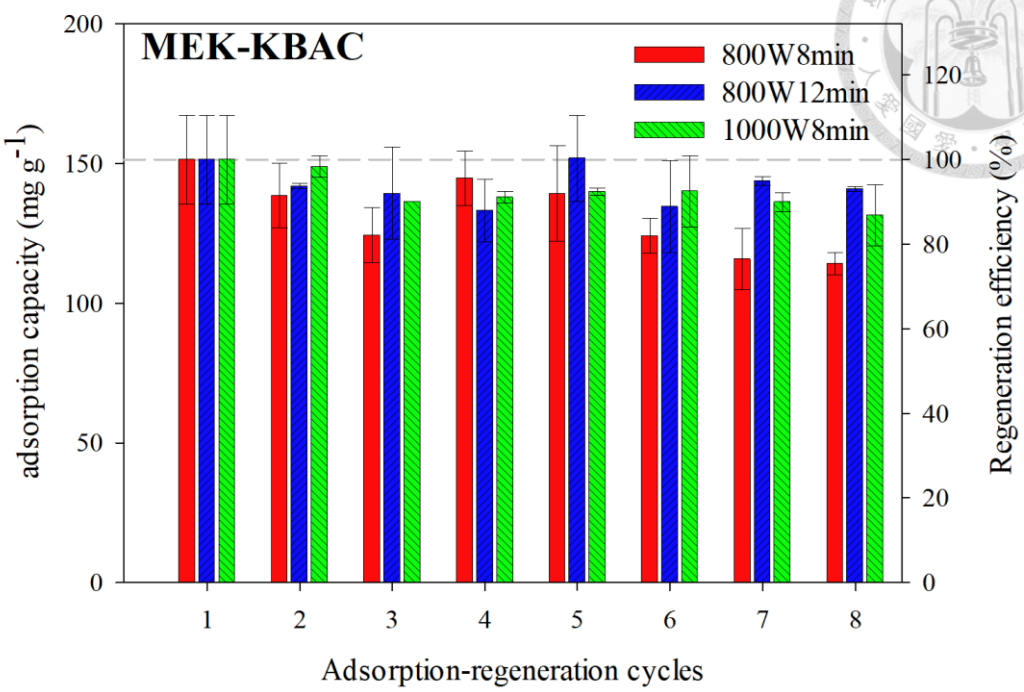

Figure 4-39 Variation in adsorption capacity of MEK-KBAC over the 8-cycle MSA test

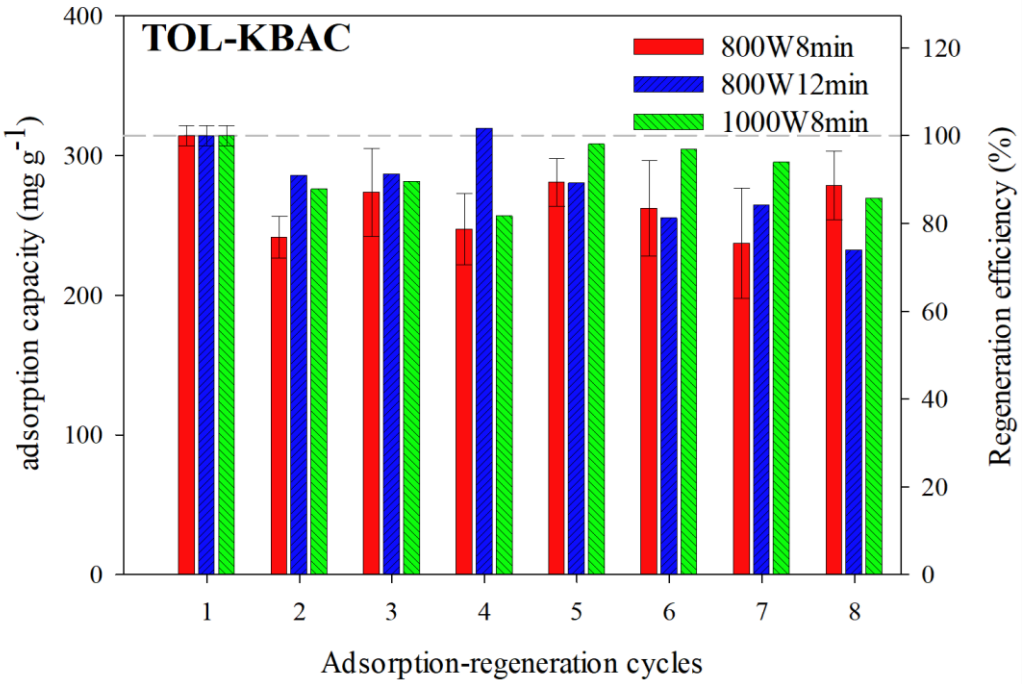

Figure 4-40 Variation in adsorption capacity of TOL-KBAC over the 8-cycle MSA test

doi:10.6342/NTU202003443

The results of the 8-cycle test of MEK-SBAC and TOL-SBAC are presented in Figures 4-41 and 4-42. The results between MEK-SBAC and TOL-SBAC showed a significant difference. Figure 4-41 shows that the adsorption capacities of all SBACs loaded with MEK were higher than their initial values after the cycles, and the improvements were undulated. However, as seen in Table 4-3, the total and microporous surface area and pore volume of MEK-SBAC all decreased after the 8-cycle MSA test (800W-8min). in other words, the increase of adsorption capacity was not owing to the improvements in the pore structure. The more likely explanation rests in the polarity of regenerated BACs. As can be seen in Table 4-1, the results of EA reflected that the percentages of H and O of MEK-KBAC grew after regeneration. The increasing surface polarity of sorbents accordingly increased its adsorption capacity of MEK (high polarity).

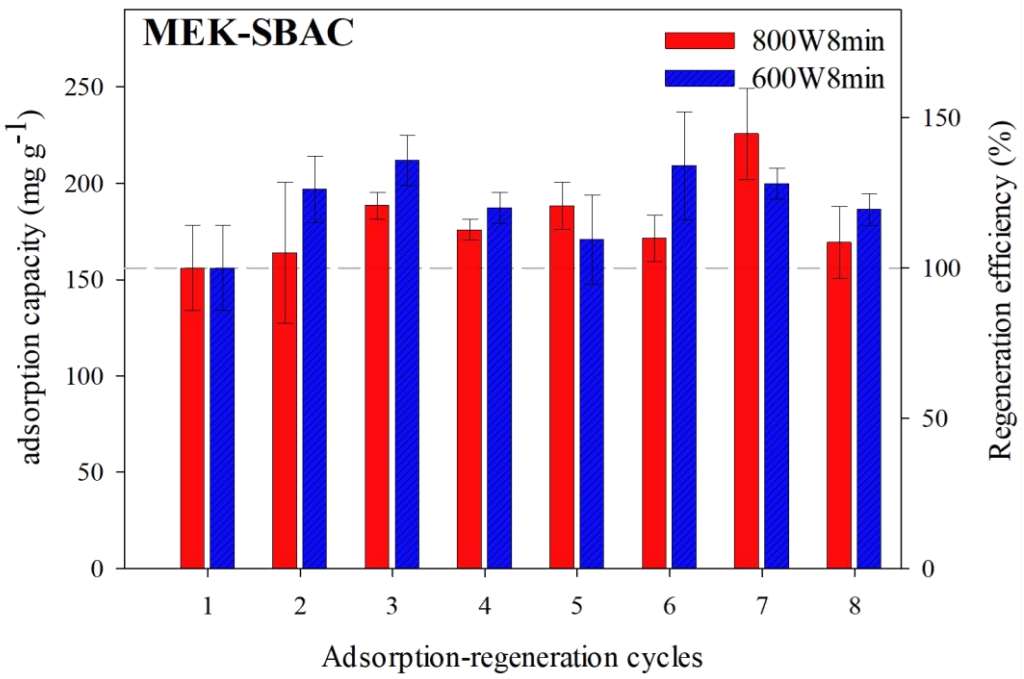

Figure 4-41 Variation in adsorption capacity of MEK-SBAC over the 8-cycle MSA test

doi:10.6342/NTU202003443

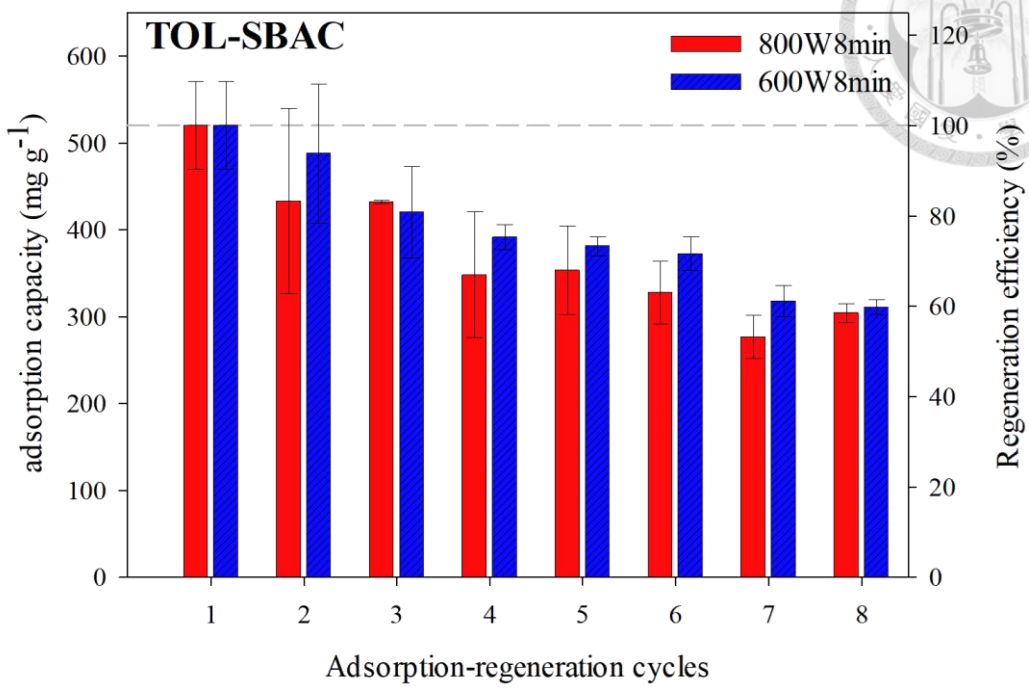

Figure 4-42 Variation in adsorption capacity of TOL-SBAC over the 8-cycle MSA test

As opposed to MEK-SBAC, the adsorption capacities of TOL-SBAC decline gradually throughout the cycles. This may be related to relatively low desorption efficiencies (around 90%, as seen in Figure 4-36). As shown in Table 4-3, the total and microporous surface area and pore volume of TOL-SBAC all significantly declined after 8-cycle of 800W-8min MSA test. Suzuki et al. (1978) have indicated that the regeneration behavior of activated carbon was significantly correlated with the aromaticity of the organic compound. TOL is a typical aromatic compound, and at high temperatures, the coke species grew faster and reached molecule sizes larger than the pores. Therefore, they became trapped in the pore structure (Korus et al., 2017). In brief, coke formation may be more significant in materials with smaller pores. SBAC is an adsorbent with more micropores and a higher micropore ratio (Table 4-2), which increased desorbate diffusion

doi:10.6342/NTU202003443

resistance during regeneration. This explained why the loss in adsorption capacity (i.e. the buildup of heel) was not notable in KBAC loaded with TOL throughout the adsorption/regeneration cycles, but resulted in upwards of a 35% loss in SBAC loaded with TOL after eight cycles. However, even though the capacities of TOL-SBAC seriously decreased, the adsorption capacities after 8 cycles were still better than TOL adsorbed onto KBAC.

doi:10.6342/NTU202003443

Chapter 5 Conclusions and Suggestions

5.1 Conclusions

This study is divided into three parts. Firstly, it aims to analyze the performances of beaded activated carbons (BACs) in adsorption towards TOL and MEK. The self-prepared BAC (SBAC) was compared with the commercial BAC (KBAC). Secondly, the spent BACs were regenerated using microwave heating, which studied the effect of regeneration performance due to microwave power output and irradiation time. Finally, cyclic adsorption/regeneration tests were conducted to prove the feasibility of this technology.

5.1.1 Adsorption Equilibrium and Kinetics

To better understand the adsorption behavior on materials, equilibrium and kinetics models were used, including the Langmuir isotherm, the Freundlich isotherm, the Dubinin-Radushkevich (D-R) isotherm, the Clausius-Clapeyron (C-C) equation, the pseudo-first-order (PFO) model, and the intraparticle diffusion (IPD) model. The results demonstrated that:

1. The saturated adsorption capacities of TOL were greater than MEK under the same operating conditions (i.e. temperature and inlet concentration) for the BACs. The main reasons were attributed to the higher boiling point, larger molecular weight, and lower polarity of TOL. SBAC was superior to KBACs in capturing VOCs. This was attributed to the much higher surface area and larger pore volume of SBAC.
2. Considering the results of both MEK and TOL adsorbed onto BACs, three isotherm models showed good fits in this study. The isosteric heat of adsorption (ΔH_s) was

doi:10.6342/NTU202003443

obtained from the D-R parameters. The ΔH_s of MEK and TOL on the SBAC were nearly constant and temperature-independent, which was possibly due to the energetic homogeneity of the surface of the adsorbent. However, the ΔH_s for TOL adsorption onto KBAC increased at higher loading. The influence of surface loading and temperature on ΔH_s were more noticeable when TOL and MEK adsorbed onto KBAC. This indicated the surface heterogeneity of KBAC.

3. The PFO and IPD models were applied to determine the external diffusion coefficient (k_1) and intraparticle diffusivities (k_p) for adsorption. Based on the value of R^2, the both kinetic model was good in describing cases. They indicated that both the external and intraparticle diffusion control was possible to be the rate-limiting step of MEK and TOL adsorbed on the adsorbent.

5.1.2 Microwave Regeneration

The spent BACs were regenerated by a novel microwave regeneration technique. The results demonstrated that:

1. The maximum signal intensity of VOCs desorbed from BACs gradually increased with the increment of microwave power, and the rates of MEK and TOL desorbed from SBAC were much faster than those desorbed from KBAC. That is, SBAC showed superior desorption performance due to the fast desorption rate and high outlet concentration.
2. The desorption efficiencies were evaluated by the change in sample weight and the mass balance of the desorption concentration curve detected by FID. As expected, an increase in irradiation power and time caused an increase in desorption

doi:10.6342/NTU202003443

efficiency. Also, MEK and TOL desorbed from SBAC showed better performance at a relatively smaller irradiation powers and time. It implied that the more efficient energy utilization on SBAC regeneration.

3. The polarity of MEK may led to a higher adsorption capability of the microwaves, and resulted in higher temperatures in certain regions of the adsorbent, as well as the desorption of impurities.
4. The desorption efficiencies of MEK-SBAC and MEK-KBAC obtained from the sample weight showed around 28.01% and 22.37% lower than evaluated by the desorption curve, respectively, while this phenomenon was only 4.31% and 4.48% in TOL-SBAC and TOL-KBAC. For MEK-SBAC, this is presumably due to the thermal decomposition of MEK into CO and CO_2. For TOL-SBAC, one possible explanation is that TOL reacted with oxygen functions on the carbon surface. Moreover, for MEK and TOL desorption from KBAC, the efficiency difference is presumably mainly due to the desorption of impurities such as sulfur.

5.1.3 Cyclic Adsorption/Desorption Test

Cyclic tests of SBAC and KBAC were conducted to demonstrate the practice of using microwave swing adsorption. Unsurprisingly, the adsorption capacities of commercial KBAC remained relatively unchanged after 8-cycle tests. However, the high microporosity of SBAC possibly caused the decrease in TOL's adsorption capacity over these 8 cycles. Additionally, the formation of coke may block pores and generate the build-up of heel in the adsorbent.

doi:10.6342/NTU202003443

5.2 Suggestions

SBAC has been proven to possess greater adsorption capacity than KBAC due to its high surface area and micropore volume. Nevertheless, it is important to emphasize that the high microporosity of SBAC may limit its repeated use. These results indicate that pore structure could be optimized to allow for great adsorption performance and fast desorption with minimum heel buildup.

Moreover, the physical properties of adsorption bed packing, including the bulk density, particle hardness, and abrasion, were important in practical applications, especially fluidization. Since this study concentrated primarily on adsorption and regeneration performance, this has not yet been tested.

Regarding regeneration, microwave heating is a rapid and energy-saving technology that can potentially replace traditional conductive heating. However, it is important to emphasize that the microwave sensitivity of the thermocouple limited the temperature measurement in our experiments. Future studies should consider a method to track the temperature of samples during microwave heating. The precise measurement of the temperature would be the next step in analyzing microwave heating behavior of adsorbent regeneration more thoroughly.

doi:10.6342/NTU202003443

Appendix A: Thermodynamic Calculation

A.1.Determination of Affinity Coefficient (β)

The affinity coefficient (β) of adsorbate is usually calculated according to the dominant interaction force of adsorbate and adsorbent. For cases where forces and interactions other than dispersion forces are important, β could be obtained from using the ratio of molecular parachors of the test (Ω) and reference (Ω_{ref}) adsorbates (Jahandar Lashaki et al., 2012):

$$\beta = \frac{\Omega}{\Omega_{\mathrm{ref}}} \tag{A-1}$$

and

$$\Omega = \frac{\gamma^{1/4}\mathrm{M}}{\rho_L} \tag{A-2}$$

where γ is the surface tension (dynes cm^{-2}) of the adsorbate in the liquid phase, M (g mol^{-1}) is the molecular weight of the adsorbate, and ρ_L (g cm^{-3}) is the density of the adsorbate in the liquid phase. The calculated parameters are in Table A-1, and benzene was selected as the reference compounds.

Table A-1 Parameters used in calculating and the affinity coefficient (β)

Adsorbate	Parameter				β
	Temperature (°C)	γ_{ref} [a] (dynes cm^{-2})	γ [a] (dynes cm^{-2})	ρ_L [b] (g cm^{-3})	
MEK	30	27.56	23.40	0.795	0.968
	40	26.25	22.28	0.785	0.970
	50	24.96	21.16	0.774	0.971
TOL	30	27.56	27.33	0.858	1.192
	40	26.25	26.15	0.848	1.193
	50	24.96	24.95	0.839	1.193

[a] (Jasper, 1972), [b] (Poling et al., 2001)

doi:10.6342/NTU202003443

A.2. Determination of Heat of Vaporization (ΔH_{vap}) and Coefficient Expansion (α)

Assuming that the limiting pore volume (W_0) is independent of temperature. The thermal expansion coefficient (α) is expressed as (Ramirez et al., 2005):

$$\alpha = \frac{\int_{\rho_c}^{\rho_b} d[\ln(\rho W_0)]}{\int_{T_b}^{T_c} dT} = \frac{1}{T_c - T_b} \ln \frac{\rho_b}{\rho_c} \tag{A-3}$$

where ρ_b and ρ_c are saturated liquid densities at normal boiling temperature (T_b) and the critical temperature (T_c). The calculated parameters and α are in Table A-2.

The heat of vaporization from bulk liquid adsorbate can be computed by using Wagner equation (Ramirez et al., 2005):

$$\begin{aligned} \Delta H_{vap} &= \frac{RT^2}{P_0}\frac{dP_0}{dT} \\ &= \frac{RT^2}{T_c}\left[\frac{-a_1 - 1.5a_2x^{0.5} + 0.5a_2x^{1.5} - 3a_3x^2 + 2a_3x^3 - 6a_4x^5 + 5a_4x^6}{(1-x)^2}\right] \end{aligned} \tag{A-4}$$

where $x = (1 - T/T_c)$. The Wagner equation constants a_1-a_4 are shown in Table A-3.

Table A-2 Parameters used in calculating and thermal expansion coefficient (α)

Adsorbate	Parameter				α
	T_b[a] (K)	T_c[a] (K)	ρ_b[a] (g cm^{-3})	ρ_c[a] (g cm^{-3})	
MEK	352.71	536.80	0.742	0.270	0.00168
TOL	383.79	591.75	0.779	0.294	0.00113

[a] (Poling et al., 2001)

Table A-3 Wagner equation constants used in calculating the heat of vaporization

Adsorbate	a_1	a_2	a_3	a_4
MEK	-7.6642	1.7175	-2.0991	-4.5861
TOL	-7.4183	1.8401	-2.1458	-3.7081

(Forero G & Velásquez J, 2011)

doi:10.6342/NTU202003443

References

Amankwah, R. K.; Pickles, C. A.; Yen, W. T. Gold Recovery by Microwave Augmented Ashing of Waste Activated Carbon. *Minerals Engineering.* **2005,** *18* (5), 517-526.

Ania, C. O.; Menéndez, J. A.; Parra, J. B.; Pis, J. J. Microwave-Induced Regeneration of Activated Carbons Polluted with Phenol. A Comparison with Conventional Thermal Regeneration. *Carbon.* **2004,** *42* (7), 1383-1387.

Ania, C. O.; Parra, J. B.; Menéndez, J. A.; Pis, J. J. Effect of Microwave and Conventional Regeneration on the Microporous and Mesoporous Network and on the Adsorptive Capacity of Activated Carbons. *Microporous and Mesoporous Materials.* **2005,** *85* (1), 7-15.

Ania, C. O.; Parra, J. B.; Menéndez, J. A.; Pis, J. J. Microwave-Assisted Regeneration of Activated Carbons Loaded with Pharmaceuticals. *Water Research.* **2007,** *41* (15), 3299-3306.

Atkinson, R. Atmospheric Chemistry of VOCs and NOx. *Atmospheric Environment.* **2000,** *34* (12-14), 2063-2101.

Atkinson, R.; Arey, J. Atmospheric Degradation of Volatile Organic Compounds. *Chemical Reviews.* **2003,** *103* (12), 4605-4638.

Ayawei, N.; Ebelegi, A. N.; Wankasi, D. Modelling and Interpretation of Adsorption Isotherms. *Journal of Chemistry.* **2017,** *2017*, 1-11.

Baird, W. M.; Hooven, L. A.; Mahadevan, B. Carcinogenic Polycyclic Aromatic Hydrocarbon-DNA Adducts and Mechanism of Action. *Environmental and Molecular Mutagenesis.* **2005,** *45* (2-3), 106-114.

Bansal, R. C.; Goyal, M., *Activated Carbon Adsorption*. CRC press: 2005.

Barratt, R. The Preparation of Standard Gas Mixtures. A Review. *Analyst.* **1981,** *106* (1265), 817-849.

Benkhedda, J.; Jaubert, J. N.; Barth, D.; Perrin, L. Experimental and Modeled Results Describing the Adsorption of Toluene onto Activated Carbon. *Journal of Chemical & Engineering Data.* **2000,** *45* (4), 650-653.

Bhandari, P. N.; Kumar, A.; Bellmer, D. D.; Huhnke, R. L. Synthesis and Evaluation of

doi:10.6342/NTU202003443

Biochar-Derived Catalysts for Removal of Toluene (Model Tar) from Biomass-Generated Producer Gas. *Renewable Energy.* **2014,** *66*, 346-353.

Binner, E.; Lester, E.; Kingman, S.; Dodds, C.; Robinson, J.; Wu, T.; Wardle, P.; Mathews, J. P. A Review of Microwave Coal Processing. *Journal of Microwave Power Electromagnetic Energy.* **2014,** *48* (1), 35-60.

Bradshaw, S. M.; Wyk, E. J. V.; Swardt, J. B. d. Preliminary Economic Assessment of Microwave Regeneration of Activated Carbon for the Carbon in Pulp Process. *Journal of Microwave Power and Electromagnetic Energy.* **1997,** *32* (3), 131-144.

Buss, E. Gravimetric Measurement of Binary Gas Adsorption Equilibria of Methane — Carbon Dioxide Mixtures on Activated Carbon. *Gas Separation & Purification.* **1995,** *9* (3), 189-197.

Cai, Q.; Huang, Z. H.; Kang, F.; Yang, J. B. Preparation of Activated Carbon Microspheres from Phenolic-Resin by Supercritical Water Activation. *New Carbon Materials.* **2004,** *42* (4), 775-783.

Çalışkan, E.; Bermúdez, J. M.; Parra, J. B.; Menéndez, J. A.; Mahramanlıoğlu, M.; Ania, C. O. Low Temperature Regeneration of Activated Carbons Using Microwaves: Revising Conventional Wisdom. *Journal of Environmental Management.* **2012,** *102*, 134-140.

Cha, C. Y.; Carlisle, C. T. Microwave Process for Volatile Organic Compound Abatement. *Journal of the Air & Waste Management Association.* **2001,** *51* (12), 1628-1641.

Cha, C. Y.; Wallace, S.; George, A. H.; Rogers, S. Microwave Technology for Treatment of Fume Hood Exhaust. *Journal of Environmental Engineering.* **2004,** *130* (3), 338-348.

Chandra, U., *Microwave Heating*. BoD–Books on Demand: 2011.

Chandrasekaran, S.; Ramanathan, S.; Basak, T. Microwave Material Processing — a Review. *AIChE Journal.* **2012,** *58* (2), 330-363.

Chang, C. T.; Chiou, C. S. Assessment of Control Strategies for Reducing Volatile Organic Compound Emissions from the Polyvinyl Chloride Wallpaper Production Industry in Taiwan. *Air Waste Management Association.* **2006,** *56* (5), 611-617.

Chang, C. T.; Jeng, F. T. Study on Fugitive Emission Model of Volatile Organic Compounds and Effects of Additives on the Emission Rate. *Toxicological &*

doi:10.6342/NTU202003443

Environmental Chemistry. **1994,** *43* (3-4), 183-202.

Chang, C. T.; Lin, K. L. Assessment of the Strategies for Reducing VOCs Emission from Polyurea-Formaldehyde Resin Synthetic Fiber Leather Industry in Taiwan. *Resources, Conservation and Recycling.* **2006,** *46* (4), 321-334.

Chang, T. Y.; Lin, S. J.; Shie, R. H.; Tsai, S. W.; Hsu, H. T.; Tsai, C. T.; Kuo, H. W.; Chiang, C. F.; Lai, J. S. Characterization of Volatile Organic Compounds in the Vicinity of an Optoelectronics Industrial Park in Taiwan. *Journal of the Air & Waste Management Association.* **2010,** *60* (1), 55-62.

Chen, Y. T.; Huang, Y. P.; Wang, C.; Deng, J. G.; Hsi, H. C. Comprehending Adsorption of Methylethylketone and Toluene and Microwave Regeneration Effectiveness for Beaded Activated Carbon Derived from Recycled Waste Bamboo Tar. *Journal of the Air & Waste Management Association.* **2020**, 616-628.

Cherbański, R. Regeneration of Granular Activated Carbon Loaded with Toluene – Comparison of Microwave and Conductive Heating at the Same Active Powers. *Chemical Engineering and Processing - Process Intensification.* **2018,** *123*, 148-157.

Chiang, H. L.; Huang, C. P.; Chiang, P. C. The Adsorption of Benzene and Methylethylketone onto Activated Carbon: Thermodynamic Aspects. *Chemosphere.* **2002,** *46* (1), 143-152.

Chiou, C. T., *Partition and Adsorption of Organic Contaminants in Environmental Systems*. John Wiley & Sons: 2003.

Choi, J. G.; Do, D. D.; Do, H. D. Surface Diffusion of Adsorbed Molecules in Porous Media: Monolayer, Multilayer, and Capillary Condensation Regimes. *Industrial & Engineering Chemistry Research.* **2001,** *40* (19), 4005-4031.

Chowdhury, S.; Mishra, R.; Saha, P.; Kushwaha, P. Adsorption Thermodynamics, Kinetics and Isosteric Heat of Adsorption of Malachite Green onto Chemically Modified Rice Husk. *Desalination.* **2011,** *265* (1), 159-168.

Cinke, M.; Li, J.; Bauschlicher, C. W.; Ricca, A.; Meyyappan, M. CO_2 Adsorption in Single-Walled Carbon Nanotubes. *Chemical Physics Letters.* **2003,** *376* (5), 761-766.

Coats, A.; Redfern, J. Thermogravimetric Analysis. A Review. *Analyst.* **1963,** *88* (1053), 906-924.

Collins, W. J.; Fry, M. M.; Yu, H.; Fuglestvedt, J. S.; Shindell, D. T.; West, J. J. Global

doi:10.6342/NTU202003443

and Regional Temperature-Change Potentials for near-Term Climate Forcers. *Atmospheric Chemistry and Physics.* **2013,** *13* (5), 2471-2485.

Cooper, C. D.; Alley, F. C., *Air Pollution Control: A Design Approach*. Waveland press: 2010.

Coss, P. M.; Cha, C. Y. Microwave Regeneration of Activated Carbon Used for Removal of Solvents from Vented Air. *Journal of the Air & Waste Management Association.* **2000,** *50* (4), 529-535.

Cvetanović, R. J.; Amenomiya, Y. A Temperature Programmed Desorption Technique for Investigation of Practical Catalysts. *Catalysis Reviews.* **1972,** *6* (1), 21-48.

Dąbrowski, A. Adsorption — from Theory to Practice. *Advances in Colloid and Interface Science.* **2001,** *93* (1-3), 135-224.

Di, Z. In *Study on Activated Carbon Adsorption of VOCs*, 6th International Conference on Mechatronics, Materials, Biotechnology and Environment (ICMMBE 2016), Atlantis Press: 2016.

Dinh, T.-V.; Choi, I.-Y.; Son, Y.-S.; Song, K.-Y.; Sunwoo, Y.; Kim, J.-C. Volatile Organic Compounds (VOCs) in Surface Coating Materials: Their Compositions and Potential as an Alternative Fuel. *Journal of Environmental Management.* **2016,** *168*, 157-164.

Do, D. D., *Adsorption Analysis: Equilibria and Kinetics*. Imperial college press London: 1998; Vol. 2.

Dubinin, M.; Stoeckli, F. Homogeneous and Heterogeneous Micropore Structures in Carbonaceous Adsorbents. *Journal of Colloid Interface Science.* **1980,** *75* (1), 34-42.

Emamipour, H.; Hashisho, Z.; Cevallos, D.; Rood, M. J.; Thurston, D. L.; Hay, K. J.; Kim, B. J.; Sullivan, P. D. Steady-State and Dynamic Desorption of Organic Vapor from Activated Carbon with Electrothermal Swing Adsorption. *Environmental Science & Technology.* **2007,** *41* (14), 5063-5069.

Fang, C. S.; Lai, P. M. C. Microwave Regeneration of Spent Powder Activated Carbon. *Chemical Engineering Communications.* **1996,** *147* (1), 17-27.

Fayaz, M.; Shariaty, P.; Atkinson, J. D.; Hashisho, Z.; Phillips, J. H.; Anderson, J. E.; Nichols, M. Using Microwave Heating to Improve the Desorption Efficiency of

doi:10.6342/NTU202003443

High Molecular Weight VOC from Beaded Activated Carbon. *Environmental Science & Technology.* **2015,** *49* (7), 4536-4542.

Foo, K. Y.; Hameed, B. H. Microwave-Assisted Regeneration of Activated Carbon. *Bioresource Technology.* **2012,** *119*, 234-240.

Forero G, L. A.; Velásquez J, J. A. Wagner Liquid–Vapour Pressure Equation Constants from a Simple Methodology. *The Journal of Chemical Thermodynamics.* **2011,** *43* (8), 1235-1251.

Fournel, L.; Mocho, P.; Brown, R.; le Cloirec, P. Modeling Breakthrough Curves of Volatile Organic Compounds On activated Carbon Fibers. *Adsorption.* **2010,** *16* (3), 147-153.

Fujita, E. M. Hydrocarbon Source Apportionment for the 1996 Paso Del Norte Ozone Study. *Science of the Total Environment.* **2001,** *276* (1-3), 171-184.

Ghafari, M.; Atkinson, J. D. Impact of Styrenic Polymer One-Step Hyper-Cross-Linking on Volatile Organic Compound Adsorption and Desorption Performance. *Journal of Hazardous Materials.* **2018,** *351*, 117-123.

Giraudet, S.; Pré, P.; Le Cloirec, P. Modeling the Heat and Mass Transfers in Temperature-Swing Adsorption of Volatile Organic Compounds onto Activated Carbons. *Environmental Science & Technology.* **2009,** *43* (4), 1173-1179.

Guo, L.; Zhang, L.; Zhang, J.; Zhou, J.; He, Q.; Zeng, S.; Cui, X.; Shi, J. Hollow Mesoporous Carbon Spheres — an Excellent Bilirubin Adsorbent. *Royal Society of Chemistry.* **2009,** (40), 6071.

Haneishi, N.; Tsubaki, S.; Abe, E.; Maitani, M. M.; Suzuki, E.-i.; Fujii, S.; Fukushima, J.; Takizawa, H.; Wada, Y. Enhancement of Fixed-Bed Flow Reactions under Microwave Irradiation by Local Heating at the Vicinal Contact Points of Catalyst Particles. *Scientific Reports.* **2019,** *9* (1), 222.

Hansen, J.; Lacis, A.; Prather, M. Greenhouse Effect of Chlorofluorocarbons and Other Trace Gases. *Journal of Geophysical Research.* **1989,** *94* (D13), 16417.

Hashisho, Z.; Rood, M.; Botich, L. Microwave-Swing Adsorption to Capture and Recover Vapors from Air Streams with Activated Carbon Fiber Cloth. *Environmental Science & Technology.* **2005,** *39* (17), 6851-6859.

Hazervazifeh, A.; Moghaddam, P. A.; Nikbakht, A. M. Microwave Dehydration of Apple

doi:10.6342/NTU202003443

Fruit: Investigation of Drying Efficiency and Energy Costs. *Journal of Food Process Engineering.* **2017,** *40* (3), e12463.

Henning, K. D.; Schäfer, S. Impregnated Activated Carbon for Environmental Protection. *Gas Separation & Purification.* **1993,** *7* (4), 235-240.

Hosseini, S.; Moghaddas, H.; Masoudi Soltani, S.; Kheawhom, S. Technological Applications of Honeycomb Monoliths in Environmental Processes: A Review. *Process Safety and Environmental Protection.* **2020,** *133*, 286-300.

Huang, Y. Y. The Temperature Dependence of Isosteric Heat of Adsorption on the Heterogeneous Surface. *Journal of Catalysis.* **1972,** *25* (1), 131-138.

Hutson, N. D.; Yang, R. T. Theoretical Basis for the Dubinin-Radushkevitch (D-R) Adsorption Isotherm Equation. *Adsorption.* **1997,** *3* (3), 189-195.

Jüntgen, H. Activated Carbon as Catalyst Support. *Fuel.* **1986,** *65* (10), 1436-1446.

Jafarinejad, S., 7-Solid-Waste Management in the Petroleum Industry. In *Petroleum Waste Treatment and Pollution Control*, S. Jafarinejad, Ed. Butterworth-Heinemann: 2017; pp 269-345.

Jagtoyen, M.; Derbyshire, F. Activated Carbons from Yellow Poplar and White Oak by H_3PO_4 Activation. *Carbon.* **1998,** *36* (7-8), 1085-1097.

Jahandar Lashaki, M.; Fayaz, M.; Niknaddaf, S.; Hashisho, Z. Effect of the Adsorbate Kinetic Diameter on the Accuracy of the Dubinin–Radushkevich Equation for Modeling Adsorption of Organic Vapors on Activated Carbon. *Journal of Hazardous Materials.* **2012,** *241-242*, 154-163.

Jones, D. A.; Lelyveld, T. P.; Mavrofidis, S. D.; Kingman, S. W.; Miles, N. J. Microwave Heating Applications in Environmental Engineering—a Review. *Resources, Conservation and Recycling.* **2002,** *34* (2), 75-90.

Kampa, M.; Castanas, E. Human Health Effects of Air Pollution. *Environmental Pollution.* **2008,** *151* (2), 362-367.

Kesselmeier, J.; Staudt, M. Biogenic Volatile Organic Compounds (VOC): An Overview on Emission, Physiology and Ecology. *Journal of Atmospheric Chemistry.* **1999,** *33* (1), 23-88.

Khan, A. R.; Ataullah, R.; Al-Haddad, A. Equilibrium Adsorption Studies of Some Aromatic Pollutants from Dilute Aqueous Solutions on Activated Carbon at

doi:10.6342/NTU202003443

Different Temperatures. *Journal of Colloid and Interface Science.* **1997,** *194* (1), 154-165.

Khan, F. I.; Kr. Ghoshal, A. Removal of Volatile Organic Compounds from Polluted Air. *Journal of Loss Prevention in the Process Industries.* **2000,** *13* (6), 527-545.

Kim, K. J.; Ahn, H. G. The Adsorption and Desorption Characteristics of a Binary Component System of Toluene and Methylethylketone on Activated Carbon Modified with Phosphoric Acid. *Carbon.* **2010,** *48* (8), 2198-2202.

Kim, K. J.; Ahn, H. G. The Effect of Pore Structure of Zeolite on the Adsorption of VOCs and Their Desorption Properties by Microwave Heating. *Microporous and Mesoporous Materials.* **2012,** *152*, 78-83.

Kodama, M.; Fujiura, T.; Ikawa, E.; Esumi, K.; Meguro, K.; Honda, H. Characterization of Meso-Carbon Microbeads Prepared by Emulsion Method. *Carbon.* **1991,** *29* (1), 43-49.

Korus, A.; Samson, A.; Szlęk, A.; Katelbach-Woźniak, A.; Sładek, S. Pyrolytic Toluene Conversion to Benzene and Coke over Activated Carbon in a Fixed-Bed Reactor. *Fuel.* **2017,** *207*, 283-292.

Laine, J.; Yunes, S. Effect of the Preparation Method on the Pore Size Distribution of Activated Carbon from Coconut Shell. *Carbon.* **1992,** *30* (4), 601-604.

Lashaki, M. J.; Fayaz, M.; Wang, H.; Hashisho, Z.; Philips, J. H.; Anderson, J. E.; Nichols, M. Effect of Adsorption and Regeneration Temperature on Irreversible Adsorption of Organic Vapors on Beaded Activated Carbon. *Environmental Science & Technology.* **2012,** *46* (7), 4083-4090.

Lee, S. W.; Cheon, J. K.; Park, H. J.; Lee, M. G. Adsorption Characteristics of Binary Vapors among Acetone, MEK, Benzene, and Toluene. *Korean Journal of Chemical Engineering.* **2008,** *25* (5), 1154-1159.

Liu, S.; Deng, R.; Li, W.; Zhu, J. Polymer Microparticles with Controllable Surface Textures Generated through Interfacial Instabilities of Emulsion Droplets. *Advanced Functional Materials.* **2012,** *22* (8), 1692-1697.

Liu, X.; Quan, X.; Bo, L.; Chen, S.; Zhao, Y. Simultaneous Pentachlorophenol Decomposition and Granular Activated Carbon Regeneration Assisted by Microwave Irradiation. *Carbon.* **2004,** *42* (2), 415-422.

doi:10.6342/NTU202003443

Lowell, S.; Shields, J. E.; Thomas, M. A.; Thommes, M., *Characterization of Porous Solids and Powders: Surface Area, Pore Size and Density*. Springer Science & Business Media: 2012; Vol. 16.

Lozano-Castelló, D.; Lillo-Ródenas, M. A.; Cazorla-Amorós, D.; Linares-Solano, A. Preparation of Activated Carbons from Spanish Anthracite. *Carbon.* **2001,** *39* (5), 741-749.

Luo, L.; Ramirez, D.; Rood, M. J.; Grevillot, G.; Hay, K. J.; Thurston, D. L. Adsorption and Electrothermal Desorption of Organic Vapors Using Activated Carbon Adsorbents with Novel Morphologies. *Carbon.* **2006,** *44* (13), 2715-2723.

Menéndez, J. A.; Arenillas, A.; Fidalgo, B.; Fernández, Y.; Zubizarreta, L.; Calvo, E. G.; Bermúdez, J. M. Microwave Heating Processes Involving Carbon Materials. *Fuel Processing Technology.* **2010,** *91* (1), 1-8.

Menon, V. C.; Komarneni, S. Porous Adsorbents for Vehicular Natural Gas Storage: A Review. *Journal of Porous Materials.* **1998,** *5* (1), 43-58.

Metaxas, A. C. Microwave Heating. *Power Engineering Journal.* **1991,** *5* (5), 237-247.

Mirzaei, A.; Leonardi, S. G.; Neri, G. Detection of Hazardous Volatile Organic Compounds (VOCs) by Metal Oxide Nanostructures-Based Gas Sensors: A Review. *Ceramics International.* **2016,** *42* (14), 15119-15141.

Mishra, A. K., *Nanomaterials for Water Remediation: Carbon-Based Materials*. Smithers Rapra: 2016; Vol. 1.

Mohamad Nor, N.; Lau, L. C.; Lee, K. T.; Mohamed, A. R. Synthesis of Activated Carbon from Lignocellulosic Biomass and Its Applications in Air Pollution Control — a Review. *Journal of Environmental Chemical Engineering.* **2013,** *1* (4), 658-666.

Monneyron, P.; Manero, M. H.; Foussard, J. N. Measurement and Modeling of Single- and Multi-Component Adsorption Equilibria of VOC on High-Silica Zeolites. *Environmental Science & Technology.* **2003,** *37* (11), 2410-2414.

Montero-Montoya, R.; López-Vargas, R.; Arellano-Aguilar, O. Volatile Organic Compounds in Air: Sources, Distribution, Exposure and Associated Illnesses in Children. *Annals of Global Health.* **2018,** *84* (2), 225-238.

Nelson, G., *Gas Mixtures: Preparation and Control*. CRC Press: 1992.

Ng, K. C.; Burhan, M.; Shahzad, M. W.; Ismail, A. B. A Universal Isotherm Model to

doi:10.6342/NTU202003443

Capture Adsorption Uptake and Energy Distribution of Porous Heterogeneous Surface. *Scientific Reports.* **2017,** *7* (1).

Nigar, H.; Garcia-Baños, B.; Peñaranda-Foix, F. L.; Catalá-Civera, J. M.; Mallada, R.; Santamaría, J. Amine-Functionalized Mesoporous Silica: A Material Capable of CO_2 Adsorption and Fast Regeneration by Microwave Heating. *AIChE Journal.* **2016,** *62* (2), 547-555.

Niknaddaf, S.; Atkinson, J. D.; Gholidoust, A.; Fayaz, M.; Awad, R.; Hashisho, Z.; Phillips, J. H.; Anderson, J. E.; Nichols, M. Influence of Purge Gas Flow and Heating Rates on Volatile Organic Compound Decomposition During Regeneration of Activated Carbon Fiber Cloth. *Industrial Engineering Chemistry Research.* **2020**.

Niknaddaf, S.; Atkinson, J. D.; Shariaty, P.; Jahandar Lashaki, M.; Hashisho, Z.; Phillips, J. H.; Anderson, J. E.; Nichols, M. Heel Formation During Volatile Organic Compound Desorption from Activated Carbon Fiber Cloth. *Carbon.* **2016,** *96*, 131-138.

Palma, V.; Barba, D.; Cortese, M.; Martino, M.; Renda, S.; Meloni, E. Microwaves and Heterogeneous Catalysis: A Review on Selected Catalytic Processes. *Catalysts.* **2020,** *10* (2), 246.

Park, J. W.; Lee, S. S.; Choi, D. K.; Lee, Y. W.; Kim, Y. M. Adsorption Equilibria of Toluene, Dichloromethane, and Trichloroethylene onto Activated Carbon Fiber. *Journal of Chemical & Engineering Data.* **2002,** *47* (4), 980-983.

Parra, J. B.; Sousa, J. C. D.; Bansal, R. C.; Pis, J. J.; Pajares, J. A. Characterization of Activated Carbons by the BET Equation — an Alternative Approach. *Adsorption Science & Technology.* **1995,** *12* (1), 51-66.

Pelekani, C.; Snoeyink, V. L. Competitive Adsorption between Atrazine and Methylene Blue on Activated Carbon: The Importance of Pore Size Distribution. *Carbon.* **2000,** *38* (10), 1423-1436.

Pereira, M. F. R.; Órfão, J. J. M.; Figueiredo, J. L. Oxidative Dehydrogenation of Ethylbenzene on Activated Carbon Catalysts. I. Influence of Surface Chemical Groups. *Applied Catalysis A: General.* **1999,** *184* (1), 153-160.

Perrich, J. R., *Activated Carbon Adsorption for Wastewater Treatment*. CRC press: 1981.

Pert, E.; Carmel, Y.; Birnboim, A.; Olorunyolemi, T.; Gershon, D.; Calame, J.; Lloyd, I.

doi:10.6342/NTU202003443

K.; Wilson, O. C. Temperature Measurements During Microwave Processing: The Significance of Thermocouple Effects. *Journal of the American Ceramic Society.* **2001,** *84* (9), 1981-1986.

Polaert, I.; Estel, L.; Huyghe, R.; Thomas, M. Adsorbents Regeneration under Microwave Irradiation for Dehydration and Volatile Organic Compounds Gas Treatment. *Chemical Engineering Journal.* **2010,** *162* (3), 941-948.

Poling, B. E.; Prausnitz, J. M.; O'connell, J. P., *The Properties of Gases and Liquids*. Mcgraw-hill New York: 2001; Vol. 5.

Popescu, M.; Joly, J. P.; Carré, J.; Danatoiu, C. Dynamical Adsorption and Temperature-Programmed Desorption of VOCs (Toluene, Butyl Acetate and Butanol) on Activated Carbons. *Carbon.* **2003,** *41* (4), 739-748.

Qi, J.; Li, J.; Li, Y.; Fang, X.; Sun, X.; Shen, J.; Han, W.; Wang, L. Synthesis of Porous Carbon Beads with Controllable Pore Structure for Volatile Organic Compounds Removal. *Chemical Engineering Journal.* **2017,** *307*, 989-998.

Ramanathan, V. Greenhouse Effect Due to Chlorofluorocarbons: Climatic Implications. *Science.* **1975,** *190* (4209), 50-52.

Ramirez, D.; Qi, S.; Rood, M. J.; Hay, K. J. Equilibrium and Heat of Adsorption for Organic Vapors and Activated Carbons. *Environmental Science & Technology.* **2005,** *39* (15), 5864-5871.

Romero-Anaya, A. J.; Lillo-Ródenas, M. A.; Linares-Solano, A. Spherical Activated Carbons for Low Concentration Toluene Adsorption. *Carbon.* **2010,** *48* (9), 2625-2633.

Romero-Anaya, A. J.; Lillo-Ródenas, M. A.; Linares-Solano, A. Activation of a Spherical Carbon for Toluene Adsorption at Low Concentration. *Carbon.* **2014,** *77*, 616-626.

Rumchev, K.; Brown, H.; Spickett, J. Volatile Organic Compounds: Do They Present a Risk to Our Health? *Reviews on Environmental Health.* **2007,** *22* (1), 39.

Ruthven, D. M., *Fundamentals of Adsorption Equilibrium and Kinetics in Microporous Solids*. Springer Berlin Heidelberg: Berlin, Heidelberg, 2006.

Seinfeld, J. H.; Pandis, S. N., *Atmospheric Chemistry and Physics: From Air Pollution to Climate Change*. John Wiley & Sons: 2016.

Shah, I. K.; Pre, P.; Alappat, B. J. Effect of Thermal Regeneration of Spent Activated

doi:10.6342/NTU202003443

Carbon on Volatile Organic Compound Adsorption Performances. *Journal of the Taiwan Institute of Chemical Engineers.* **2014,** *45* (4), 1733-1738.

Shen, K. P.; Lai, C. C.; Lin, S. S.; Wu, H. H.; Huang, J. J.; Wang, Y. M.; Chen, H. W. (1999). *Best Available Control Technology (BACT) of VOC for PU (Polyurethane) Synthetic Leather Surface Coating Industry in Taiwan*.

Sillman, S. The Relation between Ozone, NOx and Hydrocarbons in Urban and Polluted Rural Environments. *Atmospheric Environment.* **1999,** *33* (12), 1821-1845.

Singh, K. P.; Mohan, D.; Tandon, G. S.; Gupta, G. S. D. Vapor-Phase Adsorption of Hexane and Benzene on Activated Carbon Fabric Cloth: Equilibria and Rate Studies. *Industrial & Engineering Chemistry Research.* **2002,** *41* (10), 2480-2486.

Soni, V.; Singh, P.; Shree, V.; Goel, V. Effects of VOCs on Human Health. *Air Pollution and Control.* **2018**, 119-142.

Spengler, J. D.; Samet, J. M.; McCarthy, J. F., *Indoor Air Quality Handbook*. 2001.

Sui, H.; Liu, H.; An, P.; He, L.; Li, X.; Cong, S. Application of Silica Gel in Removing High Concentrations Toluene Vapor by Adsorption and Desorption Process. *Journal of the Taiwan Institute of Chemical Engineers.* **2017,** *74*, 218-224.

Sun, N.; Sun, C.; Liu, H.; Liu, J.; Stevens, L.; Drage, T.; Snape, C. E.; Li, K.; Wei, W.; Sun, Y. Synthesis, Characterization and Evaluation of Activated Spherical Carbon Materials for CO_2 Capture. *Fuel.* **2013,** *113*, 854-862.

Suzuki, M.; Misic, D. M.; Koyama, O.; Kawazoe, K. Study of Thermal Regeneration of Spent Activated Carbons: Thermogravimetric Measurement of Various Single Component Organics Loaded on Activated Carbons. *Chemical Engineering Science.* **1978,** *33* (3), 271-279.

TEPA. (2016). Taiwan Emission Data System Version 10.0 (TEDS 10.0). from Department of Air Quality Protection and Noise Control https://stat.epa.gov.tw/

Thommes, M.; Kaneko, K.; Neimark, A. V.; Olivier, J. P.; Rodriguez-Reinoso, F.; Rouquerol, J.; Sing, K. S. Physisorption of Gases, with Special Reference to the Evaluation of Surface Area and Pore Size Distribution (IUPAC Technical Report). *Pure Applied Chemistry.* **2015,** *87* (9-10), 1051-1069.

Tsao, Z. C. (2014). *The Infrared Continuous Monitoring and the Survey of Harmful Air Pollutants in Yunlin County on 2014*.

doi:10.6342/NTU202003443

Tseng, R. L. Physical and Chemical Properties and Adsorption Type of Activated Carbon Prepared from Plum Kernels by NaOH Activation. *Journal of Hazardous Materials.* **2007,** *147* (3), 1020-1027.

Vargas, A. M. M.; Cazetta, A. L.; Kunita, M. H.; Silva, T. L.; Almeida, V. C. Adsorption of Methylene Blue on Activated Carbon Produced from Flamboyant Pods (Delonix Regia): Study of Adsorption Isotherms and Kinetic Models. *Chemical Engineering Journal.* **2011,** *168* (2), 722-730.

Volkamer, R.; Jimenez, J. L.; San Martini, F.; Dzepina, K.; Zhang, Q.; Salcedo, D.; Molina, L. T.; Worsnop, D. R.; Molina, M. J. Secondary Organic Aerosol Formation from Anthropogenic Air Pollution: Rapid and Higher Than Expected. *Geophysical Research Letters.* **2006,** *33* (17).

Wang, H.; Jahandar Lashaki, M.; Fayaz, M.; Hashisho, Z.; Philips, J. H.; Anderson, J. E.; Nichols, M. Adsorption and Desorption of Mixtures of Organic Vapors on Beaded Activated Carbon. *Environmental Science & Technology.* **2012,** *46* (15), 8341-8350.

Wang, R.; Wang, L.; Wu, J., *Adsorption Refrigeration Technology: Theory and Application*. John Wiley & Sons: 2014.

Waring, C. E.; Spector, M. The Mechanism of the Thermal Decomposition of Methyl Ethyl Ketone. *Journal of the American Chemical Society.* **1955,** *77* (24), 6453-6457.

Webb, P. A.; Orr, C., *Analytical Methods in Fine Particle Technology*. Micromeritics Instrument Corp: 1997.

Wickramaratne, N. P.; Jaroniec, M. Importance of Small Micropores in CO_2 Capture by Phenolic Resin-Based Activated Carbon Spheres. *Journal of Materials Chemistry A.* **2013,** *1* (1), 112-116.

World Health Organization, Indoor Air Quality: Organic Pollutants. 1989.

Wu, F. C.; Tseng, R. L.; Juang, R. S. Initial Behavior of Intraparticle Diffusion Model Used in the Description of Adsorption Kinetics. *Chemical Engineering Journal.* **2009,** *153* (1), 1-8.

Wypych, G., *Handbook of Solvents, Volume 2: Use, Health, and Environment*. Elsevier: 2019.

Xu, C.; Cheng, L.; Shen, P.; Liu, Y. Methanol and Ethanol Electrooxidation on Pt and Pd Supported on Carbon Microspheres in Alkaline Media. *Electrochemistry*

doi:10.6342/NTU202003443

Communications. **2007,** *9* (5), 997-1001.

Yang, R. T., *Adsorbents: Fundamentals and Applications*. John Wiley & Sons: 2003.

Yuan, H. G.; Kalfas, G.; Ray, W. H. Suspension Polymerization. *Power Engineering Journal.* **1991,** *31* (2-3), 215-299.

Yuen, F. K.; Hameed, B. H. Recent Developments in the Preparation and Regeneration of Activated Carbons by Microwaves. *Advances in Colloid and Interface Science.* **2009,** *149* (1), 19-27.

Zhang, X.; Gao, B.; Creamer, A. E.; Cao, C.; Li, Y. Adsorption of VOCs onto Engineered Carbon Materials: A Review. *Journal of Hazardous Materials.* **2017,** *338*, 102-123.

Zhong, Z.; Sha, Q. e.; Zheng, J.; Yuan, Z.; Gao, Z.; Ou, J.; Zheng, Z.; Li, C.; Huang, Z. Sector-Based VOCs Emission Factors and Source Profiles for the Surface Coating Industry in the Pearl River Delta Region of China. *Science of the Total Environment.* **2017,** *583*, 19-28.

Zhou, Q.; Duan, Y. F.; Hong, Y. G.; Zhu, C.; She, M.; Zhang, J.; Wei, H. Q. Experimental and Kinetic Studies of Gas-Phase Mercury Adsorption by Raw and Bromine Modified Activated Carbon. *Fuel Processing Technology.* **2015,** *134*, 325-332.

Zhu, W.; Groen, J. C.; Kapteijn, F.; Moulijn, J. A. Adsorption of Butane Isomers and SF_6 on Kureha Activated Carbon: 1. Equilibrium. *Langmuir.* **2004,** *20* (13), 5277-5284.

doi:10.6342/NTU202003443